THE EFFECTS OF CONTACT METAMORPHISM BY THE DULUTH COMPLEX ON PROTEROZOIC FOOTWALL ROCKS IN NORTHEASTERN MINNESOTA

A THESIS
SUBMITTED TO THE FACULTY OF THE GRADUATE SCHOOL
OF THE UNIVERSITY OF MINNESOTA
BY

Shelby Jeanne Frost

IN PARTIAL FULFILLMENT OF THE REQUIREMENTS
FOR THE DEGREE OF
MASTER OF SCIENCE

Dr. John Goodge, Advisor

June 2010

ACKNOWLEDGMENTS

I would sincerely like to thank Dr. John Goodge, who served as my advisor for this study, for the hundreds of hours of academic help and guidance he provided for this study.

I am also grateful to Dr. John Swenson and Dr. Jim Miller, who both served on my committee, for taking time out of their busy schedules to talk to me about thermal modeling and the geology of the Duluth Complex.

Gratitude is also extended to Bryan Bandli for the many hours he spent helping me learn how to use a scanning electron microscope, especially when I was learning how to do EBSD analysis.

Special thanks go to Dr. John Green for providing great information about the Ely's Peak basalts, Mark Severson for helping me find the exact drill cores needed to jump start this study, and Rick Ruhanen for allowing me to come to the Hibbing DNR core shack to log core.

Lastly, I would like to thank my fiancé, Sam, for providing motivation and support to finish this thesis even though he was miles away throughout most of it.

Financial support for thin sections, chemical analyses, and other items were provided by the Precambrian Research Center research grant, the University of Minnesota – Duluth Department of Geoscience Block Grant, and an Institute on Lake Superior Geology research grant.

ABSTRACT

The Duluth Complex is composed of numerous mafic intrusions that were emplaced in northeastern Minnesota during formation of the Midcontinent Rift approximately 1.1 Ga (Miller et. al., 2002). When it intruded, the heat of this igneous body significantly affected the wall rocks around it and created a distinctive contact metamorphic aureole. Footwall rocks directly west of the Duluth Complex include the Animikie Group and the North Shore Volcanic Group.

The purpose of this research is to understand crustal conditions associated with emplacement of a large mafic igneous massif such as the Duluth Complex, and develop a better idea of the thermal state of the crust during the time of rifting. To constrain crustal conditions we must determine the effects that intrusion of the Duluth Complex had on adjacent wall rocks, in particular the Ely's Peak basalts of the North Shore Volcanic Group, and the Thomson and Virginia formations of the Animike Group. These effects include the extent and grade of metamorphism.

At the time of intrusion, metamorphic pressure was approximately 2.5 kbar and temperature was 600-700°C, based on the presence of metamorphic minerals such as orthopyroxene and wollastonite. The contact metamorphic aureole extends from the Duluth Complex into the Animikie Group for approximately 200 m and into the Ely's Peak basalts for approximately 100 m. This is consistent with estimates made by Severson (1995), Duchesne (2004) and Kilburg (1972). The criteria used to define the aureole include textures such as mortar texture and spotty slate texture in the Animikie

Group, and granoblastic texture in the Ely's Peak basalts. Porphyroblasts of metamorphic indicator minerals such as cordierite, wollastonite, garnet, and pyroxene also help define the aureole. A simple 1D thermal conduction model reproduces the conditions in the contact aureole determined by petrographic relations, and helps explain why the aureole is thin. Despite the high temperature of the intrusion, the aureole is thin because the wall rocks were fairly cool when the Duluth Complex intruded, having equilibrated over about 600 m.y. at shallow crustal levels to a typical continental geotherm. The thin contact aureole also indicates that multiple intrusions may have occurred instead of one large intrusion. This would have led to insulation of the younger intrusions and a thinner aureole. Liberation of fluids in the wall rocks by the intrusion may have also played a role in keeping the contact aureole relatively thin by lowering reaction temperatures.

TABLE OF CONTENTS

LIST OF TABLES

LIST OF FIGURES

LIST OF APPENDIXES

1. INTRODUCTION

The Duluth Complex is one of the largest igneous intrusions on Earth. Many petrogenetic aspects of the Duluth Complex have been studied extensively during the last 150 years, including the source of the melts, the emplacement history, and the relationship between the gabbros and anorthosites (Miller, et. al, 2002). Little attention has been paid, however, to the effects of contact metamorphism by the Duluth Complex on the adjacent footwall rocks to the west. Wall rocks from Duluth to the Iron Range were directly modified by intrusion of the Duluth Complex because of its large volume and high emplacement temperature, yet the degree and conditions of thermal metamorphism are poorly known.

Previous work shows that wall rocks underwent varying degrees of contact metamorphism during intrusion of the Duluth Complex. Along its southwestern margin, the contact zone at the base of the Duluth Complex shows it's effects on the Ely's Peak basalts of the North Shore Volcanic Group and units within the Animikie Group (including the Thomson and Virginia formations). For example, basalt flows at Ely's Peak show textural and mineralogical evidence of contact metamorphism within the albite-epidote, hornblende, and pyroxene hornfels facies (Kilburg, 1972). The basalts there are partly recrystallized, and a granoblastic texture is evident. Pelitic rocks of the Animikie Group contain cordierite and show evidence of syn-metamorphic deformation at the outcrop level (Severson, 1995).

The purpose of this research is to understand crustal conditions associated with emplacement of a large igneous complex, and develop a better idea of the thermal state of the crust during the time of rifting. To constrain crustal conditions, and the influence of regional crustal rifting and intrusion of large mafic igneous massifs on local thermal structure, we must determine the effects that intrusion of the Duluth Complex had on the Ely's Peak basalts and the Thomson and Virginia formations. These effects include the extent of metamorphism and how much chemical exchange took place between the igneous complex and the wall rocks. These will help in evaluation of the origin of mineralization within the wall rocks and the basal Duluth Complex.

2. GEOLOGIC BACKGROUND

2.1 Introduction

The Duluth Complex is composed of numerous mafic intrusions that were emplaced in northeastern Minnesota during formation of the Midcontinent Rift approximately 1.1 Ga (Miller et. al., 2002). It is one of the largest mafic intrusions on Earth, and includes major gabbroic and anorthositic phases (Miller et. al., 2002). When it intruded, the heat of this igneous body significantly affected the wall rocks around it, partially melting them into small pockets of granophyre found both in drill core and in outcrop of the Ely's Peak Basalts (Severson, 1995; Kilburg, 1972), and creating a contact metamorphic aureole. The wall rocks involved in this study include the Thomson and Virginia formations of the Animikie Group, and the Ely's Peak Basalts of the North Shore Volcanic Group (Figure 2.1).

2.2 Animikie Group

The Thomson and Virginia formations are part of the Paleoproterozoic Animikie Group, which also includes the Pokegama Quartzite and the Biwabik Iron Formation. The Thomson and Virginia formations make up part of the footwall rocks directly west of the Duluth Complex and north of the Ely's Peak basalts. Sediment derived from the Penokean belt was dominantly siliciclastic in composition. Deposition of the Animikie Group began between 2125 and 1930 Ma, and continued after 1878 Ma (Beck, 1988; Hemming et. al., 1990) based on U/Pb dates on zircons in volcanic ash layers (Fralich, et.

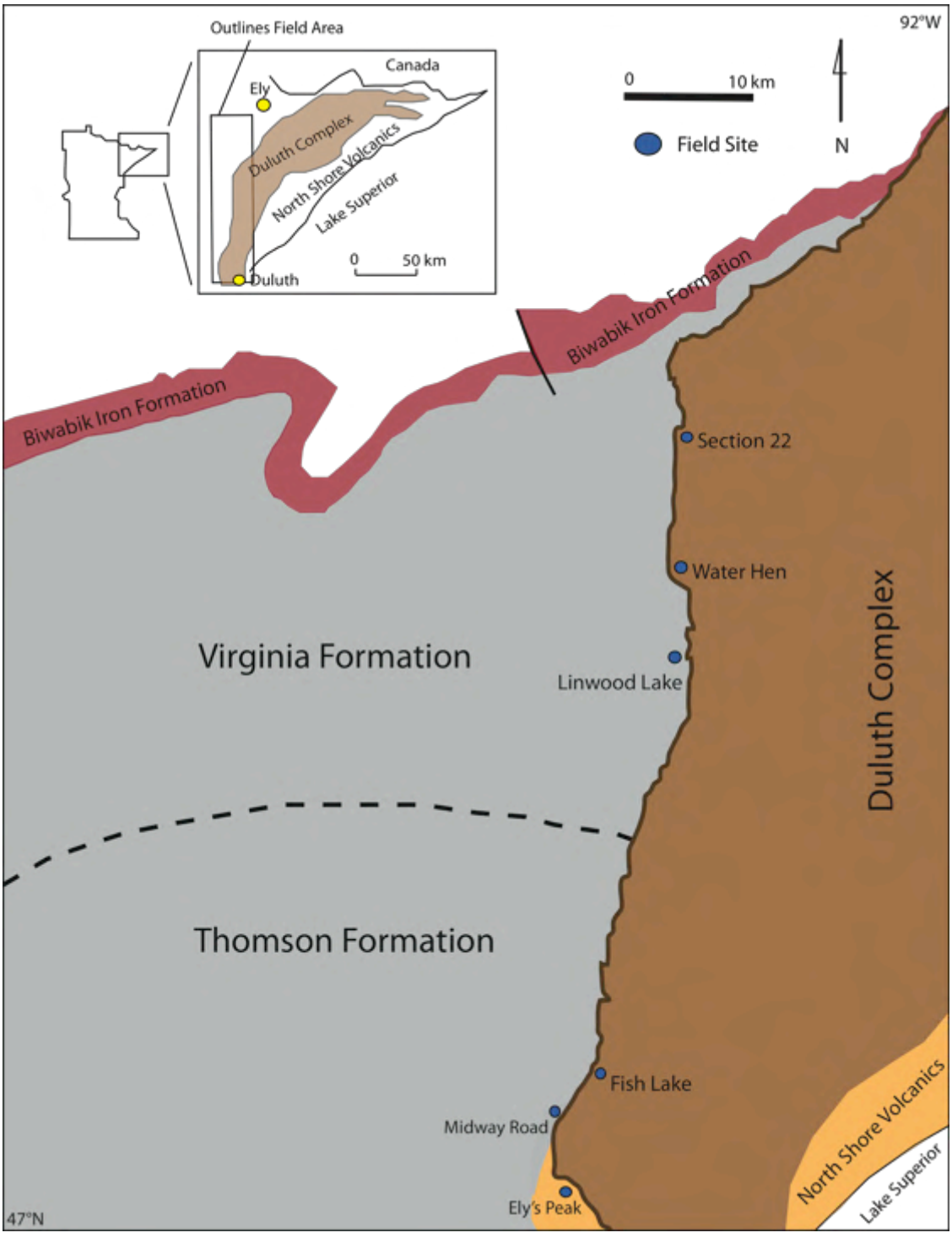

Figure 2.1. Geologic map of the study area modified from Severson (1995), showing field sites (blue circles). The dotted line separating the Virginia Formation from the Thomson Formation represents a change from steep bedding in the southern area to shallow bedding in the northern area.

al, 1998). Ages and provenances of these sediments have changed over time. Initially they were derived from the north (from the Superior Craton) as part of a rift-margin basin thinning to the south. Then as the Penokean belt developed, the provenance shifted to the south with foreland-basin deposits shed towards the north.

The Thomson Formation consists of intercalated metagraywacke, metasiltstone, and slate that underlie the Virginia Formation. The Thomson siliciclastic assemblage is approximately 900 m thick (Morey and Ojakangas, 1970). The Virginia Formation is a thick, well-bedded sequence of weakly metamorphosed argillite, siltstone and greywacke, representing the uppermost part of the Animikie Group (Ojakangas, et. al, 2001; Peterson and Severson, 2002). In general, the siliciclastic metasedimentary rocks are quartz-rich, containing detrital plagioclase feldspar, muscovite, and biotite. Bedding in the Virginia Formation is relatively steep to the south, and to the north it becomes more shallow in attitude. The thickness of this unit is poorly constrained and ranges from more than 500 m on average to less than 10 m near the northeastern contact with the Duluth Complex (Ripley, 2001).

2.3 Ely's Peak Basalts

Footwall rocks to the west of the Duluth Complex include the Ely's Peak flood basalt unit of the North Shore Volcanic Group (Mesoproterozoic), a thick package of tholeiitic lavas that form the northwest limb of the Midcontinent Rift synclinorium. The Ely's Peak basalts are a north-south trending, wedge-shaped section of basalt flows that make up the base of the North Shore Volcanic Group (Goldich et. al., 1961). This unit is

exposed for nearly 13 km along strike and is 360 m thick, and it is composed of at least 20 separate flows (Kilburg 1972). Although each flow has a unique structure and petrology, the flows are dominantly porphyritic, diabasic, and ophitic, with the basal flow being pillowed, and they are characterized by reversed magnetic polarity (Green, 2002). Plagioclase is the dominant phenocryst phase in all of the flows and makes up 28-55% of the rocks, but it is commonly hydrothermally altered. Two main types of pyroxene are found throughout the flows. The first type is diopsidic augite, which occurs both as ophitic grains and phenocrysts. The second type is subcalcic augite, which occurs as ophitic grains. Ilmenite and magnetite are the dominant opaque minerals found in the flows. These minerals also show evidence of hydrothermal alteration. Interflow sediments, mainly sandstone, are rare and are only found in discontinuous lenses (Kilburg, 1972).

2.4 Duluth Complex

The Duluth Complex in northeast Minnesota is one of the largest mafic intrusive complexes in the world. This intrusive massif was emplaced into flood basalts during formation of the Mesoproterozoic Midcontinent Rift approximately 1.1 Ga. It extends 240 km from Duluth to the northeastern tip of Minnesota, and it is approximately 5000 km^2 in area and 13 km thick (Miller et. al., 2002). A mixture of anorthositic, troctolitic, gabbroic, granodioritic, and granitic intrusive bodies make up the entire complex, while the base of the complex is composed of a layered series of troctolite and ferrogabbro. Many of the individual intrusions are relatively thin tabular bodies. These intrusions are

the result of pulses of magmatic activity that occurred during four stages of rifting over a period of 23 million years (Davis and Paces, 1990; Paces and Miller, 1993; Davis and Green, 1997; Zartman et. al, 1997): the early, latent, main, and late magmatic stages (Miller and Vervoort, 1996). The early magmatic stage (1109 to 1107 Ma) represents the impact of a mantle plume head with the lithosphere, heating of the lithosphere by mantle-derived melts, and contamination of those melts by interaction with the lower crust. The latent magmatic stage (1107 to 1102 Ma) represents a period of continued mantle plume upwelling and melting, extensive crustal underplating, and lower crustal melting. The main magmatic stage (1102 to 1094 Ma) represents the start of crustal separation, the evacuation of lower crustal magma chambers, and continued mantle plume melting. Lastly, the late magmatic stage (1094 to 1086 Ma) represents the loss of the plume heat due to plate drift and thermal collapse of the rift basin (Miller, et. al., 2002). Various intrusions of the Duluth Complex were emplaced during the early and main magmatic stages (Paces and Miller, 1993; Vervoort, unpub. data, 2001). The anorthositic and mafic layered intrusions that are the focus of this study were emplaced during the main stage.

The Duluth Complex is divided into four general rock series based on age, lithology, internal structure, and structural position within the complex (Miller and Severson, 2002). The first series is the felsic series, which consists of mostly granophyric granite that occurs as a semicontinuous mass of intrusions emplaced during early stage magmatism (~1108 Ma). The early gabbro series consists of layered sequences of dominantly gabbroic cumulates that occur along the northeastern contact of the Duluth Complex. These sequences were also emplaced during early stage

magmatism (~1108 Ma). The anorthositic series is a structurally complex suite of foliated plagioclase-rich gabbroic cumulates that was emplaced during main stage magmatism (~1099 Ma). Finally, the layered series is a suite of stratiform troctolitic to ferrogabbroic cumulates that comprises at least eleven different mafic layered intrusions along the base of the Duluth Complex. These intrusions were emplaced during main stage magmatism after the anorthositic series (~1099 Ma). This study focuses on the layered series because it occurs along the base of the Duluth Complex.

Massive sulfide mineralization is documented at the base of the complex in many areas, and sulfur-isotope data indicate that Paleoproterozoic footwall rocks are the source of the sulfur in the mineralized parts of the Duluth Complex (Ripley, 1981; Andrews and Ripley, 1989; Peterson and Severson, 2002).

2.5 Contact Metamorphism of the Wall Rocks

Volcanic and sedimentary footwall rocks were directly affected by intrusion of the Duluth Complex, but the extent and degree of metamorphism is unclear. As stated above, they also may be the source for some of the sulfide mineralization found at the base of the Duluth Complex and in other localized areas. While numerous studies have been conducted on igneous petrology of the basal Duluth Complex, little is known about its affects on the directly adjacent wall rocks.

Kilburg (1972) observed that basalts at Ely's Peak are recrystallized to fine-grained hornfels at the contact and show a granoblastic texture. He identified brittle shearing within 180 m of the contact, which is characterized by brecciated zones cross-

cutting the flows. He also documented granophyre pods occurring near the contact and interpreted them to be partial melting of the basalt. Mineralogical data are lacking but the metamorphism is interpreted to be albite-epidote, hornblende, and pyroxene hornfels facies.

Kilburg also studied scattered outcrops of the Thomson Formation immediately west of the Duluth Complex and noted intense folding with axes that trend east-west, and bedding that dips steeply north and south. At the contact the Thomson is metamorphosed to a fine-grained hornfels texture (Kilburg, 1972). Severson (1995) noted that near the contact the argillite is massively cordierite-bearing and characterized by cordierite, potassium feldspar, orthopyroxene, and biotite. Granophyre pods were found in this unit, as in the Ely's Peak basalts, suggesting that temperatures in the contact aureole were sufficient to cause partial melting of the wall rocks. The Thomson Formation becomes increasingly folded and recrystallized towards the contact (Severson, 1995).

Severson also studied the Virginia Formation at several outcrops near Linwood Lake and in drill core (Severson, 1995). The Virginia Formation is also cordierite-bearing near the contact, and it shows significant increases in deformation and degree of metamorphism approaching the contact. Metamorphic textures are superimposed on the original sedimentary protoliths, and informal mineral zonation was defined near the contact (Severson, 1996). Cordieritic metasediments are found directly adjacent to the contact. Cordierite is so abundant in places that bedding has been obliterated. A disrupted unit lies beneath the cordierite-rich layer and is characterized by chaotic bedding, partial melt zones, and intense structural deformation. Below the disrupted unit

lies a recrystallized unit that is the higher-grade metamorphic equivalent of the disrupted unit. There is no visible bedding and this layer contains boudins of metasiltstone and calc-silicate hornfels that are possibly metamorphosed concretions. Based on depth of core, the lowest division near the contact consists of graphitic argillite and a bedded pyrrhotite layer in the basal 61 m of the Virginia Formation. This division contains small amounts of staurolite and sillimanite (Severson, 1996). Severson (1994) and Zanko (1994) proposed that this last layer of bedded pyrrhotite provided a local sulfur source for the pyrrhotite-dominated massive-sulfide mineralization at the base of the Duluth Complex. Localized massive sulfide deposits occur at the Serpentine and Dunka pits, and in the Local Boy ore zone (Hauck et. al., 1997).

3. PREVIOUS WORK

3.1 Animikie Group

Extensive ore deposit study has been conducted on various properties of the Duluth Complex, but little research has been done on the associated wall rocks. Labotka (1984) studied the northern part of the Animikie Group (Rove Formation) to determine the role of water in the contact metamorphic aureole created by intrusion of the Duluth Complex. He described the mineral assemblage crd-bt-ms-qtz-kfs and determined that contact metamorphism resulted from the discontinuous reaction:

$$\text{chl-ms-qtz} \rightarrow \text{crd-bt-}H_2O$$

and the continuous reaction:

$$\text{ms-bt-qtz} \rightarrow \text{crd-kfs-}H_2O$$

Using mass balance equations he showed that the contact metamorphism of the Rove Formation was isochemical and in chemical equilibrum, except for a loss of 0.6-2.7 wt% H_2O. Labotka also constructed a one-dimensional heat conduction model to determine the width of the thermal aureole and the temperature of the thermal gradient. His model indicated the width of the contact metamorphic aureole to be 180 m, and temperatures along the thermal gradient ranged from 500-620°C. He theorized that as the temperature increased, devolitalization reactions occured and were capable of buffering fluid composition.

Severson (1995), in a study for the Natural Resources Research Institute (NRRI), of the geology of the southern portion of the Duluth Complex, also investigated wall

rocks along the contact. He discovered extensive deformation of the Thomson and Virginia formations that increased with proximity to the contact with the Duluth Complex. He also noted diagnostic metamorphic minerals in these rocks, including cordierite.

Building on his initial observations of the Animikie Group, Severson and Peterson (2002) described several metamorphic zones present in the Virginia Formation near the contact within multiple drill core sites. From the contact outward, they defined four zones based on metamorphic attributes. The cordierite-rich metasediments zone lies directly beneath the basal contact of the Duluth Complex. This zone is characterized by cordierite-rich metasediments that are bluish-gray in color, and bedding that has been mostly obliterated by contact metamorphism. With greater depth in the drill hole, the cordierite-rich metasediments are underlain by a disrupted unit. This unit consists of well-bedded argillites that are highly deformed. Bedding is chaotic and randomly oriented, and small scale folding and faulting are common. There are also abundant zones of partial melt in this unit, lending an overall texture that appears to be a combination of partial melting and intense structural deformation that Severson and Peterson believe is related to emplacement of the Duluth Complex. The next unit (recrystallized unit) is a high-grade metamorphic equivalent to the disrupted unit. All bedding is obliterated and decussate medium-grained biotite is very common. Within this zone are boudins of siltstone and calc-silicate and patches of the disrupted unit. The deepest units of graphitic argillite and bedded pyrrhotite units comprise the lower 61 m of the Virginia Formation. This rock commonly contains as much as 5% disseminated

pyrrhotite, and more minor amounts of staurolite and sillimanite. Where this unit was intruded by the Duluth Complex it provided a local sulfur source for the pyrrhotite-dominated massive sulfide mineralization at the base of the Duluth Complex.

Duchesne (2004) completed a petrographic and geochemical study of the Virginia Formation in order to establish mineralogical and microstructural aspects of the contact aureole due to intrusion of the Duluth Complex. She concluded that at the time of intrusion, metamorphic pressure was approximately 2-2.5 kbar, and the temperature was greater than 650°C. She also hypothesized that the temperature could have reached at least 750°C due to the presence of orthopyroxene. Duchesne identified many microstructures that are characteristic of partial melting and show evidence of flow and segregation. Geochemical analysis revealed a degree of melting more than 26%, but the separation of melt and residuum is not extensive. She hypothesized that this could be due to only minor deformation of the country rocks during intrusion, or that cooling after contact metamorphism occurred rapidly.

3.2 Ely's Peak Basalts

Winchell (1899) published a description of the geology and petrography of the flows in the vicinity of Ely's Peak, and Sandberg (1938) briefly described the Ely's Peak basalts when he published a strip map of the flows along the North Shore of Lake Superior from Duluth to Two Harbors. Sandberg distinguished seven separate flows and estimated the thickness to be approximately 800 m. Schwartz (1949) used Winchell and Sandberg's work when he published a report on the geology of the Duluth area, but he

did not elaborate any more than the previous workers. Green (1968, 1972) collected samples of several of the flows for petrographic study and suggested the Ely's Peak basalts as a problem deserving further attention.

Kilburg (1972) provided the only detailed petrologic and geochemical study of the Ely's Peak basalts. During his study he determined that the whole area has undergone burial and possible hydrothermal metamorphism to the upper zeolite and/or lower greenschist facies, and he also identified a contact metamorphic aureole that extends approximately 100 meters outward from the contact with the Duluth Complex. He noted that the basalt had been recrystallized to a granoblastic pyroxene hornfels near the contact. Kilburg estimated pressures during metamorphism to have been between 2 and 2.5 kbars although it is not clear which metamorphic event is associated with this pressure range. Temperatures during burial metamorphism were though to be between 290°C and 370°C, and temperatures during contact metamorphism to have been between 600°C and 700°C.

3.3 Duluth Complex

For the purpose of this study, igneous evolution of the Duluth Complex will refer to previous study by Miller and Severson (2002). They identified four major stages of magmatic activity related to thermal and dynamic changes within the plume and plume-impacted lithosphere. This is noteworthy because the intrusion of the Duluth Complex could cause very different metamorphic patterns if it was injected in multiple pulses rather than one large intrusion.

4. FIELD AND LABORATORY METHODS

4.1 Mapping

Field mapping was completed over a period of four weeks during the summer of 2009 in order to confirm and refine existing mapping done by James Kilburg in 1971 and Mark Severson in 1991. New mapping was done in order to better define textural variation across the Ely's Peak basalt flows, and to document variation in mineral growth with increasing distance from the contact between the Duluth Complex and the wall rocks. Mapping was done on topographic maps at a scale of 1:24,000.

The study area for the Ely's Peak Basalts covered portions of the Esko and West Duluth quadrangles (46.6816°N, 92.2538°W). Mapping focused on the "E" flow identified by Kilburg (1972) because this flow contained the best and most distinct exposure from the contact. Evidence of contact metamorphism was noted such as the presence of hornfels texture, and flow tops containing amygdules filled with possible metamorphic minerals. Field work addressed whether the contact zone between the Ely's Peak basalts and the Duluth Complex is sharp or gradational, and whether mixing has occurred between the two formations.

Field mapping of the Thomson Formation was very limited due to poor outcrop. Outcrop of the Thompson Formation was found along Midway Road west of Duluth in the Esko quadrangle (46.7898°N, 92.1010°W). The contact between the Thomson Formation and the Duluth Complex is not exposed along Midway Road. The closest distance between an outcrop of Thomson Formation and an outcrop of Duluth Complex

is approximately 500 m. Although preexisting deformation from the Penokean Orogeny is evident, some primary depositional structures are preserved, including gradation of sandy beds to slaty beds and the presence of large calc-silicate inclusions, which may be altered concretions. "Spotted slate" texture, an indication of contact metamorphism, was also observed an estimated 200 m away from the contact and helps to determine the scale of the contact aureole.

Mapping of the Virginia Formation was also completed in the summer of 2009. Like the Thompson Formation, mapping was limited to a few sparse outcrops and centered around Linwood Lake on portions of the Harris Lake quadrangle (45.3527°N, 92.1238°W). Pre-existing deformation due to the Penokean Orogeny can be readily observed throughout the Virginia Formation; however Severson (1995) also described deformation he ascribed to intrusion of the Duluth Complex at outcrops near Linwood Lake. These outcrops were revisited, and textural and mineral variation was defined, including the presence of cordierite, a mineral commonly found in contact metamorphic aureoles.

4.2 Drill Core

Drill core of the Animikie Group was studied and sampled from the Minnesota Department of Natural Resources repository in Hibbing. Seven holes were selected from areas just north of Duluth to Virginia along the contact. Holes were selected if they crossed the contact between the Duluth Complex and the Animikie Group. Drill holes were either vertical or angled, but all crossed the contact at some point.

Holes FHL-1 and FHL-2 near Fish Lake Reservoir in Minnesota (46.9566, -92.2785) were logged, sampled, and used to construct a lithologic section of the Thomson Formation adjacent to the contact. These two cores were the longest cores sampled, and show deformed and disrupted bedding in some sections. Textural and mineralogical evidence of contact metamorphism and regional metamorphism were noted. Both outcrop and drill core samples were used to define textural and mineralogical variations.

Cordierite was observed in core from the Virginia Formation (Severson, 1995), so new core logging was done to define textural and mineral variation and enhance our understanding from outcrop exposure. Holes CN-3, CN-6, CN-10, and CN-11 in the Water Hen area of Minnesota (47.2549°N, 92.0364°W), and hole A-1 from the Section 22 drilling area near Hoyt Lakes (47.5551°N, 92.1179°W) were also logged and sampled. These holes were shorter than the Thomson Formation core and did not show as much textural variation, but they still contained mineralogical evidence of metamorphism.

4.3 Sample Collection

Hand samples were collected from outcrops mapped in each unit. These hand samples were used to make thin sections for petrographic study, and polished probe sections. Thin sections were also made from drill core samples of the Thomson and Virginia formations. Thin sections, notes, and maps from the Ely's Peak basalts and the Thompson and Virginia formations obtained from previous workers (Kilberg, Green, Dahlberg) were studied to obtain more detail about the textural variation and mineral growth that occur in those units.

4.4 Thermal Modeling

Conductive thermal modeling was used to evaluate the thermal gradient within the wall rocks after intrusion of the Duluth Complex. Thermal modeling was conducted using a simple set of algorithms in Microsoft Excel™. Physical conditions at the contact and the thickness of the thermal aureole were also estimated using modeling. Model parameters included the volume of the magma, which intruded the country rocks in multiple pulses. The geometry and surface area of the contact, thermal conductivities of igneous and wall rock units, the temperature of the wall rocks prior to intrusion, and the emplacement temperature of the Duluth Complex, which was derived from igneous phase relationships and thermodynamic modeling, were also introduced into this model. Modeling was developed to determine how long the thermal aureole would take to expand into the wall rocks and over what distance a temperature greater than 400° C occurred. The completed model will be compared with sample data to develop a more comprehensive spatial picture of contact metamorphism.

4.5 Optical Petrography

Seventy-seven thin sections were studied using petrographic microscopes. Petrographic methods determined the main mineral assemblages and textures present in each rock unit. In the Animikie Group, relict sedimentary minerals were identified, as well as regional metamorphic minerals that grew during the Penokean Orogeny. For the Ely's Peak basalts, relict igneous minerals were identified, as well as minerals associated with regional burial metamorphism. In both rock types, contact metamorphic mineral

assemblages and textures were identified. The equilibrium contact metamorphic mineral assemblages were the primary focus and distinguished from primary igneous and/or sedimentary minerals and minerals formed during earlier regional metamorphism. Textural growth relationships were observed to see which were related to thermal contact effects. Textures were documented to determine whether any older pre-contact metamorphism minerals still exist or if they have been replaced.

4.6 Mineral Analysis and Chemistry

The JEOL JSM-6490LV scanning electron microscope (SEM) at the University of Minnesota-Duluth was used to conduct an elemental analysis of 22 polished thin sections, including samples from each rock unit. The SEM is a key tool in this research because imaging and chemical analysis of fine-grained phases leads to better identification of the minerals present due to the effects of contact metamorphism. Data collected on the SEM were organized and interpreted using Oxford Instruments INCA™ software

Using a combination of secondary electron imaging (SEI) and backscattered electron imaging (BSE), minerals were identified and determined to be either relict sedimentary, regional metamorphic, or contact metamorphic in origin. Textural and compositional variations throughout individual grains were also noted, which can provide evidence of metamorphism or fluid flow.

The composition of each mineral was identified using the Oxford Instruments Energy 250 energy-dispersive spectrometer (EDS) system. Mineral composition variation that could be related to conditions relative to distance from the contact zone was

noted. Mineral compositions are also useful in determining pressure-temperature conditions. Both standardless and standardized point analysis methods were used to determine mineral compositions. Standardless point analysis uses an internal reference energy spectrum to determine the element proportions in a sample. However, it cannot account for matrix effects, so this type of analysis is best limited to anhydrous minerals only. In samples where standardless analysis was done for anhydrous minerals, cations were normalized to 100% based on the number of oxygens in the mineral's chemical composition. Standardized point analysis uses a set of reference materials of known composition to define the x-ray energy peaks prior to analysis of unknowns. Standardized analysis was done for hydrous minerals using Smithsonian Institution standards and an assigned number of oxygens in the mineral compositions.

Mineral lattice structures were determined using the HKL NordlysII electron backscatter diffraction (EBSD) system. The system collects patterns due to interference of an electron beam with the internal crystallographic structure of a mineral, referred to as Kikuchi bands. The resulting electron backscatter pattern is then compared to a set of reference diffraction patterns to determine a crystallographic structure. Using this information and the chemical composition of the mineral determined by EDS, it is possible to identify a phase based on its chemical composition and crystal structure. Unfortunately, due to poor polish on the probe sections, few minerals yielded Kikuchi band patterns that could be used for accurate phase identification. More analysis needs to be done to determine mineral structure.

5. FIELD OBSERVATIONS

5.1. Section 22

Section 22 is the northernmost site in the field area. Six holes were drilled in this area, but for this study only one was sampled that was drilled obliquely in the Duluth Complex and crosses the contact into the Virginia Formation (Figure 5.1). The core obtained is A-1, and the area of interest in the core occurs between 420' and 563' (Figure 5.2.). From 420' to 479' the core is massive and has no preserved bedding. The rock is gray, fine-grained and cordierite-rich. At 479' there is a granophyric bleb containing pegmatitic mica. Evidence of metamorphism such as the presence of cordierite ceases at 516', and the core is uniformly very fine-grained until the end of the hole (563').

5.2 Water Hen Area

Water Hen is a drilling site located south of the Section 22 area that also contains drill holes that start in the Duluth Complex and cross into the Virginia Formation (Figure 5.3). Four cores were sampled from this site. Cores CN-3 (Figure 5.4) and CN-6 (Figure 5.5) cross the contact at an angle, while cores CN-10 (Figure 5.6) and CN-11 (Figure 5.7) are vertical.

Core CN-3 was studied from 307' to 461'. Between 307' and 320' the core penetrated igneous rocks of Duluth Complex, which consists of a mixture of a norite and a pyroxenite. Between 320' and 383' the core is fairly uniform and consists of light grey

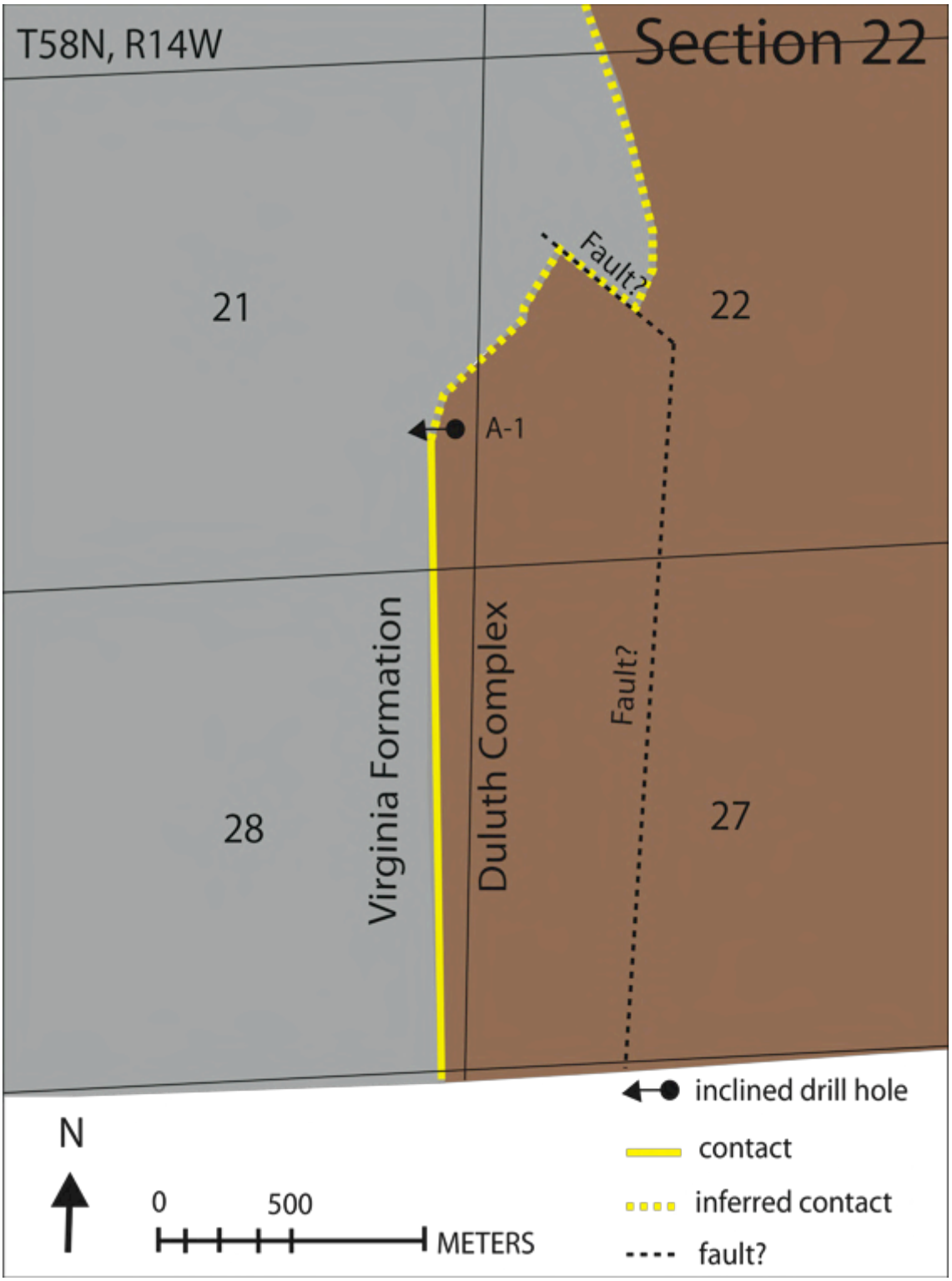

Figure 5.1. Geologic map of the Section 22 area (47.5551, -92.1179), modified from Severson (1995), showing the location of drill hole A-1.

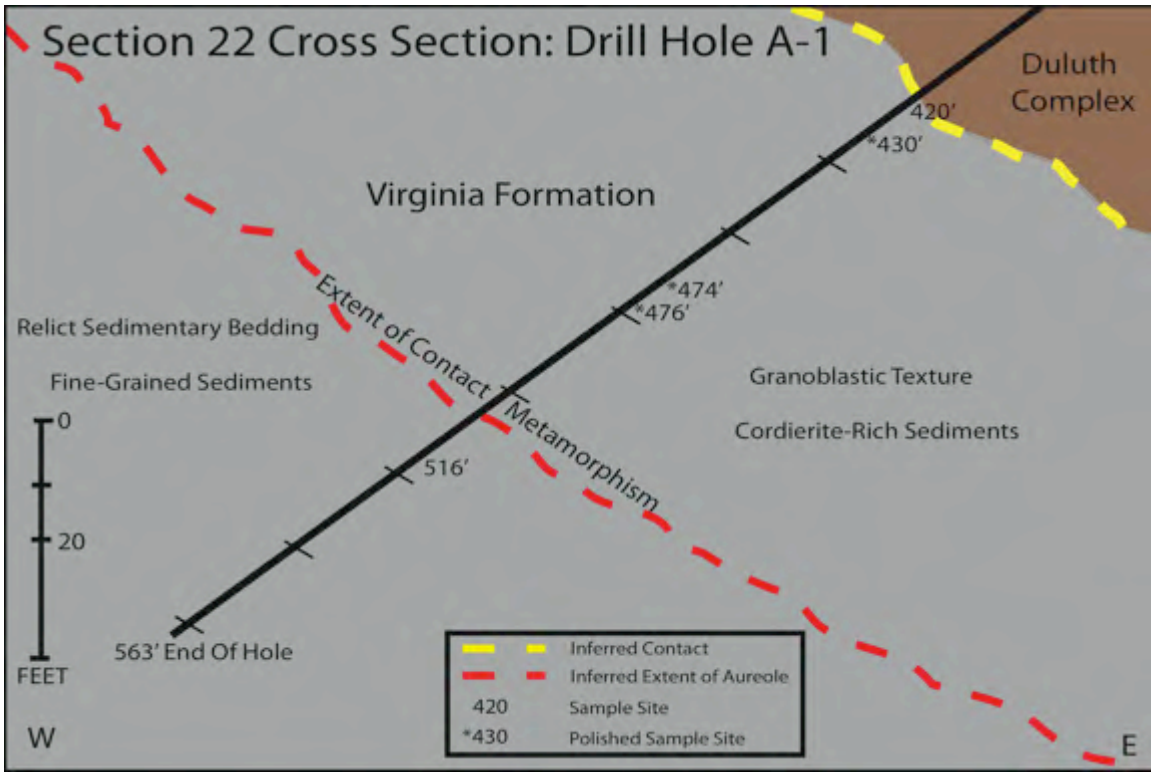

Figure 5.2. Cross section through drill hole A-1. The angle of the drill hole is schematic. The geologic contact and the extent of contact metamorphism are inferred based on hand sample and thin section analysis of drill hole A-1. Above the inferred extent of contact metamorphism, samples exhibit a granoblastic texture and are cordierite-rich. Below the boundary relict sedimentary bedding is visible. The extent of the contact metamorphic aureole could occur anywhere between 476' and 516' due to the lack of data between samples.

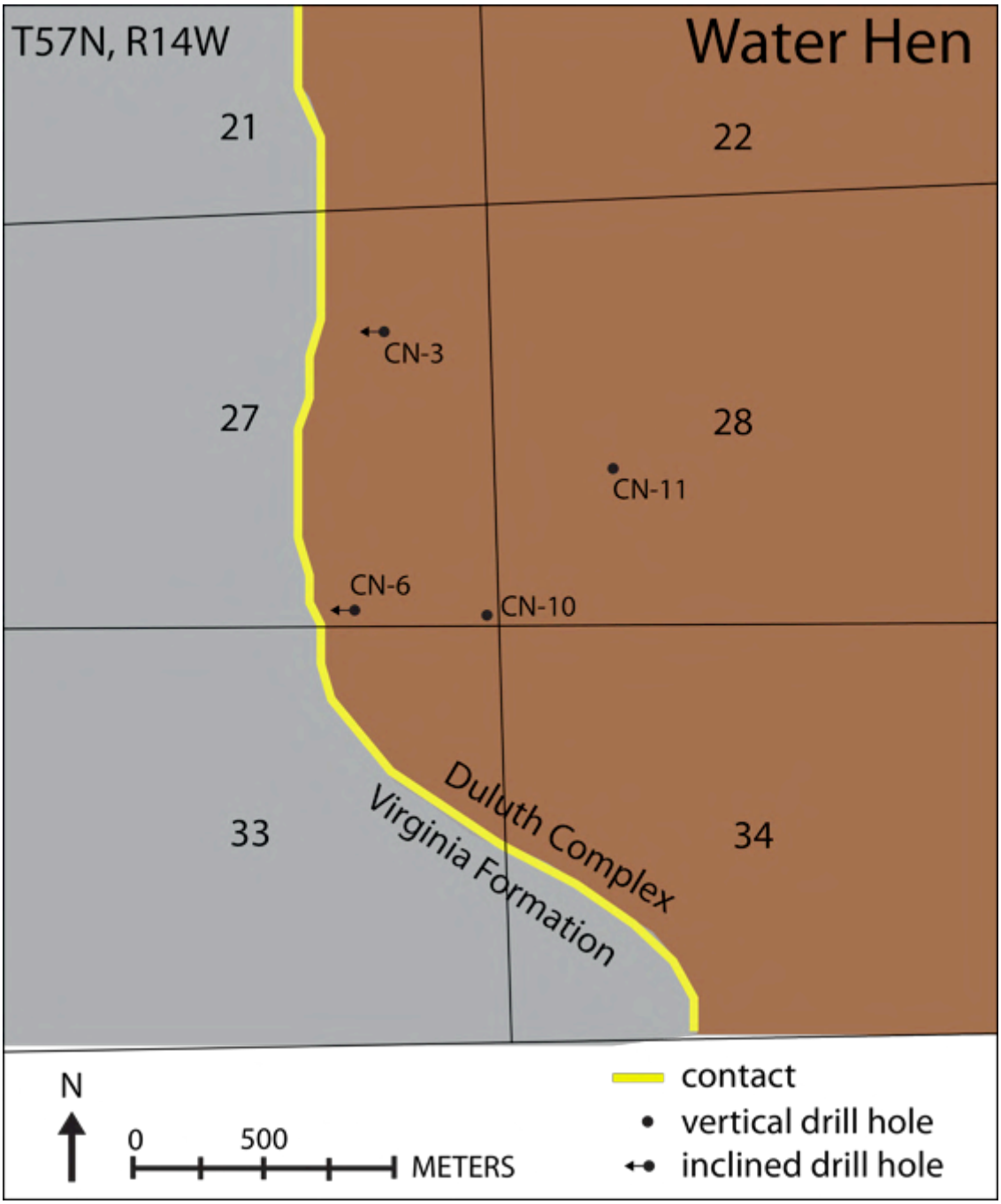

Figure 5.3. Geologic map of the Water Hen area (47.2549°N, 92.0364°W), modified from Severson (1995), showing the location of drill holes CN-3, CN-6, CN-10, and CN-11.

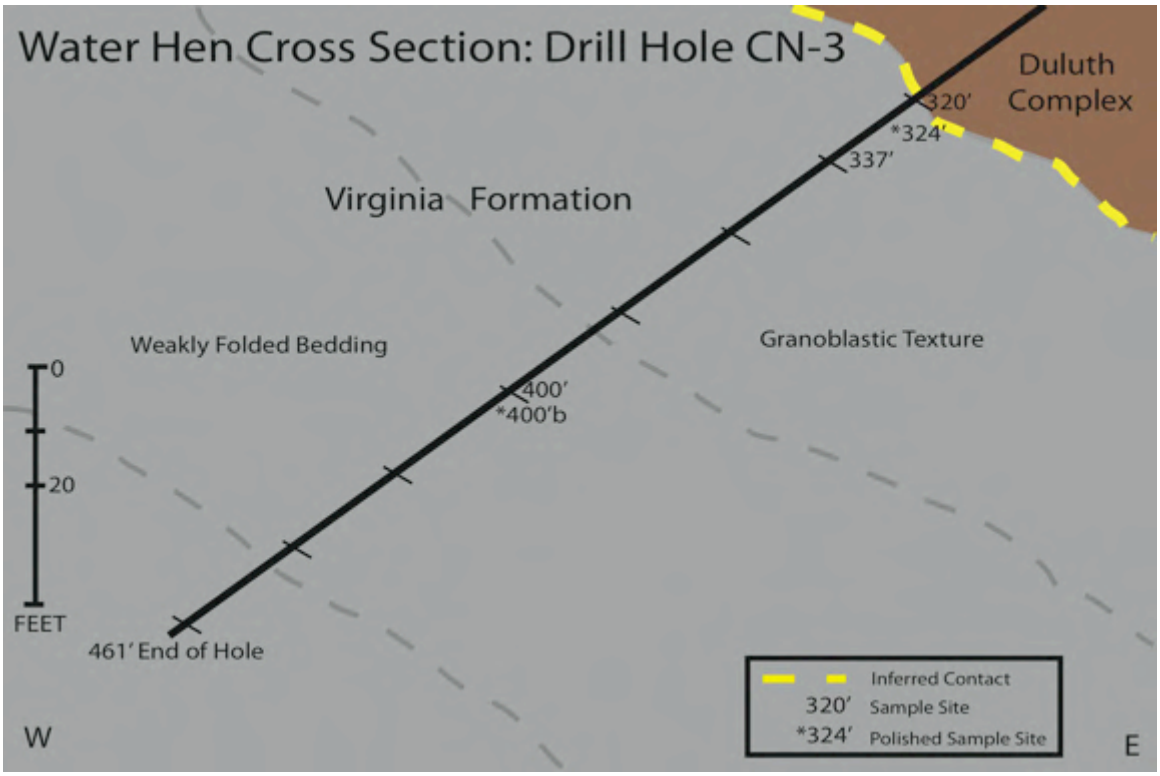

Figure 5.4. Cross-section through drill hole CN-3. The angle of the drill hole is schematic and the contact is inferred based on data observed in hand sample and thin section. Gray lines delineate zones that have been determined from metamorphic changes found in thin section. From the contact to 383' the rock exhibits a granoblastic texture, and between 383' and 445' weakly folded beds are visible.

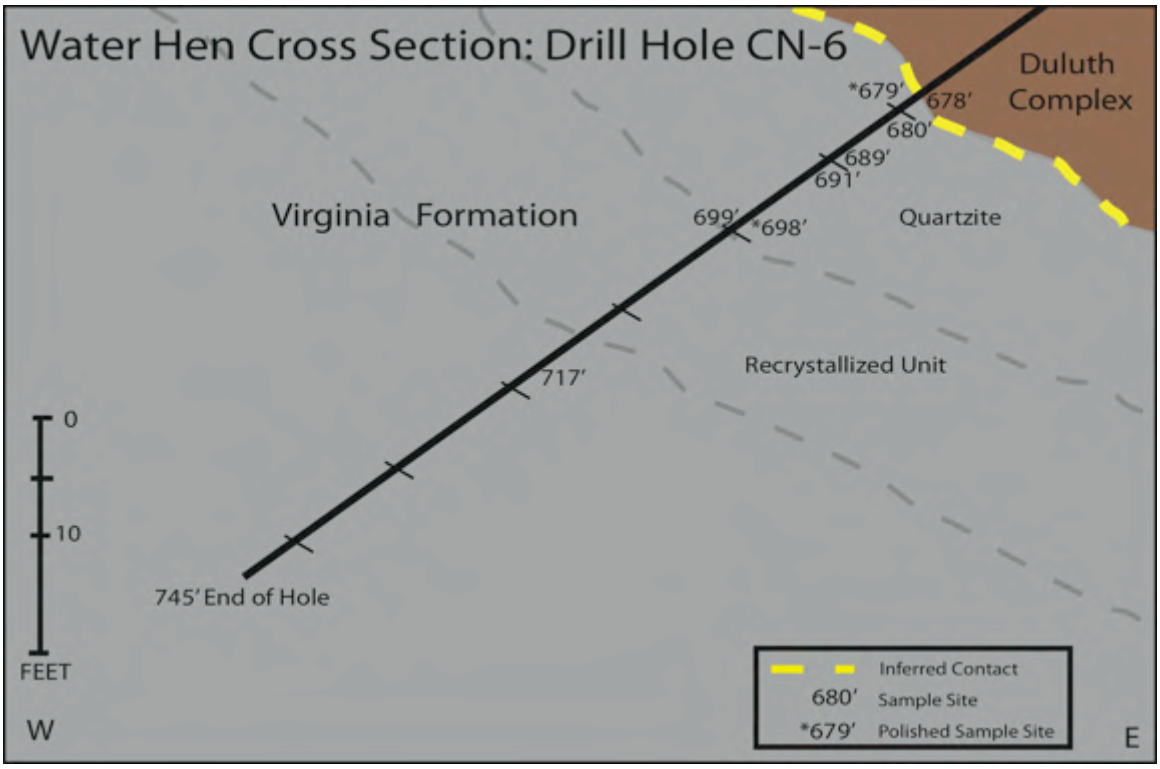

Figure 5.5. Cross-section through drill hole CN-6. The angle of the drill hole is schematic and the contact is inferred. Gray lines divide areas that show different metamorphic textures. From the contact to 699' the rock is a quartzite. Below 699' to 712' it is a recrystallized unit.

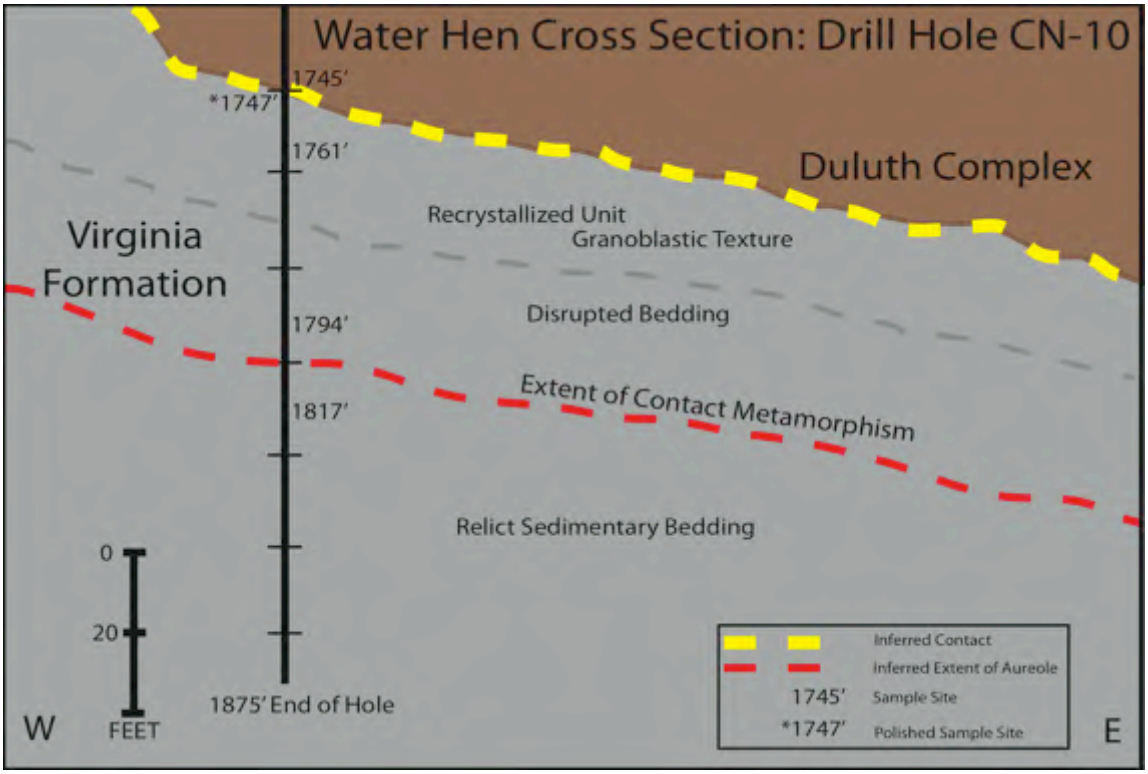

Figure 5.6. Cross-section through drill hole CN-10. The contact is inferred and the extent of contact metamorphism is based on observations made in both hand sample and thin section. The extent of the contact metamorphic aureole could occur anywhere from 1794' to 1817' due to the lack of data in between samples. From the contact to 1774' the rock is the recrystallized unit and exhibits a granoblastic texture. From 1774' to 1806' the rock contains disrupted bedding, and below the extent of contact metamorphism the rock exhibits relict sedimentary bedding.

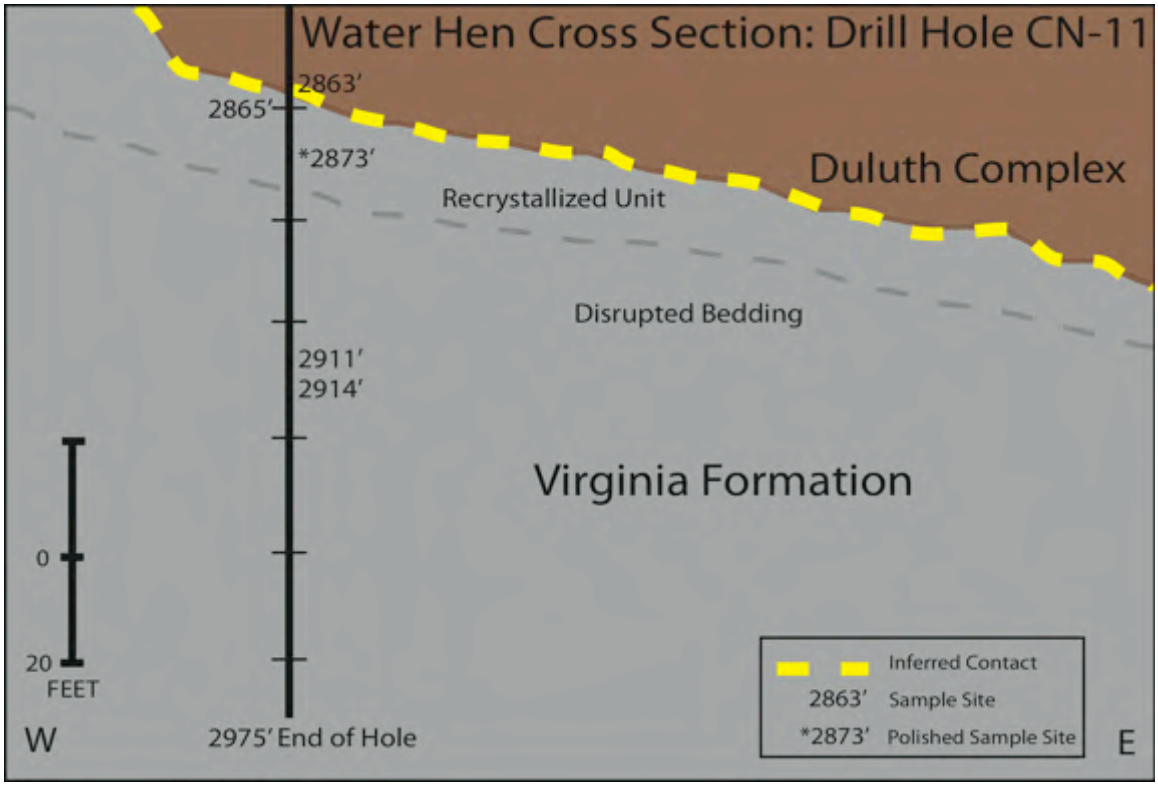

Figure 5.7. Cross-section through drill hole CN-11. The contact is inferred. From the contact to 2876' the rock consists of the recrystallized unit. Below that, disrupted bedding is observed.

metagreywacke with fine-grained patches nestled inside coarser-grained zones. From 383’ to 445’ bedding is visible with weakly folded beds. Metamorphic pyroxene also becomes more abundant leading to a general darkening of the core color. The core continues to be uniform from 445’ to the end of the hole at 461’.

Core CN-6 was studied from 678’ to 745’. Between 678’ and 689’ it is quartz-rich and is identified as a quartzite. Grains are less than 1 mm. From 689’ to 694’ potassium feldspar is present. From 694’ to 698’ the core consists of pure quartzite again, and at 699’ it contains a small amount of cordierite. Between 699’ and 712’ it is made up of the recrystallized unit of the Virginia Formation. The recrystallized unit is a high-grade metamorphic argillite, and is classified as a diatexite (Sawyer, 1999). It is identified by decussate randomly oriented biotite flakes up to 1.5 mm, and partial melt making up 20-30% of the rock. Slight foliation may indicate a remnant texture of regional metamorphism. Large biotite grains are prevalent through the end of the core at 745’.

Core CN-10 was studied from 1745’ to 1875’. Between 1745’ and 1774’ the core contains recrystallized rocks of the Virginia Formation, evident as medium-coarse-grained biotite-rich metasediments with possible disrupted bedding. From 1774’ to 1806’ it shows stronger disrupted bedding, with darker elliptical pods typically made up of finer-grained rock that may represent metamorphosed concretions. The pods are 2-4 cm and have no uniform direction. Between 1806’ to 1845’ the core shows preserved relict sedimentary bedding within metagreywacke. Evidence of contact metamorphism stops at

1806', and the rock continues to have a continuous texture until the end of the hole at 1875'.

Core CN-11 was studied from 2863' to 2975'. Between 2863' to 2876' it is comprised of the recrystallized unit seen in the other cores, and is very coarse-grained with large flecks of biotite approximately 1mm in width. From 2876' to 2914' it exhibits disrupted bedding, likely due to regional metamorphism. The bedding dips approximately 50° relative to the hole, indicating a moderate eastward dip, and the rock is light grey with large 1mm flecks of biotite. From 2914' to the end of the hole at 2975' the rock alternates between the disrupted bedding unit and a white chert.

5.3 Linwood Lake

Linwood Lake is adjacent to the contact between the Duluth Complex and the Virginia Formation (Figure 5.8). Severson noted three outcrops in the area, but during field mapping only one outcrop was located due to new housing developments and heavy vegetation. In hand sample, the Virginia Formation at Linwood Lake is light grey and very fine-grained. Quartz, calcite, plagioclase, and muscovite were identified. Due to very poor exposure, no bedding or other features were visible.

5.4 Fish Lake

South of Linwood Lake is the Fish Lake site. This site straddles the contact between the Duluth Complex and the Thomson Formation, and holes were drilled on the shore of Island Lake near Fredenberg Township (Figure 5.9). Two cores were sampled

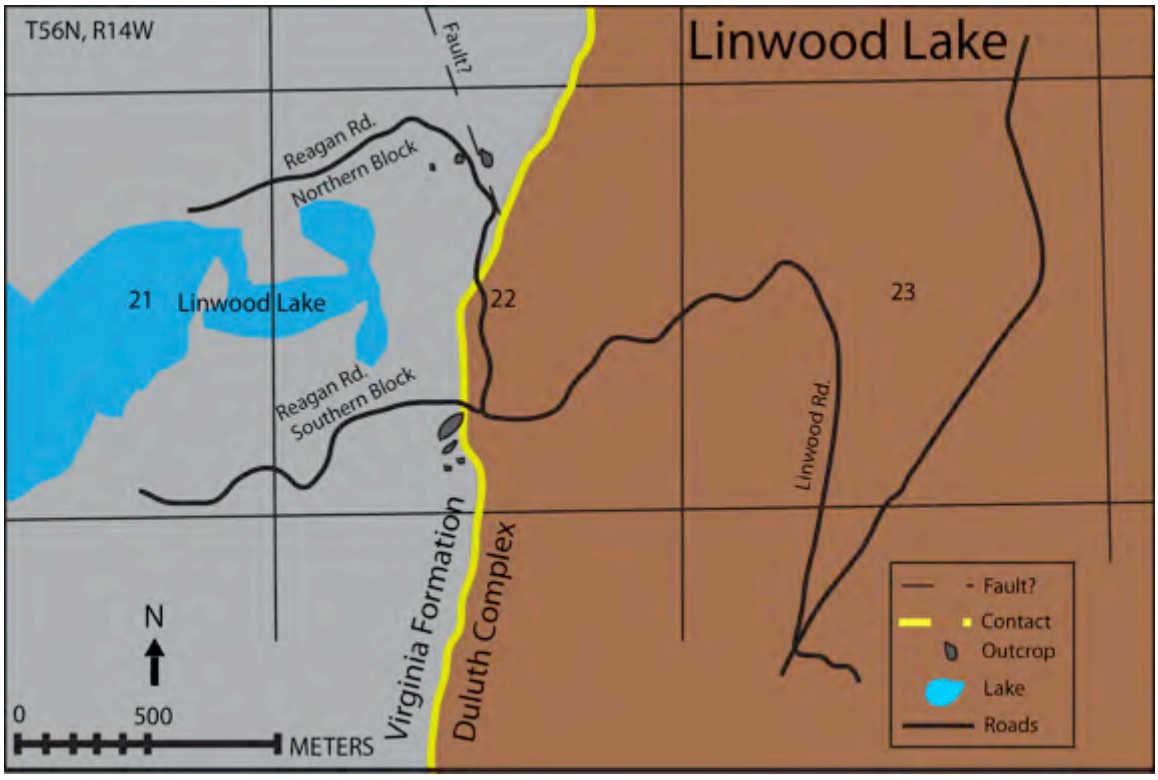

Figure 5.8. Geologic map of the Linwood Lake area (45.3527°N, 92.1238°W), modified from Severson (1995), showing the location of outcrop.

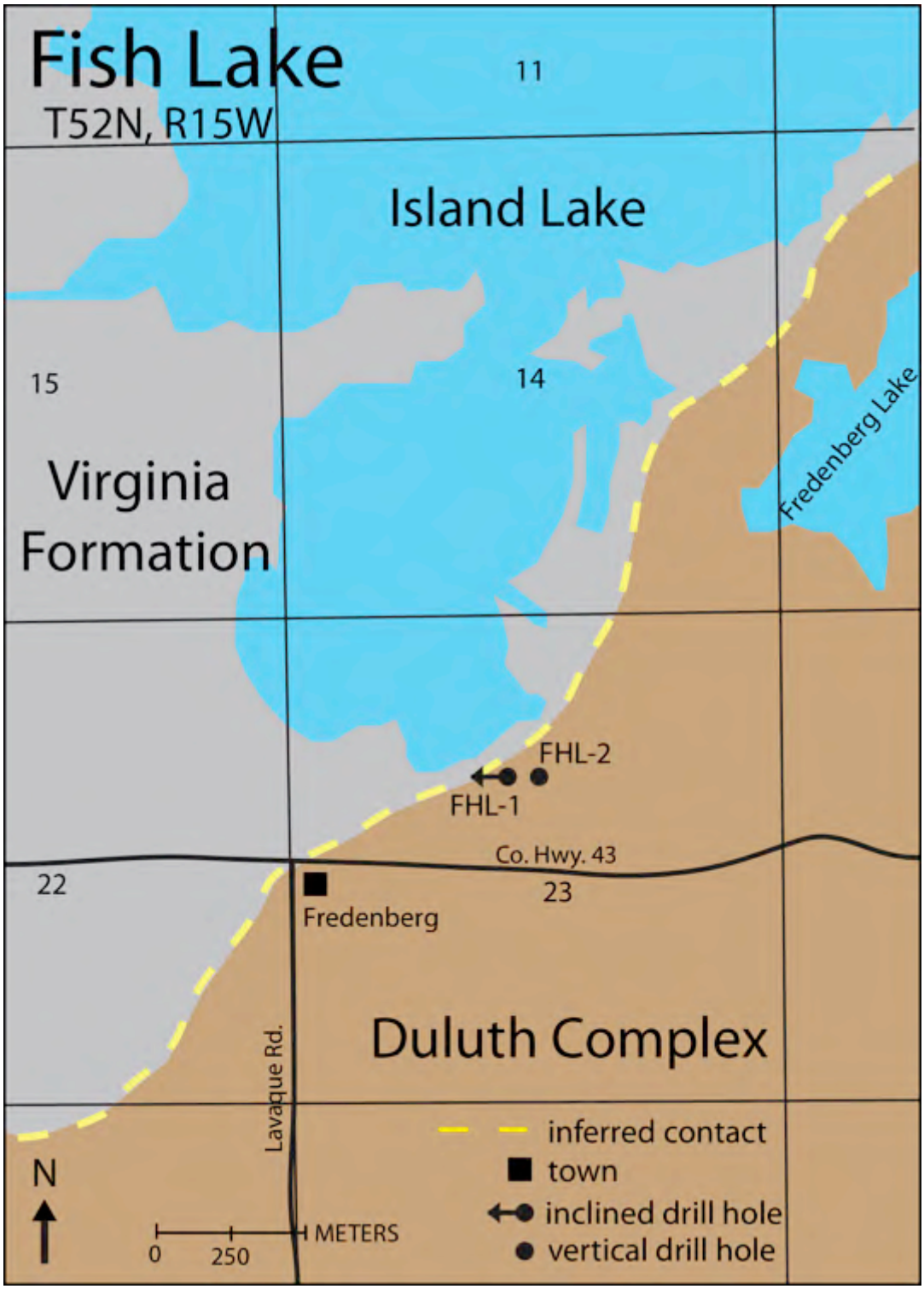

Figure 5.9. Geologic map of the Fish Lake drilling site showing the approximate locations of drill holes FHL-1 and FHL-2.

from the Fish Lake field site, FHL-1 and FHL-2 (Figure 5.10). Core FHL-1 was studied from 490' to 1003' and was the longest hole studied. The contact between the Duluth Complex and the Thomson Formation occurs at 492' and the area surrounding it is very dark grey, coarse-grained and sulfide rich from 492' to 553'. Between 553' to 570' is a chaotic mix of rock that Severson (1995) described as a large partially-melted argillite with granophyre pods or lenses. The granophyre is light pink to white in color and is medium- to coarse-grained with intergrowths of quartz and feldspar. The pods are small, ranging from 4 cm thick to 24 cm thick, and do not have mafic selvedges, therefore Severson and Peterson's hypothesis of partial melting seems plausible. From 570' to 605' the core consists of disrupted bedding with finer-grained lenses previously described in the Virginia Formation. The pod-shaped lenses range in size from 2-4 cm and have no dominant alignment direction. From 605' to 621' these lenses increase in size from 1-8 cm and the rock becomes more coarse-grained overall. From 621' to 669' the core alternates between sulfide-rich well-bedded layers dipping 45° and thick-bedded white cherts. From 669'-705' the core exhibits disrupted bedding with fine-grained lenses again, but this time bedding is more evident and the lenses are mostly sub-horizontal. From 705' to 780' the core becomes finer-grained and the bedding shallows out to approximately 15-40°. Evidence of metamorphism ceases at approximately 780' with the appearance of well-bedded argillite. Wispy veins and granophyre pods break up the bedding until from 780' to the end of the hole at 1003' the core is well-bedded and bedding continues to shallow to 10-15°.

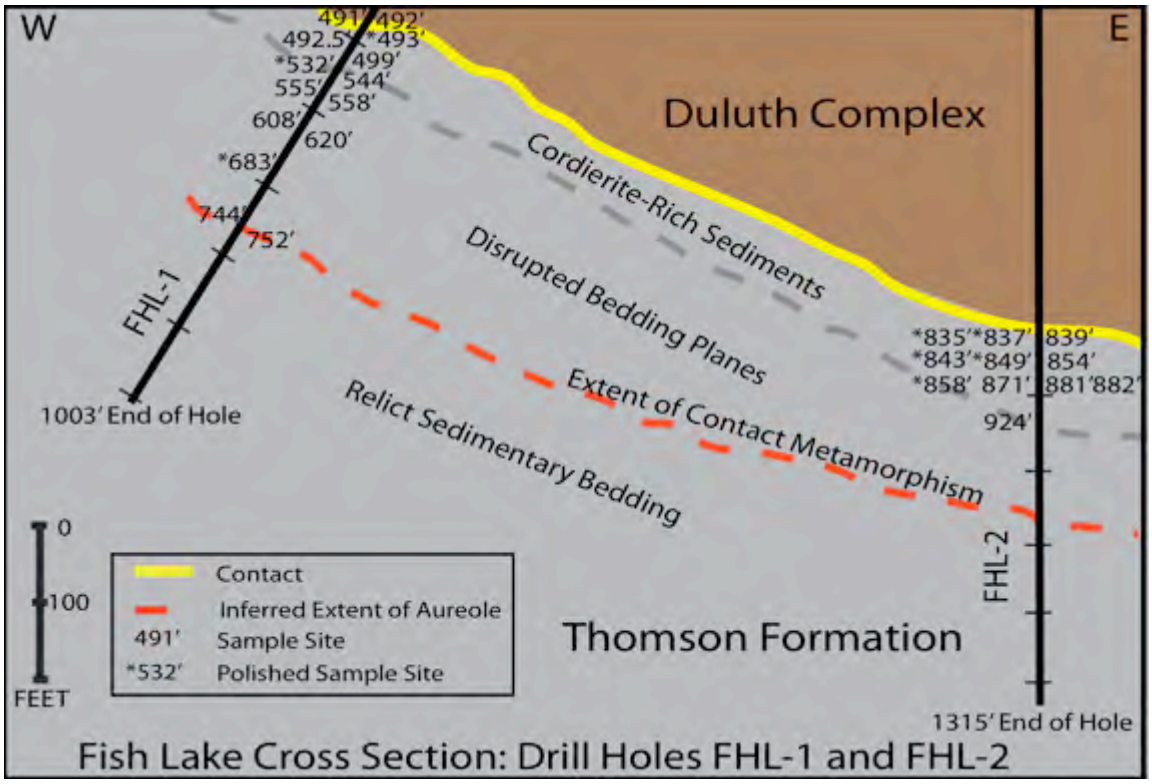

Figure 5.10. Cross-section through holes FHL-1 and FHL-2 modified from Severson (1995). The contact between rock units is known from correlating the drill holes. The extent of contact metamorphism is inferred from data observed in hand sample and in thin section. The extent of the contact aureole could be from 744' to 752' in drill hole FHL-1 due to evidence of relict sedimentary bedding. It is harder to determine the extent in hole FHL-2 because of a lack of evidence, but it is inferred to be approximately 1198'.

Core FHL-2 was studied from 829’ to 1315’. The contact between the Duluth Complex and the Thomson Formation occurs at 837’, and from 837’ to 855’ the core is very coarse-grained and sulfide-rich. From 855’ to 875’ the core becomes very fine-grained moving away from the contact, although it is still sulfide-rich. Between 875’ and 921’ the core becomes coarse-grained again and the amount of sulfides increases, then from 921’ to 931’ the core becomes fine-grained once more. From 931’ to 941’ it exhibits convoluted bedding with possible lenses but hydrothermal alteration has overprinted everything. From 941’ to 968’ disrupted bedding is present with lenses that are slightly more elongated than those found in FHL-1. Lenses range from 1-5 cm and bedding dips 30° on average. Between 976’ and 1016’ it consists of light grey, undisturbed, very fine-grained horizontally-bedded metagraywacke. From 1016’ to 1024’ the core is made up of folds where the hinge of the fold follows the length of the core. At 1024’ the rock returns to undisturbed bedding. The core alternates between undisturbed bedding and folds from 1024’ to 1059’. From 1059’ to 1080’ the core becomes coarser-grained and mica-rich. Some sigmoidal beds are present but overall bedding is dipping 20-45° with some localized folds. From 1080’ to 1180’ the bedding ranges from convoluted to disrupted, with localized folds. The rock is still mica-rich and coarse-grained. Between 1180’ to 1198’ is a disrupted zone with folded beds, steep bedding approximately 75°, and possible lenses are aligned with the bedding. From 1198’ to the end of the hole at 1315’ the core exhibits massive sub-horizontal bedding that is very uniform and biotite-rich. Severson (1995) describes localized pegmatitic

veins, some partial melt zones, and localized disrupted bedding, but overall the core exhibits horizontal bedding.

5.5 Midway Road

The Midway Road field site is a series of outcrops that border the contact between the Thomson Formation and the Ely's Peak basalts, which are being pinched out to the north by the Duluth Complex (Figure 5.11). The Thomson Formation crops out as a dark grey fine-grained metagraywacke containing quartz, plagioclase, potassium feldspar, muscovite, and biotite. Trace minerals include pyrite, apatite, and detrital zircons. This rock has beds trending 090 75 and grading from slaty to sandy in areas north to south along the outcrop (Figure 5.12). In some of the sandier sections convoluted bedding is preserved. Large calcite concretions or nodules are present near the contact and range in size from 2-10 cm (Figure 5.13). The slaty sections of the Thomson Formation are pelitic and contain black 0.25 mm flecks commonly referred to as "spotty slate" which are neoblastic metamorphic grains of cordierite. Sulfides are present throughout the area and are thought to have come from the Duluth Complex (Peterson and Severson, 2002). Veins of quartz cross-cut the Thomson Formation perpendicular to bedding.

5.6. Ely's Peak Area

The Ely's Peak basalts are typically dark green-black coarse-grained basalt containing plagioclase, augite, and olivine pseudomorphs. Although over 20 different flows are known in this area, this study focuses on the "E" flow mapped by Kilburg

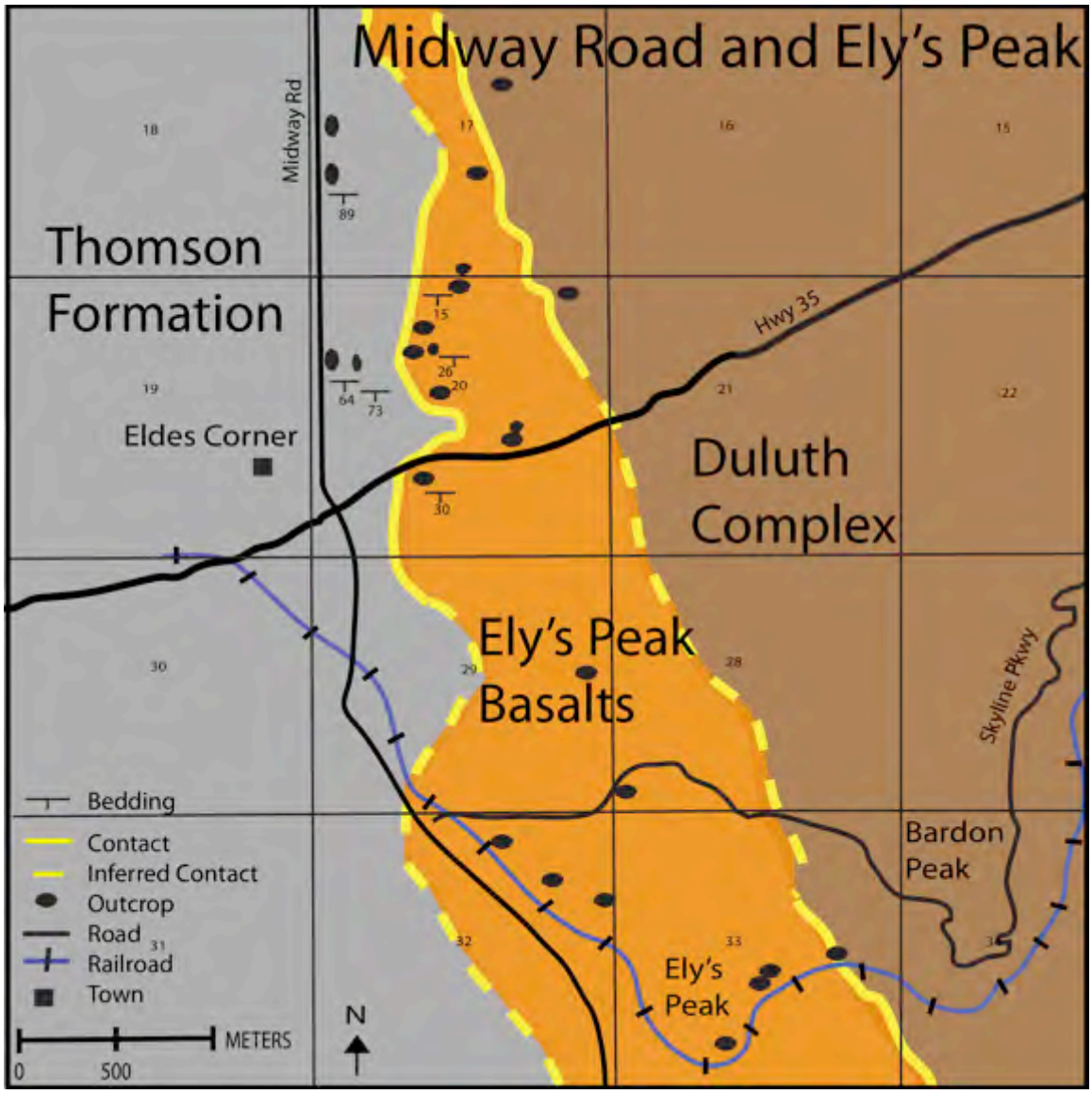

Figure 5.11. Geologic map of the Midway Road field site and Ely's Peak area showing outcrops of the Duluth Complex, the Ely's Peak Basalts, and the Thomson Formation.

Figure 5.12. Outcrop of massive Thomson Formation metagraywackes along Midway Road. Note how poorly exposed the surface is, which is why the majority of the study was conducted on drill core. Hammer for scale.

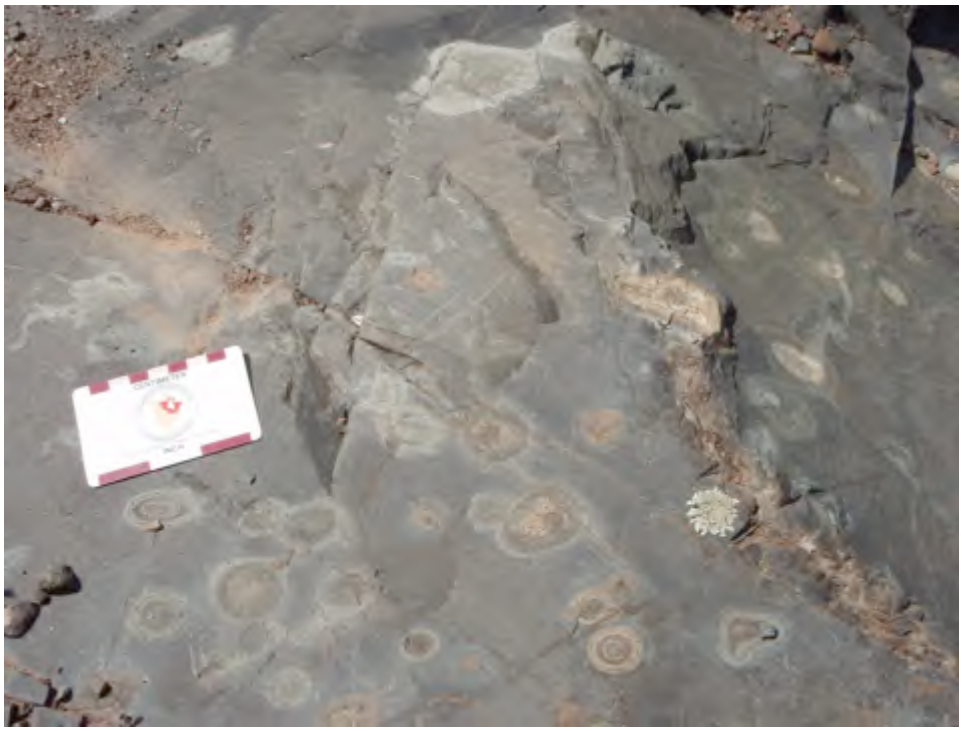

Figure 5.13. Concretions within Thomson Formation metagraywacke. They formed secondary to the original deposition of the sediments, and are possibly associated with diagenetic cementation of the Thomson Formation.

(1972), which crops out along an abandoned railroad bed on Ely's Peak (Figure 5.11). The flows tilt approximately 30° and strike north-south. They are approximately 13 km long and approximately 2.5 km wide. Within 100 m of the contact the basalts become recrystallized to a very dense hornfels. The top of the E flow is filled with amygdules that contain crystalline epidote and concentric rings of plagioclase, amphibole, and clinopyroxene (Kilburg, 1972). The contact is gradational, not discrete, and is associated with small pockets of pegmatites (Figure 5.14). Sulfides are also present in small pockets near the contact, which provide evidence of possible fluid flow.

Figure 5.14. Photograph of the gradational contact between the Ely's Peak Basalts on the left-hand side of the picture and the Duluth Complex on the right. Yellow line represents the contact, hammer for scale.

6. PETROGRAPHIC RELATIONS

6.1 Mineral Assemblages in the Animikie Group

The Animikie Group was subjected to two metamorphic events that overprinted primary detrital minerals of the Thomson and Virginia formations. Minerals associated with the original deposition in the Animikie basin (~2.3 Ga) are considered relict sedimentary minerals. Mineral assemblages associated with the Penokean Orogen (~1.8 Ga) formed during regional metamorphism (M_1), and these in turn were partially replaced during intrusion of the Duluth Complex (~1.1 Ga) within a contact metamorphic aureole (M_2). Mineral abbreviations used here follow those recommended by Kretz (1983) (Appendix A).

6.2 Relict Sedimentary Minerals of the Animikie Group

When the Animikie Group was deposited, it consisted of argillites, siltstones, and graywackes that ranged from sandy, to clay-rich, to calcite-rich (Peterson and Severson, 2002). Main framework minerals associated with original deposition of the Animikie Group are quartz, plagioclase feldspar, potassium feldspar, clays, and muscovite (Figure 6.1). Locally the rocks contain abundant calcite, including calcite concretions in some areas. This suggests the sedimentary protoliths were cemented by silica and/or calcite. It is important to note that sulfides such as pyrite and sphalerite are also thought to be associated with either initial deposition or early diagenesis (Peterson and Severson, 2002), and they are a possible source of the massive sulfide deposits found at the base of

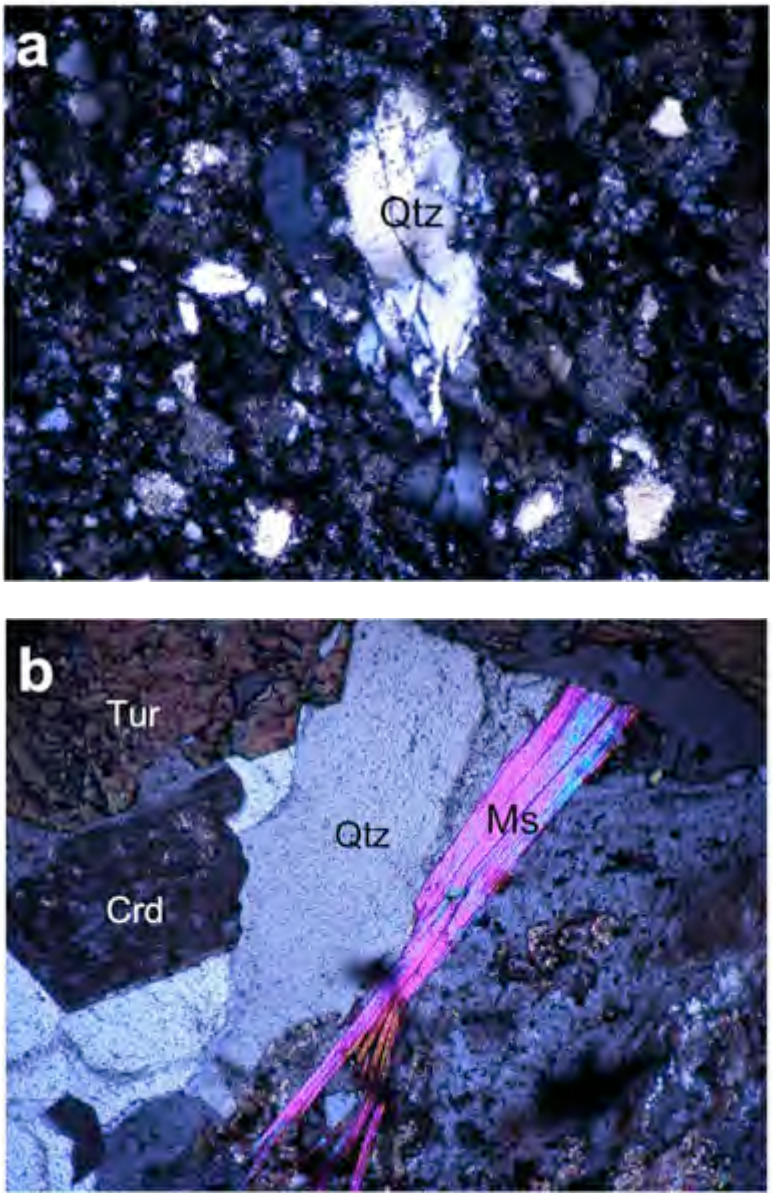

Figure 6.1. (a) Photomicrograph of relict sedimentary quartz (Qtz) grain in sample MR-01-A taken in crossed polarized light (XPL) with a field of view of 2 mm. This mineral was identified as relict sedimentary in origin due to its undulating extinction and broken edges. Both of these observations indicate that the quartz grain underwent deformation, probably due to the Penokean Orogeny, of a relict sedimentary mineral after deposition. (b) Photomicrograph of relict detrital muscovite (Ms) in sample A-1-476 taken in XPL with a field of view of 2 mm. This mineral is interpreted as relict sedimentary because it has been bent and the ends are splitting. Splitting along cleavage planes and the coarse grain size relative to framework grains indicate it is detrital, and the bent shape could have occurred either during deposition, compaction, or Penokean deformation. Together, these features of coarse muscovite indicate it is detrital in origin.

the Duluth Complex. Other trace minerals include titanite, ilmenite, rutile, apatite, and zircon. Relict sedimentary or early metamorphic minerals including biotite, quartz, and pyrite occur as inclusions in poikiloblasts of contact metamorphic minerals (Figure 6.2), and relict sedimentary bedding is preserved in thin section (Figure 6.3).

6.3 Regional Metamorphic Minerals of the Animikie Group (M_1)

After deposition, the Animikie Group was subjected to higher temperatures and pressures during the Penokean Orogeny than during deposition. This condition led to biotite, muscovite, plagioclase feldspar, and quartz growth over a broad area. Regional metamorphic minerals such as biotite are distinguished from relict sedimentary minerals and contact metamorphic minerals on the basis of porphyroblasts having a preferred orientation and a more bent and broken texture than the contact metamorphic porphyroblasts (Figure 6.4). Weakly folded bedding planes identifiable in thin section may also be an indication of regional metamorphism and deformation (Figure 6.5).

6.4 Contact Metamorphic Minerals of the Animikie Group (M_2)

Peak metamorphic mineral assemblages found in the Animikie Group vary significantly depending on position relative to the contact with the Duluth Complex. The highest-grade peak metamorphic minerals found in the Animike Group are cordierite, orthopyroxene, and clinopyroxene. In this section, the peak metamorphic mineral assemblage is described for each field area, along with other associated minerals.

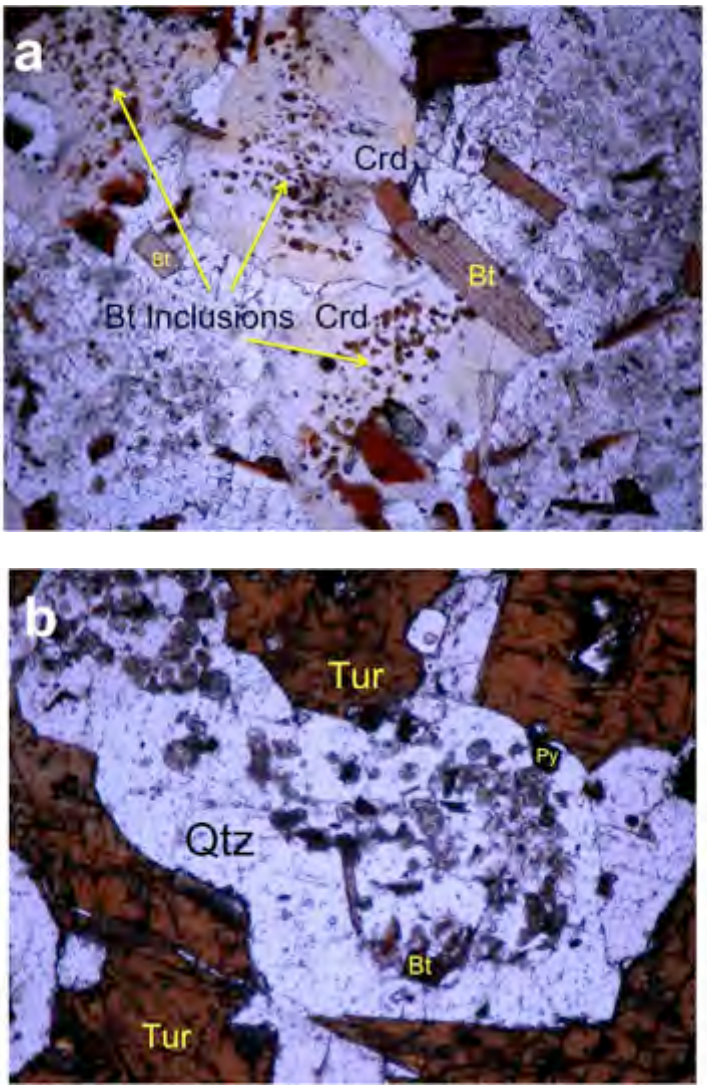

Figure 6.2. (a) Photomicrograph of inclusions of biotite (Bt) inside contact metamorphic cordierite (Crd) in sample A-1-430 taken in XPL with a field of view of 2 mm. Note the rectangular shape of the biotite and their similar orientation relative to the cordierite poikiloblast. The biotite could have grown during regional metamorphism and later been included during cordierite growth; they could also have formed during contact metamorphism as a by-product of cordierite crystallization. They are probably not relict detrital grains because they are fine-grained, polygonal, and have a grain-shape alignment. (b) Photomicrograph of inclusions of relict sedimentary biotite (Bt) and pyrite (Py) inside recrystallized quartz (Qtz) that is included in a large tourmaline (Tur) crystal. The photo was taken from sample A-1-474 in XPL with a field of view of 2 mm. The biotite and pyrite are identified as relict sedimentary because they are identified as inclusions in a quartz grain enclosed by tourmaline, which means they existed before the growth of both quartz and tourmaline crystals.

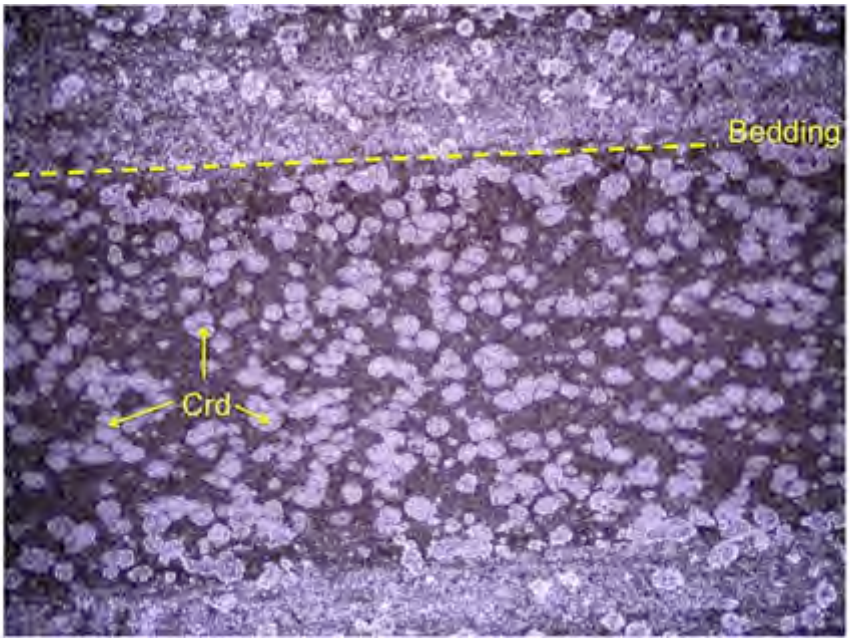

Figure 6.3. Photomicrograph of graded bedding in sample MR-03-B in plane polarized light (PPL) with a field of view of 2 mm. The matrix of the sediment is composed of biotite, muscovite, plagioclase, and quartz. Graded bedding is overprinted by small cordierite (Crd) porphyroblasts that create a "spotty slate" texture.

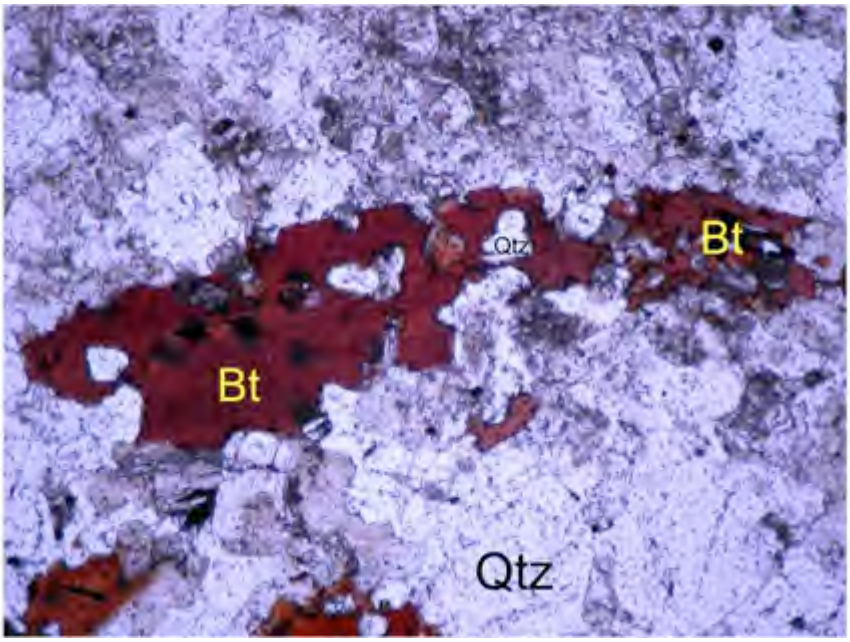

Figure 6.4. Photomicrograph of regional metamorphic biotite (Bt) in sample C-11-2873 in PPL with a field of view of 2 mm. The biotite can be distinguished from relict sedimentary biotite by its poikiloblastic texture and quartz inclusions. It is distinguished from contact metamorphic biotite poikiloblasts by its rough edges and preferred orientation. In this photomicrograph the biotite has slightly bent cleavage, perhaps from deformation during or after the Penokean Orogeny.

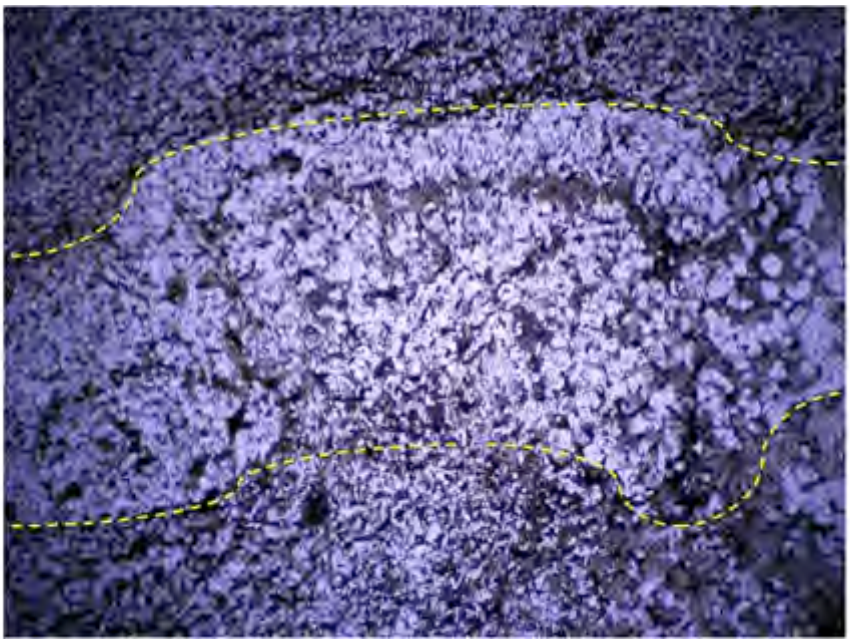

Figure 6.5. Photomicrograph of disrupted bedding in sample F-1-752 in PPL with a field of view of 2 mm. Yellow dotted lines delineate the disrupted bedding, which is thought to have been folded during the Penokean Orogeny; therefore it is associated with regional metamorphism.

Interpretations of the spatial variation in mineral assemblage will be discussed in a later chapter.

The northernmost field site is Section 22 (Figure 5.1), and in this area the peak metamorphic mineral assemblage is cordierite-gedrite-biotite. Cordierite is identified as tabular poikiloblasts approximately 1 mm wide that contain inclusions of relict quartz, and pyrite, and pieces of biotite that have formed as a by-product of cordierite formation (Figure 6.6). In the matrix, new biotite is also identified as large platy 1 mm wide poikiloblasts that typically show radiation damage halos from enclosed zircons. Gedrite, as amorphous growths on biotite and has no uniform shape. Due to its poor optical properties, gedrite was identified as an amphibole optically, and as gedrite due to its chemical composition. At low pressures cordierite, gedrite, and biotite can be stable at temperatures as low as 450°C, so the area experienced only mild contact metamorphic conditions (Deer, et al., 2002). Other minerals associated with contact metamorphism in the area include muscovite, quartz, spinel, and pentlandite that has overgrown pyrite. The contact metamorphic aureole in this area extends approximately 20-28 m and is identified by the presence of mineral porphyroblasts noted above and mortar texture (Figure 6.7).

Farther south, the next field site is Water Hen (Figure 5.3). In this area, the peak metamorphic mineral assemblage is ferrosilite-cordierite-gedrite. Optically ferrosilite and gedrite were only identified as orthopyroxene and amphibole, respectively, and their more detailed identification of their compositions was determined by energy dispersive

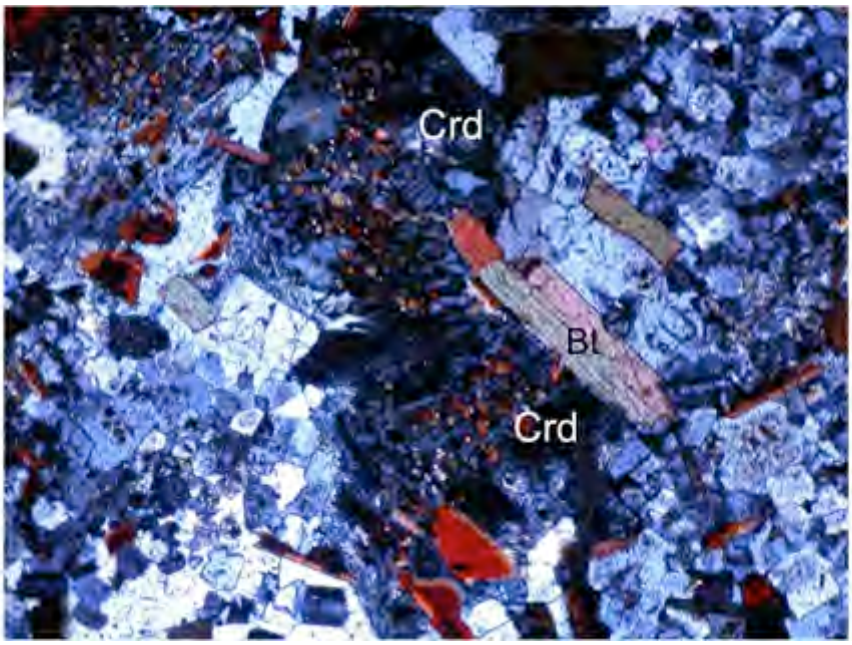

Figure 6.6. Photomicrograph of cordierite (Crd) poikiloblasts in sample A-1-430 taken in XPL with a field of view of 2 mm. The poikiloblasts range from 1-4 mm in width and contain inclusions of biotite (Bt). The similar size and orientation of the biotite inclusions shows that they may be a by-product of a cordierite growth reaction. The fan-like twinning pattern is characteristic of cordierite. Biotite porphyroblasts are also in equilibrium next to the cordierite poikiloblasts.

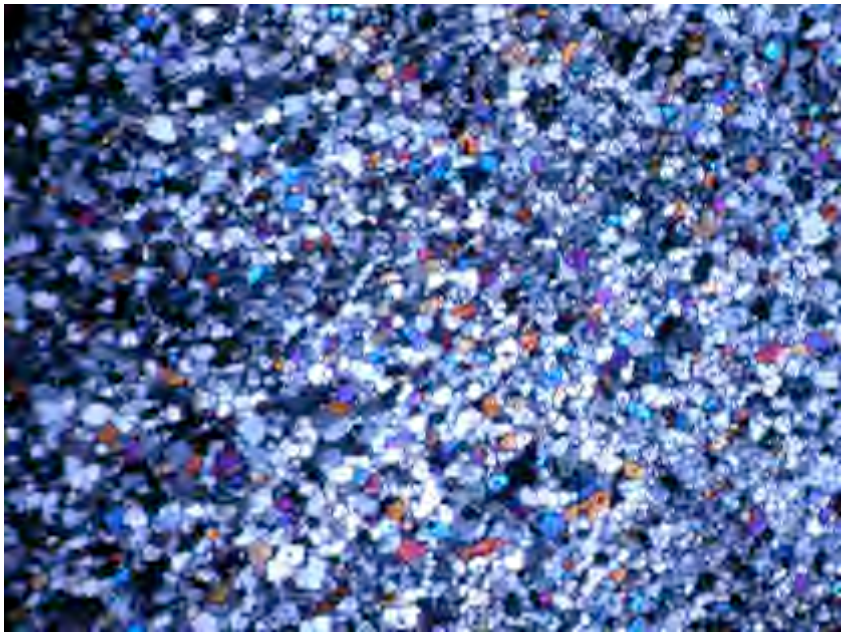

Figure 6.7. Photomicrograph showing an elegant mortar texture commonly found in contact aureoles in sample C-3-324 taken in XPL with a field of view of 2 mm. The minerals making up this texture include quartz, augite, and sulfides.

spectrometry (EDS). For the purpose of distinguishing the different types of orthopyroxenes and clinopyroxenes identified in this study, I will refer to compositional varieties identified by EDS. Analytical results obtained by EDS are discussed in the next chapter.

Ferrosilite is identified as small flecks that are reacting from or with biotite (Figure 6.8). Small fine-grained crystals of ferrosilite are associated with acicular shards of biotite, which together form a rhombohedral shape. They may be reacting with each other, but there is space between minerals that are filled in by background matrix. This suggests an overall reaction in which biotite and gedrite and forming with other phases as a replacement for something else as yet unidentified. Well-formed euhedral porphyroblasts of ferrosilite were never identified in this study. Cordierite is tabular and poikiloblastic, and gedrite is found as amorphous shapes associated with ferrosilite. The assemblage cordierite-ferrosilite-gedrite is stable at temperatures around 700°C (Spear, 1993), so this area was subjected to higher-grade metamorphism than Section 22. Other minerals associated with contact metamorphism in this area include clinopyroxenes such as augite and hedenburgite, and wollastonite, which forms from the reaction of quartz and calcite and is a good indicator of contact metamorphism (Figure 6.9). Rocks in this area also contain biotite, muscovite, alkali feldspar, and quartz, but these phases have recrystallized from pre-existing assemblages. The contact metamorphic aureole at this site extends approximately 70 m, and is identified by porphyroblasts and mortar texture (Figure 6.7).

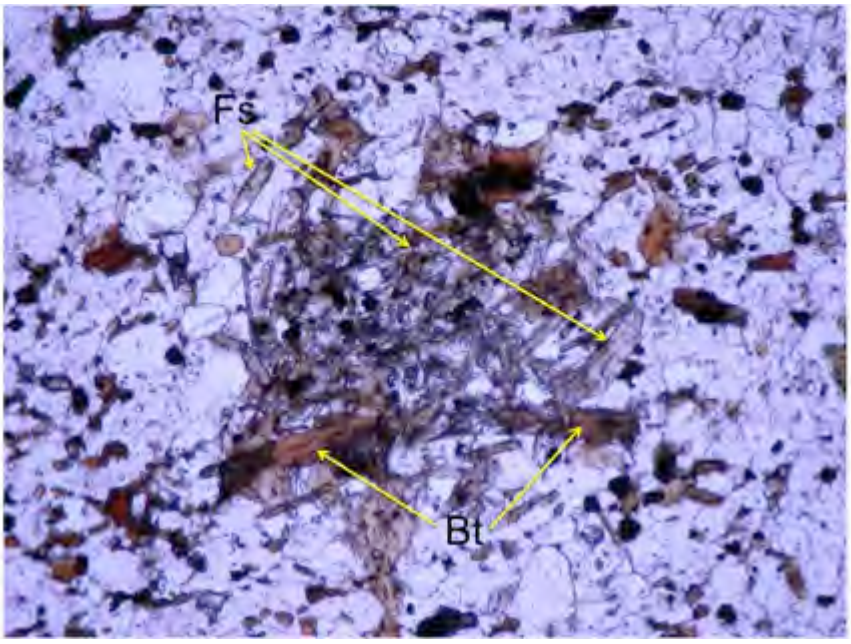

Figure 6.8. Photomicrograph of fine ferrosilite (Fs) crystals associated with biotite (Bt) in sample C-11-2914 taken in PPL with a field of view of 2 mm. It is hard to identify grains of ferrosilite optically, but they were positively identified by their composition. Small grains of ferrosilite and multiple crystals of acicular biotite are associated together in a rhombohedral shape. The biotite and ferrosilite could together be a replacement of an older porphyroblast, the biotite could be replacing an old ferrosilite porphyroblast, or the ferrosilite could be reacting from the biotite. It is unlikely that ferrosilite is reacting to produce biotite because the ferrosilite is not a continuous larger crystal. Likewise biotite reacting to produce ferrosilite seems unlikely, so the first hypothesis seems the most reasonable.

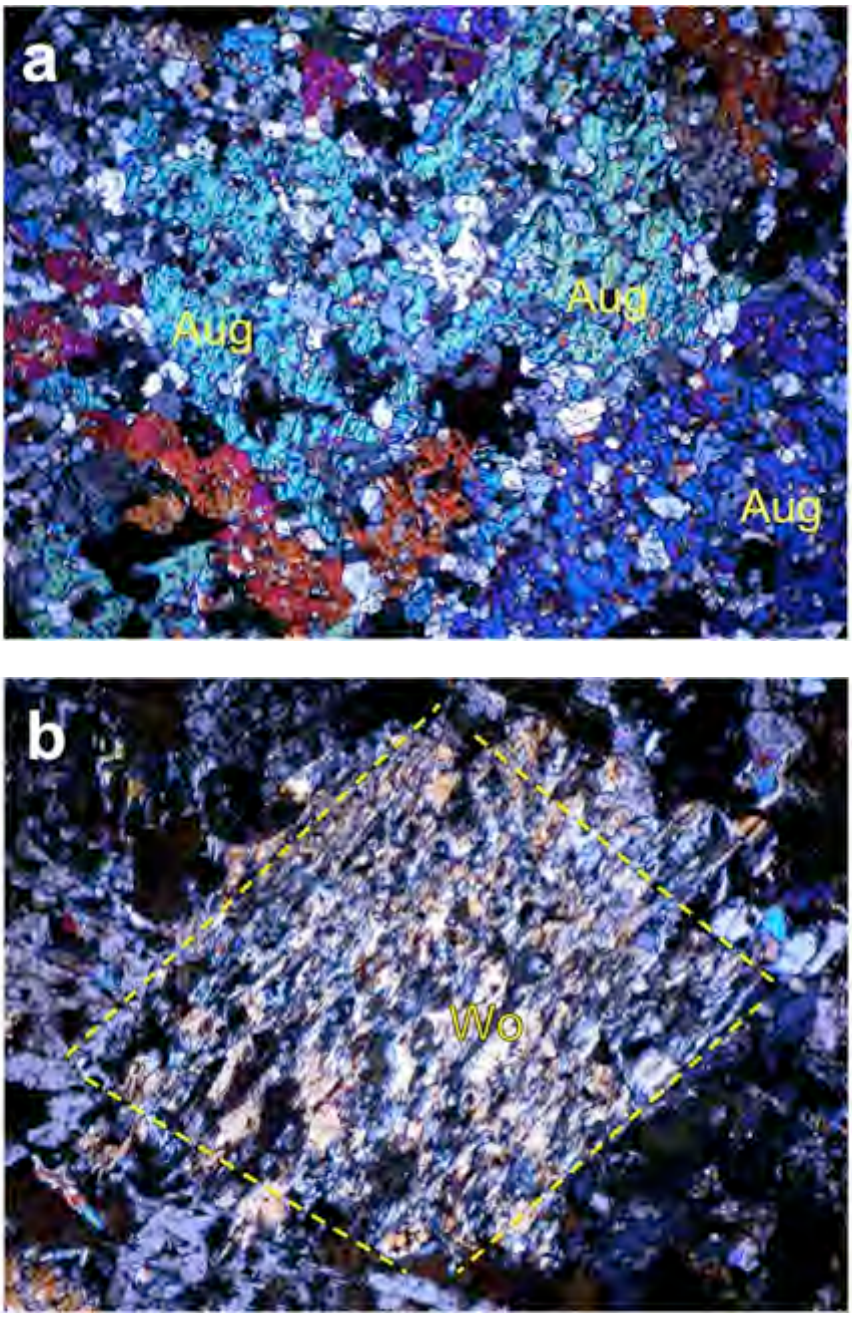

Figure 6.9. (a) Photomicrograph of several augite (Aug) poikiloblasts containing inclusions of quartz and sulfides in sample C-3-324 taken in XPL with a field of view of 2 mm. Augite poikiloblasts can be up to 1-2mm, especially near fluid-filled fractures. (b) Photomicrograph of wollastonite (Wo) in sample C-3-400b taken in XPL with a field of view of 2 mm. Wollastonite is a good indicator mineral of contact metamorphism, and is commonly mistaken for pyroxene because it has a similar shape and birefringence. It was distinguished from pyroxene using EDS.

The peak metamorphic mineral assemblage at Linwood Lake (Figure 5.8) is enstatite-augite-cordierite. Enstatite is only identified as small crystals reacting with biotite, as in the case of ferrosilite (Figure 6.8). Augite, in contrast, occurs as very large poikiloblasts containing inclusions of quartz and pyrite, and ranges in size from 0.25-4 mm (Figure 6.9). Cordierite occurs as 1 mm poikiloblasts containing inclusions of quartz, and pyrite, and also contains biotite formed as a by-product. Enstatite-augite-cordierite is stable at temperatures of about 700°C (Spear, 1993), so this site was subjected to the same degree of heating as the Water Hen area. Other minerals associated with contact metamorphism at this site include gedrite, muscovite, and recrystallized quartz. The width of the contact metamorphic aureole is unknown for this site due to a lack of exposure, but the outcrop that was sampled is approximately 30 m from the contact with the Duluth Complex (Severson, 1994) and it contains porphyroblasts of the three peak metamorphic minerals. Therefore the contact aureole is a minimum of 30 m wide.

The Fish Lake field site (Figure 5.9) has a peak metamorphic mineral assemblage of ferrosilite-cordierite-gedrite. Ferrosilite occurs similarly to the Water Hen field site. It is found in tiny crystals associated with acicular plates of biotite, which together form a rhombohedral shape. Like the Water Hen site, ferrosilite is not identified as euhedral porphyroblasts. Cordierite is identified as large tabular porphyroblasts and exhibits a wavy texture, possibly due to twinning (Figure 6.10). Gedrite has an amorphous shape and is found associated with ferrosilite. This mineral assemblage is stable at temperatures around 700°C (Spear, 1993), coinciding with the metamorphic conditions at

both Linwood Lake and Water Hen. Other minerals associated with the contact metamorphic assemblage at this site include biotite, muscovite, alkali feldspar, quartz, sphene, and pentlandite. At this field site, the contact metamorphic aureole extends approximately 30-40 m based on the presence of porphyroblasts of cordierite and ferrosilite.

The Midway Road field site (Figure 5.11) has two peak metamorphic mineral assemblages: cordierite-gedrite-biotite, and garnet-augite-gedrite. The two assemblages formed in rocks of different bulk composition at this field site, where one is more calcium-rich, allowing for the growth of garnet and augite instead of cordierite. Cordierite, garnet, and augite all are identified as euhedral poikiloblasts containing inclusions of biotite, quartz and pyrite (Figure 6.11). Gedrite occurs as an amorphous shape that is associated with augite and biotite. Biotite occurs as tabular porphyroblasts that are larger and have more defined borders than biotite associated with regional metamorphism. These mineral assemblages are stable at temperatures around 600°C (Spear, 1993), so this field site was subjected to slightly lower temperature conditions than Water Hen, Linwood Lake, and Fish Lake. Other minerals associated with the contact metamorphic assemblage at this site include muscovite, alkali feldspar, and quartz. The contact metamorphic aureole at this site is hard to determine due to limited outcrop, but the outcrop sampled does exhibit signs of contact metamorphism such as spotted slate texture, poikiloblastic texture, and the presence of contact metamorphic minerals such as cordierite and garnet. Thomson Formation sampled at this site is farther away from the contact (approximately 250 m) than other field sites, and it is separated

Figure 6.10. Photomicrograph of a twinned cordierite (Crd) porphyroblast in sample F-2-837 taken in XPL with a field of view of 2 mm. Note the wavy texture of the cordierite, which is a common texture due to its affinity for twinning.

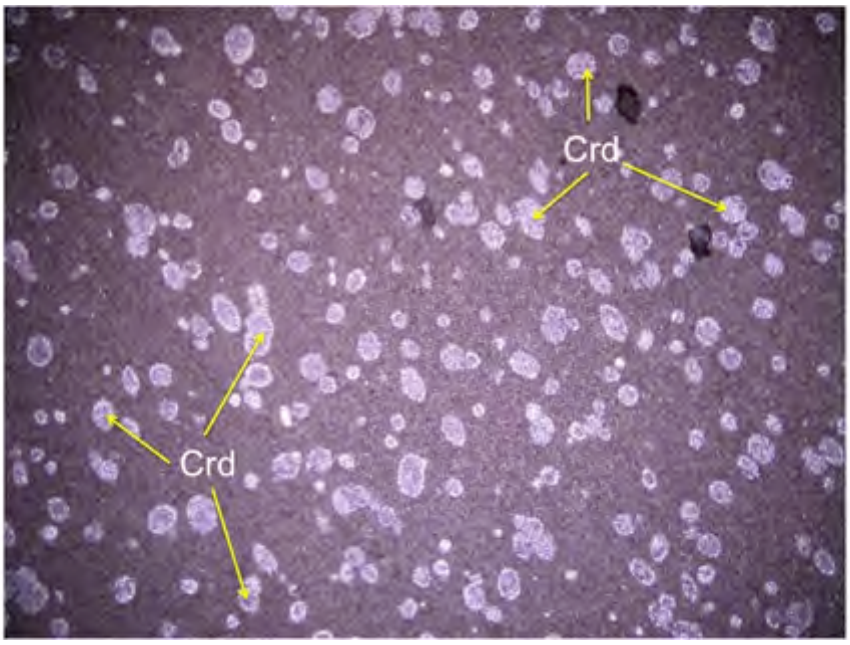

Figure 6.11. Photomicrograph of cordierite (Crd) poikiloblasts in sample MR-03-B taken in PPL with a field of view of 2 mm. The poikiloblasts have grown in a pattern called "spotty slate," which is commonly found in contact metamorphic aureoles. They contain inclusions of biotite, muscovite, and pyrite.

from the Duluth Complex intrusions by the Ely's Peak Basalts, making an accurate estimate of the width of the aureole difficult.

6.5 Retrograde Metamorphism and Alteration in the Animikie Group

After the intrusion of the Duluth Complex, the Animikie Group cooled and underwent retrograde metamorphism. This retrograde metamorphism, and possibly some fluid flow associated with fractures in the rocks produced new mineral growth. Minerals associated with this retrograde metamorphism include chlorite and possibly tourmaline (Figure 6.12). Tourmaline could have also grown syn-contact metamorphism if the intrusion of the Duluth Complex liberated water. Figure 6.13 and Table 6.1 illustrate the relationships between the four different stages of minerals discussed above.

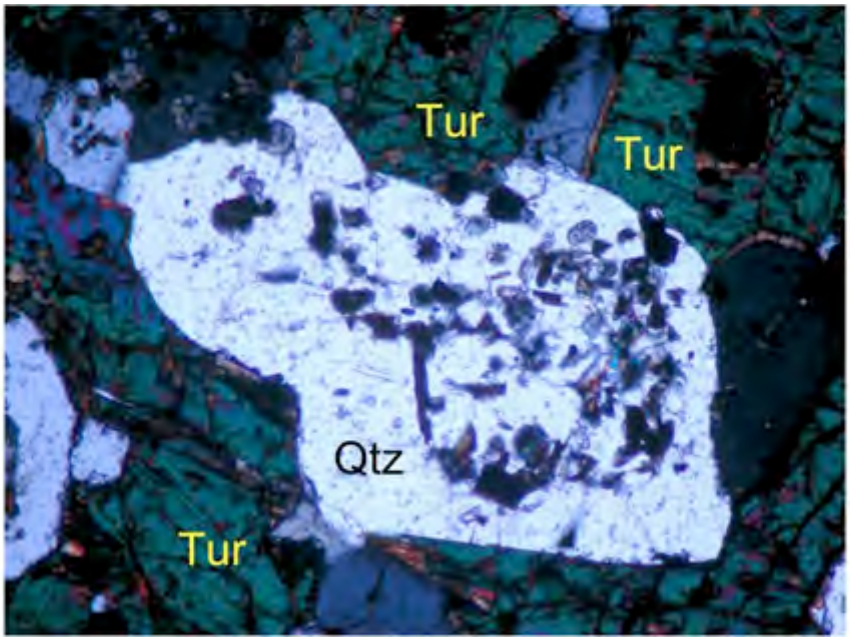

Figure 6.12. Photomicrograph of tourmaline (Tur) in sample A-1-474 taken in XPL with a field of view of 2 mm. The tourmaline in this photo is approximately 10 mm wide and is associated with fluid flow through fractures in Thomson Formation metagraywackes, which are fairly common in the rock. It also contains inclusions of recrystallized quartz. Since the quartz itself contains inclusions of earlier relict sedimentary minerals such as biotite and pyrite, it is thought that the tourmaline occurred either during the contact metamorphism, due to liberation of water from the intrusion, or after.

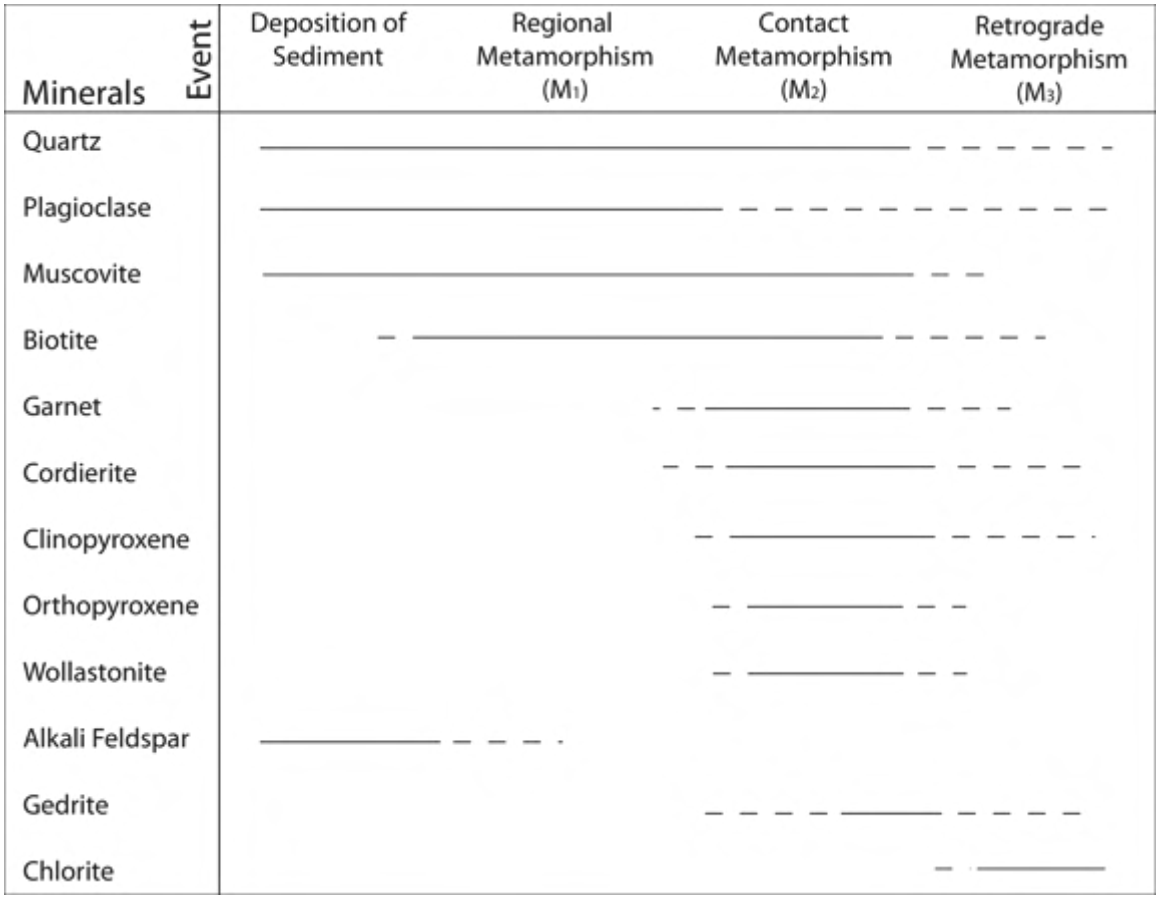

Figure 6.13. Timeline showing the growth stages of relict sedimentary, regional metamorphic (M_1), contact metamorphic (M_2), and late metamorphic mineral growth due to cooling and possible fluid flow (M_3) in the Animikie Group. The dashed lines show uncertain beginning and end of mineral growth, and solid lines show periods of definite crystallization or recrystallization.

Table 6.1. Table listing minerals present in each sample taken from the Animikie Group. Minerals are divided up into contact metamorphic minerals, relict sedimentary minerals, and accessory minerals.

	Contact Metamorphic Minerals							
Sample	Crd	Opx	Cpx	Wo	Grt	Ged	Bt	Ms
Section 22								
A-1-430	x					x	x	x
A-1-474	x					x	x	
A-1-476	x						x	x
Water Hen								
C-3-324			x			x		
C-3-400b	x		x	x				x
C-6-679			x			x	x	x
C-6-698							x	x
C-10-1747	x	x	x			x	x	x
C-11-2873	x					x	x	x
C-11-2914	x	x	x			x	x	x
Linwood Lake								
LL-1-09	x	x	x			x		x
Fish Lake								
F-1-493	x					x	x	
F-1-532	x					x	x	x
F-1-683	x						x	x
F-2-835	x	x				x	x	
F-2-837	x					x	x	x
F-2-843	x					x	x	x
F-2-849	x	x				x	x	x
F-2-858	x	x				x	x	x
Midway Road								
MR-01-A			x		x	x		x
MR-01-E	x					x	x	
MR-03-B	x					x	x	x

Table 6.1. Table listing minerals present in each sample taken from the Animikie Group. Minerals are divided up into contact metamorphic minerals, relict sedimentary minerals, and accessory minerals.

	Relict Sedimentary Minerals				
Sample	Ms	Kfs	Pl	Cal	Qtz
Section 22					
A-1-430	x	x	x		x
A-1-474		x			x
A-1-476	x	x	x		x
Water Hen					
C-3-324			x		x
C-3-400b	x		x		x
C-6-679	x	x	x		x
C-6-698	x	x	x		x
C-10-1747	x	x	x		x
C-11-2873	x	x	x		x
C-11-2914	x		x		x
Linwood Lake					
LL-1-09	x		x	x	x
Fish Lake					
F-1-493		x	x		x
F-1-532	x	x	x		x
F-1-683	x		x		x
F-2-835		x	x		x
F-2-837	x	x	x		x
F-2-843	x		x		x
F-2-849	x	x			x
F-2-858	x	x	x		x
Midway Road					
MR-01-A	x	x	x		x
MR-01-E	x		x		x
MR-03-B	x	x	x		x

Table 6.1. Table listing minerals present in each sample taken from the Animikie Group. Minerals are divided up into contact metamorphic minerals, relict sedimentary minerals, and accessory minerals.

	Accessory Minerals										
Sample	Py	Sph	Pent	Spn	Ilm	Rt	Ap	Tur	Chl	Spl	Zr
Section 22											
A-1-430	x										x
A-1-474	x		x				x	x			x
A-1-476	x				x		x	x	x	x	
Water Hen											
C-3-324	x										x
C-3-400b					x			x			x
C-6-679					x		x				
C-6-698							x				x
C-10-1747					x		x				
C-11-2873					x		x				x
C-11-2914	x				x						
Linwood Lake											
LL-1-09					x		x		x		
Fish Lake											
F-1-493	x			x	x	x		x		x	
F-1-532	x						x		x		x
F-1-683							x				x
F-2-835		x			x						
F-2-837	x		x		x	x	x	x			
F-2-843	x					x		x	x		
F-2-849						x		x			
F-2-858	x	x				x		x	x		
Midway Road											
MR-01-A	x				x		x		x		
MR-01-E	x				x		x				
MR-03-B	x				x						x

6.6 Mineral Assemblages in the Ely's Peak Basalts

The Ely's Peak basalts were initially extruded during opening of the Midcontinent Rift (~1.1 Ga). They were subjected to burial metamorphism due to subsequent lava flows and sediments being deposited above them and then contact metamorphosed by the intrusion of the Duluth Complex.

6.7 Initial Mineralogy of the Ely's Peak Basalts

When the Ely's Peak basalts were initially crystallized, olivine, augite, and plagioclase were the main phenocryst and groundmass phases (Kilberg, 1972). All of the minerals grew with euhedral or subhedral shapes and can be as big as 1-2 mm. As the rocks cooled, olivine became unstable and was largely replaced by pseudomorphs of serpentine. Magnetite and ilmenite are the dominant opaque minerals.

6.8 Regional Burial Metamorphism of the Ely's Peak Basalts

After the Ely's Peak Basalts were erupted, they were buried by the deposition of overlying flows and sediments. This led to a rise in pressure and temperature, and ultimately to a hydrothermal burial metamorphism in the greenschist facies. Most of the primary igneous structures and textures are still preserved, although certain minerals are altered. The alteration of olivine to either chlorite or serpentine is one indication of burial metamorphism, as is the "dusty" look of plagioclase (Kilburg, 1972), (Figure 6.14). Augite alters to actinolite along grain boundaries, and ilmenite and magnetite alter to

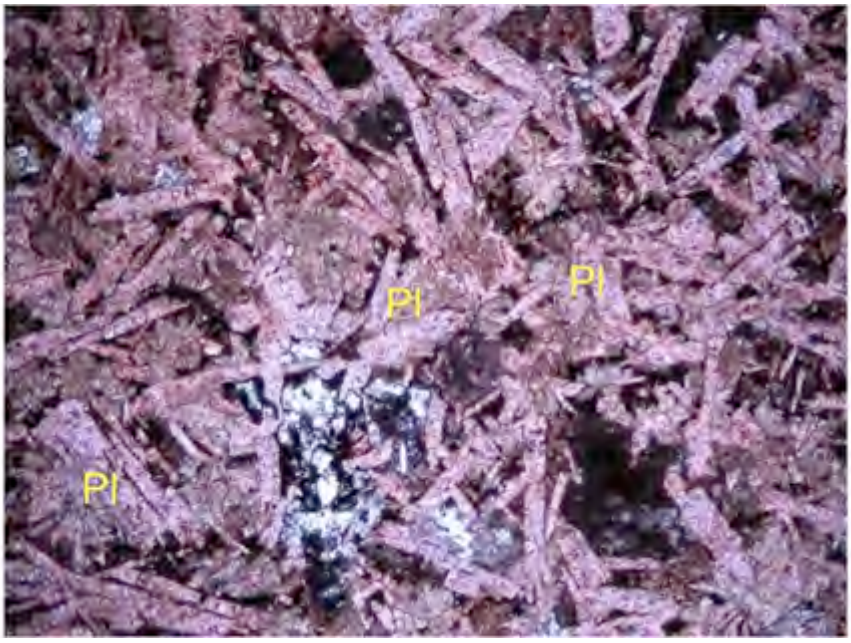

Figure 6.14. Photomicrograph of plagioclase feldspar (Pl) that has been affected by hydrothermal burial metamorphism in sample EP-7-09 taken in PPL with a field of view of 2 mm. The "dusty" texture of the plagioclase is due to sericitization as it breaks down. The red coloring of the plagioclase in the photomicrograph is due to ilmenite altering to magnetite.

sphene and hematite. In the flow top amygdules, epidote and potassium feldspar are present.

6.9 Contact Metamorphism in the Ely's Peak Basalts

When the Duluth Complex intruded into the Ely's Peak Basalts, it metamorphosed the basalts into a granofels of the pyroxene-hornfels facies. The innermost part of the aureole extends about 100 meters out from the contact and has a peak metamorphic mineral assemblage of augite-gedrite-plagioclase (Figure 6.15). The only olivine present was that associated with original crystallization, and it has been replaced by serpentine pseudomorphs. Gedrite was identified through mineral composition and is possibly associated with the olivine pseudomorphs. This mineral assemblage is stable at temperatures of approximately 600-700°C (Spear, 1993), which is similar to the average temperature that the Animikie Group was subjected to during contact metamorphism. Small pockets of sulfides and pegmatites also occur near the contact. Between 100-300 meters away from the contact, but still showing a granofels texture, the peak metamorphic mineral assemblage becomes biotite-hornblende-plagioclase. This mineral assemblage is stable at temperatures ranging from 400-600°C (Spear, 1993). Farther from the contact the basalt loses its granofels appearance. Primary igneous textures reappear, and the basalt exhibits signs of burial metamorphism (Figure 6.16). Table 6.2 shows all of the minerals associated with the Ely's Peak Basalts, and their relationship to one another.

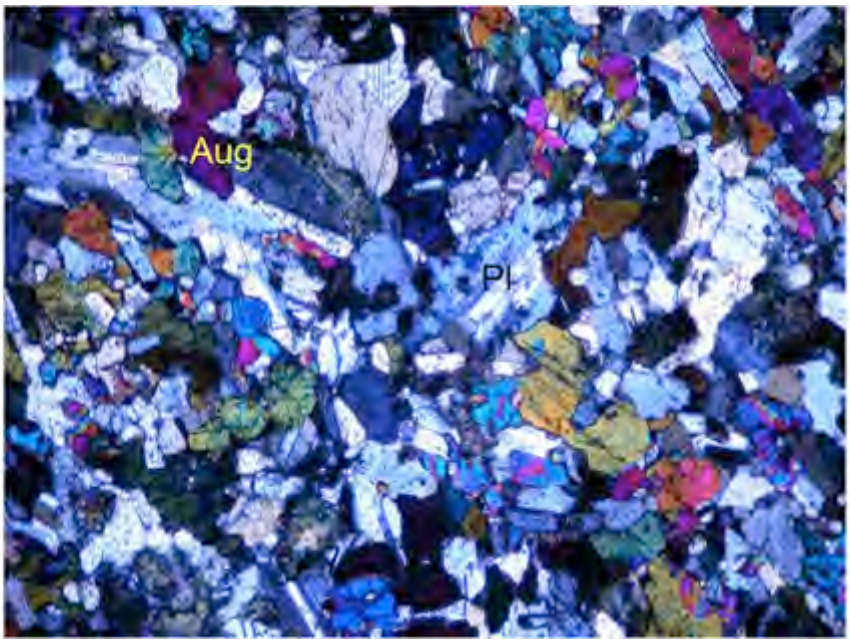

Figure 6.15. Photomicrograph showing augite (Aug) and plagioclase (Pl) in a well-formed granoblastic texture in sample EP-3-09b taken in XPL with a field of view of 2 mm. The plagioclase has lost its bladed appearance and is equant in some areas, which is characteristic of a granoblastic texture.

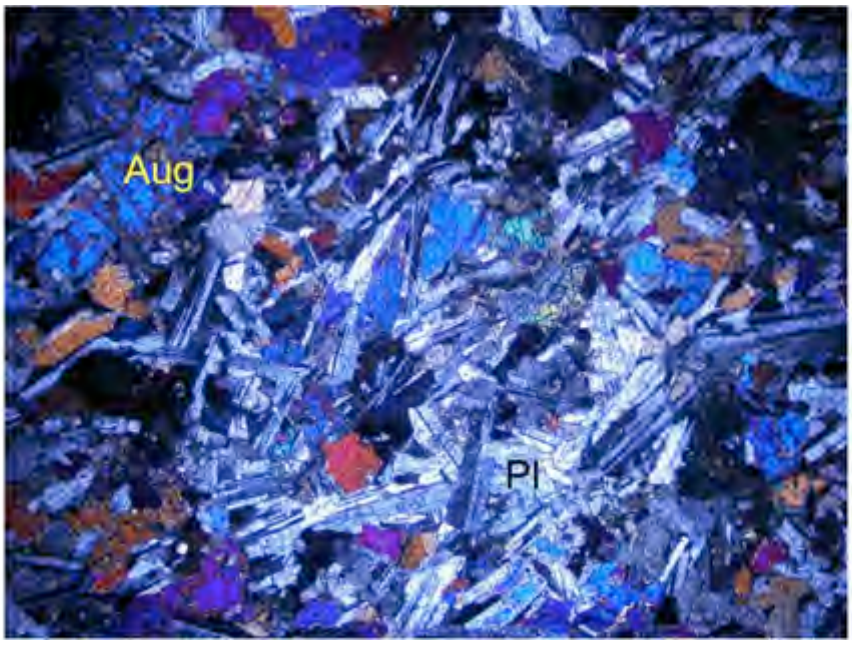

Figure 6.16. Photomicrograph showing augite (Aug) and plagioclase (Pl) outside of the contact metamorphic aureole in sample EP-7-09 taken in XPL with a field of view of 2 mm. There is no granoblastic texture, plagioclase is growing in elongate lathes, and augite is taking on a tabular shape.

Table 6.2. Table of minerals in the Ely's Peak basalts. Minerals are listed as primary igneous phases, metamorphic mineral assemblages, and accessory minerals.

	Primary Minerals			**Metamorphic Minerals**		
Sample	Ol	Aug	Pl	Aug	Ged	Pl
Ely's Peak						
EP-3-09b	x	x	x	x	x	x
EP-6-09	x	x	x	x	x	x
EP-7-09	x	x	x	x	x	x

	Accessory Minerals							
Sample	Bt	Ms	Spn	Ilm	Ap	Py	Kfs	Ep
Ely's Peak								
EP-3-09b		x	x	x	x	x	x	x
EP-6-09	x	x		x				
EP-7-09			x	x				

7. MINERAL TEXTURES AND ANALYSIS

7.1 Introduction

The JEOL JSM-6490LV Scanning Electron Microscope (SEM) was used for three main purposes. Both secondary electron imaging (SEI) and backscattered electron imaging (BSE) were used to gather high-resolution images of the minerals and determine textural and compositional changes. Energy dispersive spectroscopy (EDS) was used to determine the chemical composition of the minerals, allowing a better identification to be made. Lastly, electron backscatter diffraction (EBSD) was used to determine the crystal lattice structure of a mineral, which when combined with chemical composition can help with mineral identification.

7.2 Imaging

Secondary electron images (SEI) of the minerals were acquired in order to determine textural characteristics. SEI images show grain boundaries, highlight twinning, help to determine the best point for EDS analysis, and allow for an examination of how well the thin section has been polished. The only mineral that had textural changes of note was cordierite due to its affinity for twinning (Figure 7.1).

Backscattered electron images (BSE) are important because they show textural relationships at high-resolution and qualitatively show compositional differences in a mineral. This is extremely useful when conducting EDS analysis because it allows high spatial-resolution location of spot analyses. BSE imaging can also indicate rims

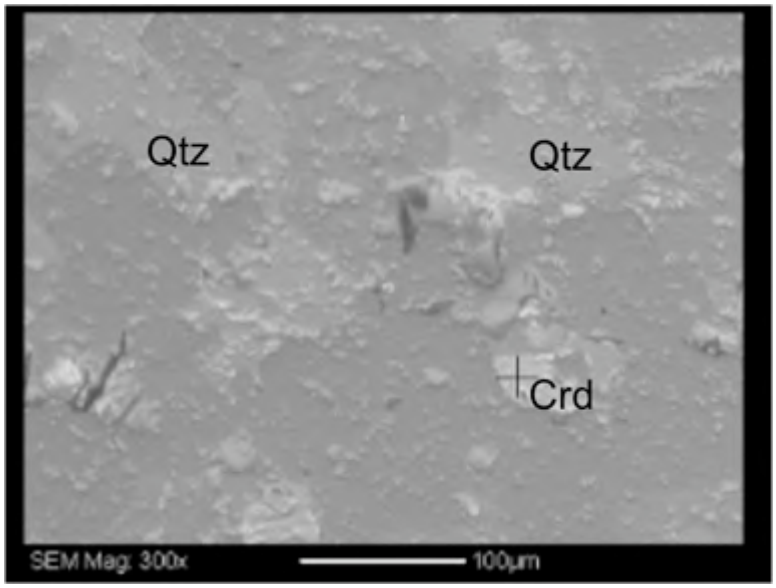

Figure 7.1. SEI image showing the difference in texture between cordierite (Crd) and quartz (Qtz) in sample A-1-430. Note that the cordierite is raised higher than the quartz. This is because cordierite is very hard, making it hard to polish smooth on a thin section.

versus cores in certain minerals, and exsolution structures. Backscattered electron imaging sharply defines mineral grain boundaries because of the contrast in compositions, allowing for a quick determination of mineral phases. The higher the average atomic number of a mineral, as given by its bulk composition, the brighter its appearance in BSE. For example, quartz, plagioclase, and alkali feldspar are hard to distinguish from one another because they are all high in silica and typically appear dark, but pyrite stands out because it is high in sulfur and iron, which have higher atomic numbers (Figure 7.2).

7.3 Mineral Compositions

Energy dispersive spectroscopy (EDS) analysis is the most important type of analysis in this study. EDS allows a mineral to be analyzed for its chemical composition. The Oxford Instruments Energy 250 system with an INCA xACT Si-drift detector was used to determine the chemical composition of minerals from the study area. EDS was commonly used as a compliment to optical petrography in order to help identify fine-grained minerals, and it was used to quantitatively determine mineral compositions that reflect the conditions of formation during the time of the Midcontinent Rift.

Analysis of cordierite by EDS was a great benefit because cordierite is very difficult to distinguish from plagioclase and other minerals optically, so the SEM was used to confirm its presence (Figure 7.3). Analysis of cordierite shows that many have

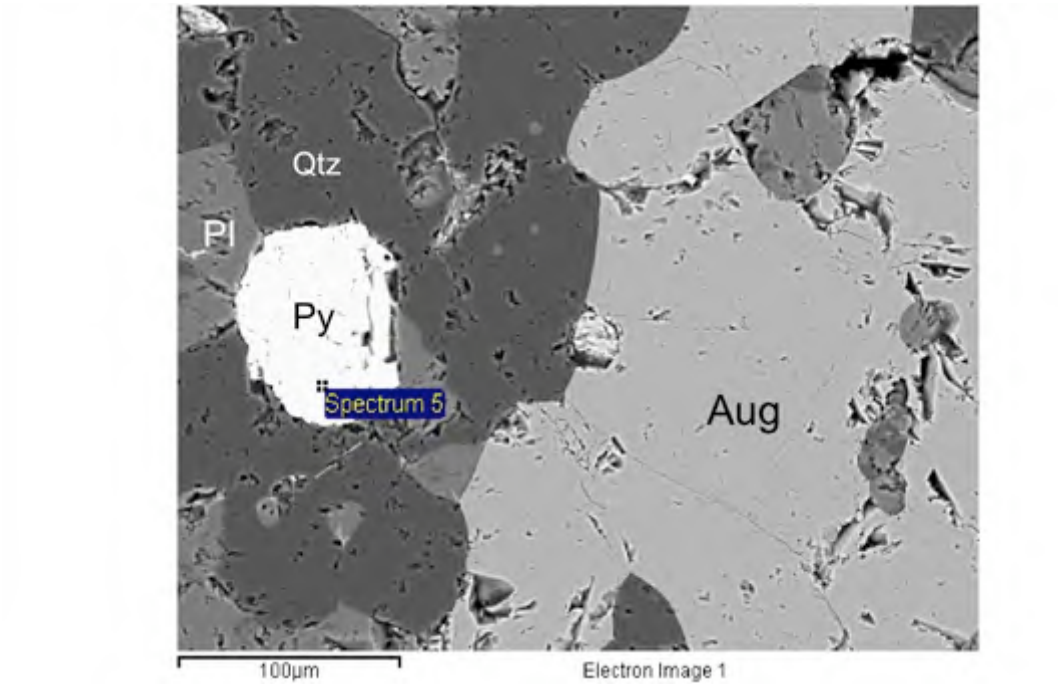

Figure 7.2. BSE image of pyrite (Py) and augite (Aug) showing the difference in composition between the two minerals in sample C-3-324. The spectrum label is where the chemical composition of the mineral was analyzed. Pyrite is brighter than augite in a BSE image because it contains elements which have higher atomic numbers, so scatter more incoming beam electrons and show up more brightly on a BSE image. Quartz and plagioclase feldspar are darker because their mineral composition consists of minerals that have lower atomic numbers such as silica.

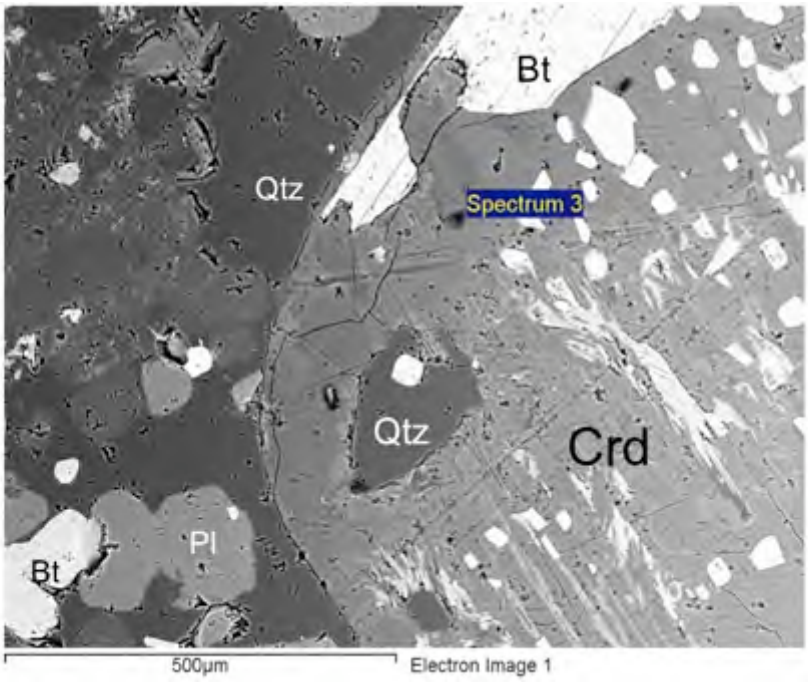

Figure 7.3. BSE image of a cordierite (Crd) poikiloblast containing inclusions of quartz (Qtz), biotite (Bt). The biotite occurs as both the polygonal bright crystals in the cordierite poikiloblast, and as wispy minerals, perhaps due to their reaction with cordierite. This image was taken from sample A-1-430. The spectrum label is where the chemical composition of the mineral was analyzed, and is marked in bold on Table 7.1.

Table 7.1. Table of representative chemical analyses of cordierite. All analyses were done in standardized mode with cation proportions based on 18 oxygens.

Representative Analyses of Cordierite

	Virginia Formation					
Field Site	Section 22					
Sample No.	A-1-430	A-1-430	**A-1-430**	A-1-430	A-1-430	A-1-430
Site No.	1	2	**3**	4	5	6
No. Analyses	2	3	**1**	4	5	3
Wt %						
SiO_2	45.92	42.44	**49.77**	42.04	49.93	51.13
TiO_2	0.00	0.00	**0.00**	0.00	0.00	0.00
Al_2O_3	33.38	33.88	**33.88**	33.37	32.78	32.39
FeO	5.66	8.31	**2.96**	8.20	3.44	4.04
MgO	3.59	4.39	**2.10**	4.42	2.31	2.84
MnO	0.00	0.00	**0.00**	0.00	0.00	0.00
CaO	0.00	0.34	**0.00**	0.26	0.22	0.00
Na_2O	0.50	0.44	**0.61**	0.08	0.51	0.44
K_2O	4.41	2.93	**6.19**	2.89	7.40	7.05
Total	93.46	92.73	**95.52**	91.26	96.59	97.89
Total Cations	(Based on the Smithsonian Institution osumilite, pyrope, oliviine, and microcline standards and 18 O)					
Norm Factor	2.73	2.67	**2.82**	2.64	2.82	2.86
Si	5.04	4.76	**5.29**	4.78	5.31	5.36
Al(iv)	0.96	1.24	**0.71**	1.22	0.69	0.64
SUM	6.00	6.00	**6.00**	6.00	6.00	6.00
Al(vi)	3.36	3.23	**3.54**	3.24	3.42	3.36
Ti	0.00	0.00	**0.00**	0.00	0.00	0.00
Fe	0.52	0.78	**0.26**	0.78	0.31	0.35
Mg	0.59	0.73	**0.33**	0.75	0.37	0.44
Mn	0.00	0.00	**0.00**	0.00	0.00	0.00
Ca	0.00	0.04	**0.00**	0.03	0.03	0.00
Na	0.11	0.10	**0.13**	0.02	0.11	0.09
K	0.62	0.42	**0.84**	0.42	1.00	0.94
Total	**11.19**	**11.30**	**11.10**	**11.24**	**11.22**	**11.19**
X(Fe)	0.47	0.51	**0.44**	0.51	0.46	0.44
X(Mg)	0.53	0.49	**0.56**	0.49	0.54	0.56
Ca+Na+K	0.72	0.56	**0.97**	0.47	1.13	1.03
X(Ca)	0.00	0.07	**0.00**	0.07	0.02	0.00
X(Na)	0.15	0.17	**0.13**	0.04	0.09	0.09
X(K)	0.85	0.75	**0.87**	0.89	0.89	0.91

Representative Analyses of Cordierite (Cont.)

	Virginia Formation					
Field Site	Section 22					
Sample No.	A-1-430	A-1-430	A-1-430	A-1-430	A-1-430	A-1-430
Site No.	7	8	9	10	11	12
No. Analyses	3	2	2	3	4	4
Wt %						
SiO_2	43.18	49.44	40.23	42.24	48.93	47.37
TiO_2	0.00	0.00	0.00	0.00	0.00	0.00
Al_2O_3	34.30	34.18	31.54	31.69	33.39	33.57
FeO	7.86	11.68	10.56	9.99	3.92	4.55
MgO	4.44	6.72	5.85	5.79	2.76	2.97
MnO	0.00	0.00	0.00	0.00	0.00	0.00
CaO	0.00	0.00	0.36	0.21	0.00	0.15
Na_2O	0.61	0.33	0.00	0.33	0.46	0.37
K_2O	2.93	0.00	2.42	2.95	5.82	6.93
Total	93.32	102.35	90.96	93.20	95.28	95.91
Total Cations	(Based on the Smithsonian Institution osumilite, pyrope, oliviine, and microcline standards and 18 O)					
Norm Factor	2.70	2.98	2.59	2.66	2.80	2.78
Si	4.79	4.97	4.66	4.76	5.24	5.11
Al(iv)	1.21	1.03	1.34	1.24	0.76	0.89
SUM	6.00	6.00	6.00	6.00	6.00	6.00
Al(vi)	3.27	3.02	2.96	2.97	3.45	3.37
Ti	0.00	0.00	0.00	0.00	0.00	0.00
Fe	0.73	0.98	1.02	0.94	0.35	0.41
Mg	0.73	1.01	1.01	0.97	0.44	0.48
Mn	0.00	0.00	0.00	0.00	0.00	0.00
Ca	0.00	0.00	0.04	0.03	0.00	0.02
Na	0.13	0.06	0.00	0.07	0.10	0.08
K	0.41	0.00	0.36	0.42	0.79	0.95
Total	**11.28**	**11.07**	**11.40**	**11.41**	**11.13**	**11.31**
X(Fe)	0.50	0.49	0.50	0.49	0.44	0.46
X(Mg)	0.50	0.51	0.50	0.51	0.56	0.54
Ca+Na+K	0.55	0.06	0.40	0.52	0.89	1.05
X(Ca)	0.00	0.00	0.11	0.05	0.00	0.02
X(Na)	0.24	1.00	0.00	0.14	0.11	0.07
X(K)	0.76	0.00	0.89	0.81	0.89	0.91

high potassium levels (2-7 wt% K_2O) relative to typical cordierite with potassium levels of ~1% wt% K_2O (Table 7.1). After further analysis I determined that this cordierite is a rare type of high-potassium cordierite that is found in dry, low-pressure high-temperature environments like that found near a contact metamorphic aureole (Schreyer et. al., 1990). The analyses show that many cordierites in these rocks are relatively Fe-rich compared to most cordierite, which is Mg-rich. Cordierites in the contact metamorphosed Animikie rocks have X_{Fe} ranging from 0.44-0.51, which is notably high even though the concentrations of Fe and Mg are similar. This may reflect stability of Fe-rich cordierite at low temperatures relative to Mg-rich varieties. Only a few studies have been done to date on high-potassium cordierite. Of those studies, Hentschel (1977) and Miyashiro and Iiyama (1954) mentioned that Fe^{3+} may be present in high-potassium cordierite, which may help to explain the high levels of Fe found in this study.

EDS analysis was also useful for identifying orthopyroxene and clinopyroxene (Figure 7.4). Ferrosilite and hypersthene are the main orthopyroxenes, and augite and hedenbergite are the main clinopyroxenes (Table 7.2). These were confirmed by comparing them to published analyses of these minerals (Deer, et al., 2002). EDS analysis confirmed that these homogeneous pyroxenes contained intermediate Ca contents between 10-40%. Due to this composition and their homogeneity, it is thought that the pyroxenes are metamorphic rather than igneous pyroxenes. They are not exsolved texturally so they may have been rehomogenized during high-temperature diffusion.

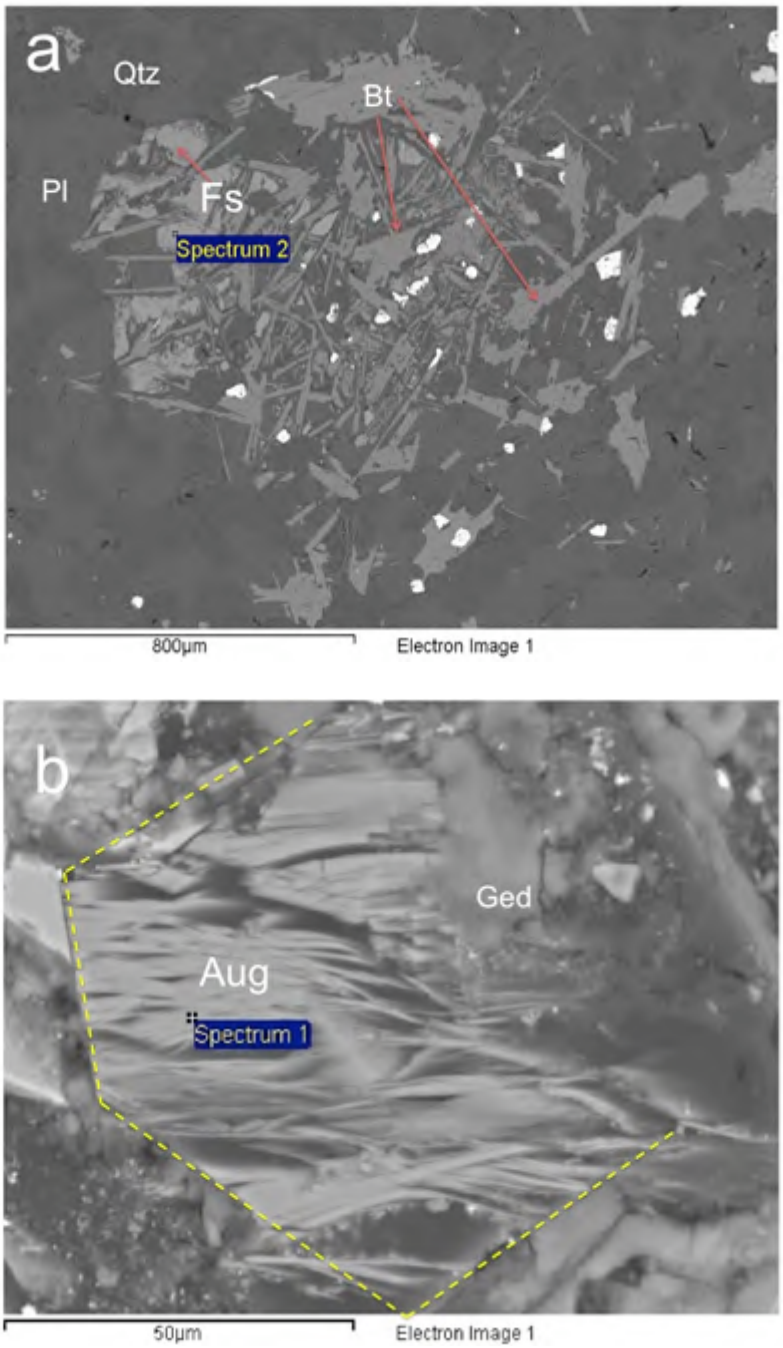

Figure 7.4. (a) BSE image of ferrosilite (Fs) associated with biotite (Bt) in sample C-11-2914. This association of small ferrosilite crystals and acicular biotite forming a rhombohedral shape is common in the Animikie rocks, and no single, large orthopyroxene porphyroblasts were found. (b) BSE image of augite (Aug) reacting with gedrite (Ged) in sample C-3-400b. Amoeboidal gedrite is commonly found associated with pyroxene. In both photomicrographs the spectrum label is where chemical composition was analyzed, which is shown in bold in Table 7.2.

Table 7.2. Table of standardless representative analyses of ortho- and clinopyroxene based on 6 oxygens. Each pyroxene has been identified based on the ratio of calcium, iron, and magnesium using the method stated in Deer, et al. (2002). The two main clinopyroxenes identified are augite and hedenbergite. The two main orthopyroxenes identified are ferrosilite and hypersthene.

Representative Analyses of Pyroxene

	Clinopyroxene					
	Augite	Hedenbergite	Augite	Subcalcic Augite	Subcalcic Augite	Subcalcic Augite
	Virginia Formation					
Field Site	Water Hen				Linwood Lake	
Sample No.	C-3-324	**C-3-400b**	C-10-1747	C-10-1747	LL-1-09	LL-1-09
Site No.	1	**1**	3	4	1	3
No. Analyses	4	**4**	2	1	4	4
Wt %						
SiO_2	54.00	**51.94**	55.10	53.02	57.11	54.14
TiO_2	0.54	**0.00**	0.00	0.83	0.00	0.37
Al_2O_3	0.89	**0.00**	0.00	5.58	1.64	7.16
FeO	14.08	**22.40**	14.61	17.99	6.40	8.29
MgO	10.75	**2.35**	10.46	11.36	17.92	17.60
MnO	0.34	**0.93**	0.00	0.00	0.06	0.00
CaO	19.40	**22.38**	19.36	10.27	16.87	11.62
Na_2O	0.00	**0.00**	0.00	0.56	0.00	0.62
K_2O	0.00	**0.00**	0.00	0.38	0.00	0.00
Total	100.00	**100.00**	99.53	99.99	100.00	99.80
Total Cations (Based on 6 O)						
Norm Factor	2.64	**2.51**	2.64	2.67	2.78	2.79
Si	2.04	**2.07**	2.09	1.98	2.05	1.94
Al(iv)	-0.04	**-0.07**	-0.09	0.02	-0.05	0.06
Al(vi)	0.08	**0.07**	0.09	0.23	0.12	0.24
Ti	0.02	**0.00**	0.00	0.02	0.00	0.01
Fe	0.44	**0.75**	0.46	0.56	0.19	0.25
Mg	0.61	**0.14**	0.59	0.63	0.96	0.94
Mn	0.01	**0.03**	0.00	0.00	0.00	0.00
Ca	0.78	**0.96**	0.79	0.41	0.65	0.45
Na	0.00	**0.00**	0.00	0.04	0.00	0.04
K	0.00	**0.00**	0.00	0.02	0.00	0.00
Total	**3.94**	**3.94**	**3.93**	**3.91**	**3.93**	**3.93**
X(Fe)	0.24	**0.41**	0.25	0.35	0.11	0.15
X(Mg)	0.33	**0.08**	0.32	0.39	0.53	0.58
X(Ca)	0.43	**0.52**	0.43	0.26	0.36	0.27

Representative Analyses of Pyroxene (Cont.)

	Clinopyroxene				
	Subcalcic Augite	Subcalcic Augite	Subcalcic Augite	Subcalcic Augite	Subcalcic Augite
	Virginia Fm	Ely's Peak Basalts			
Field Site	Linwood Lake	Ely's Peak			
Sample No.	LL-1-09	EP-3-09b	EP-3-09b	EP-6-09	EP-7-09
Site No.	4	4	5	2	1
No. Analyses	4	2	4	3	3
Wt %					
SiO_2	58.32	54.14	56.45	55.20	54.10
TiO_2	0.00	0.00	0.37	0.00	0.47
Al_2O_3	2.10	5.84	3.50	3.61	3.98
FeO	8.84	13.50	11.66	16.72	17.27
MgO	18.41	16.03	15.77	12.29	11.66
MnO	0.20	0.16	0.07	0.24	0.13
CaO	12.13	10.07	11.98	11.17	10.64
Na_2O	0.00	0.27	0.21	0.56	0.73
K_2O	0.00	0.00	0.00	0.00	0.47
Total	100.00	100.01	100.01	99.79	99.45
Total Cations (Based on 6 O)					
Norm Factor	2.80	2.74	2.76	2.69	2.66
Si	2.08	1.97	2.04	2.05	2.03
Al(iv)	-0.08	0.03	-0.04	-0.05	-0.03
Al(vi)	0.17	0.22	0.19	0.21	0.21
Ti	0.00	0.00	0.01	0.00	0.01
Fe	0.26	0.41	0.35	0.52	0.54
Mg	0.98	0.87	0.85	0.68	0.65
Mn	0.01	0.00	0.00	0.01	0.00
Ca	0.46	0.39	0.46	0.44	0.43
Na	0.00	0.02	0.01	0.04	0.05
K	0.00	0.00	0.00	0.00	0.02
Total	**3.89**	**3.92**	**3.89**	**3.90**	**3.92**
X(Fe)	0.15	0.25	0.21	0.32	0.33
X(Mg)	0.57	0.52	0.51	0.41	0.40
X(Ca)	0.27	0.23	0.28	0.27	0.26

Representative Analyses of Pyroxene

	Orthopyroxene				
	Ferrosilite	Ferrosilite	Ferrosilite	Hypersthene	Ferrosilite
	Virginia Formation				Thomson Fm
Field Site	Water Hen			Linwood Lake	Fish Lake
Sample No.	C-10-1747	**C-11-2914**	C-11-2914	LL-1-09	F-2-835
Site No.	4	**2**	3	1	1
No. Analyses	2	**3**	3	3	2
Wt %					
SiO_2	57.90	**56.47**	52.17	48.13	53.35
TiO_2	0.00	**0.00**	0.00	0.00	0.00
Al_2O_3	0.00	**1.59**	1.64	6.45	1.32
FeO	26.97	**25.99**	33.46	26.78	30.77
MgO	13.83	**15.02**	12.18	16.04	14.18
MnO	0.32	**0.64**	0.28	0.41	0.39
CaO	0.99	**0.28**	0.27	1.78	0.00
Na_2O	0.00	**0.00**	0.00	0.00	0.00
K_2O	0.00	**0.00**	0.00	0.29	0.00
Total	100.01	**99.99**	100.00	99.88	100.01
Total Cations (Based on 6 O)					
Norm Factor	2.66	**2.67**	2.56	2.60	2.59
Si	2.17	**2.11**	2.04	1.85	2.05
Al(iv)	-0.17	**-0.11**	-0.04	0.15	-0.05
Al(vi)	0.17	**0.18**	0.11	0.14	0.11
Ti	0.00	**0.00**	0.00	0.00	0.00
Fe	0.85	**0.81**	1.09	0.86	0.99
Mg	0.77	**0.84**	0.71	0.92	0.81
Mn	0.01	**0.02**	0.01	0.01	0.01
Ca	0.04	**0.01**	0.01	0.07	0.00
Na	0.00	**0.00**	0.00	0.00	0.00
K	0.00	**0.00**	0.00	0.01	0.00
Total	**3.84**	**3.87**	**3.94**	**4.02**	**3.93**
X(Fe)	0.51	**0.51**	0.60	0.45	0.55
X(Mg)	0.47	**0.48**	0.39	0.51	0.45
X(Ca)	0.02	**0.01**	0.01	0.04	0.00

As with other fine-grained phases difficult to identify in thin section, garnet (Figure 7.5) and gedrite (Figure 7.6) were identified and chemically analyzed by EDS. Garnet has very high amounts of calcium that identified the mineral as a grossular-rich garnet (Table 7.3). . Garnet was found in only one site: MR-01-A. This is because this site was more calcite-rich and when it was subjected to contact metamorphism, it producted garnet porphyroblasts instead of cordierite. Gedrite was identified on the basis of silica content, proportions of octahedral cations, and a lack of calcium (Deer, et al., 2002) (Table 7.4).

Wollastonite is an interesting pyroxenoid mineral associated with contact metamorphism (Figure 7.7). It was not identified in thin section due to its similarity to pyroxene, and the degree of mineral alteration. However, using EDS, wollastonite was identified and it is an indicator mineral of both contact metamorphism, and the presence of calcium-rich zones in the study area. Wollastonite was only found at one site in the study area, much like garnet. Again this is due to the high amount of calcium at the site relative to the other field sites, because wollastonite forms from the reaction between calcite and quartz (Table 7.5).

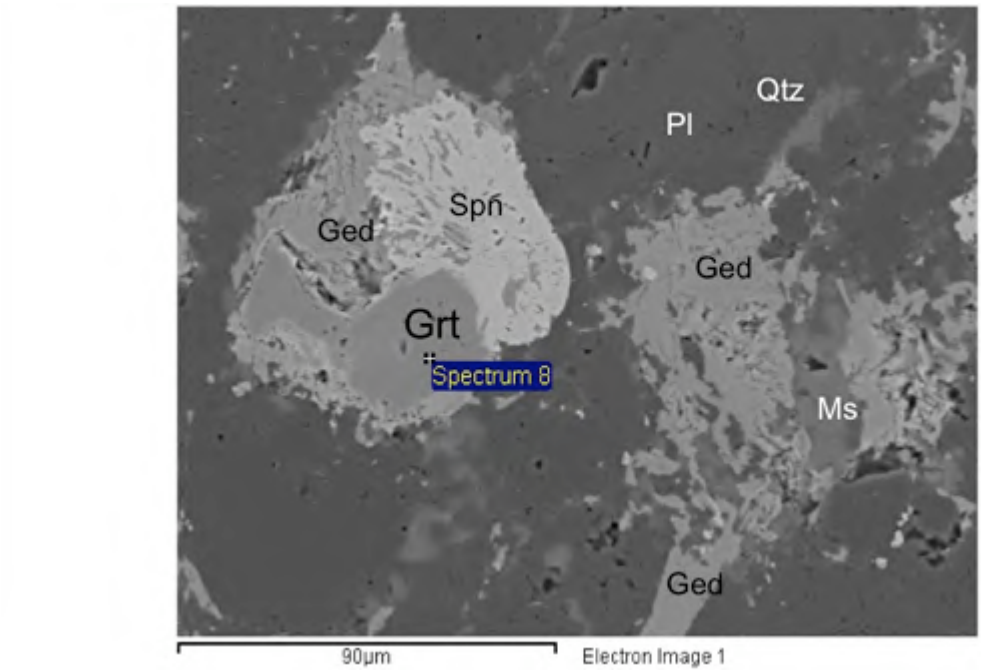

Figure 7.5. BSE image of a garnet (Grt) porphyroblast in sample MR-01-A. Garnet is reacting with gedrite (Ged) and sphene (Spn) and is possibly being replaced by them. Garnet was only identified by EDS, not optically. Spectrum label represents the area of chemical composition analysis, which is marked in bold on Table 7.3.

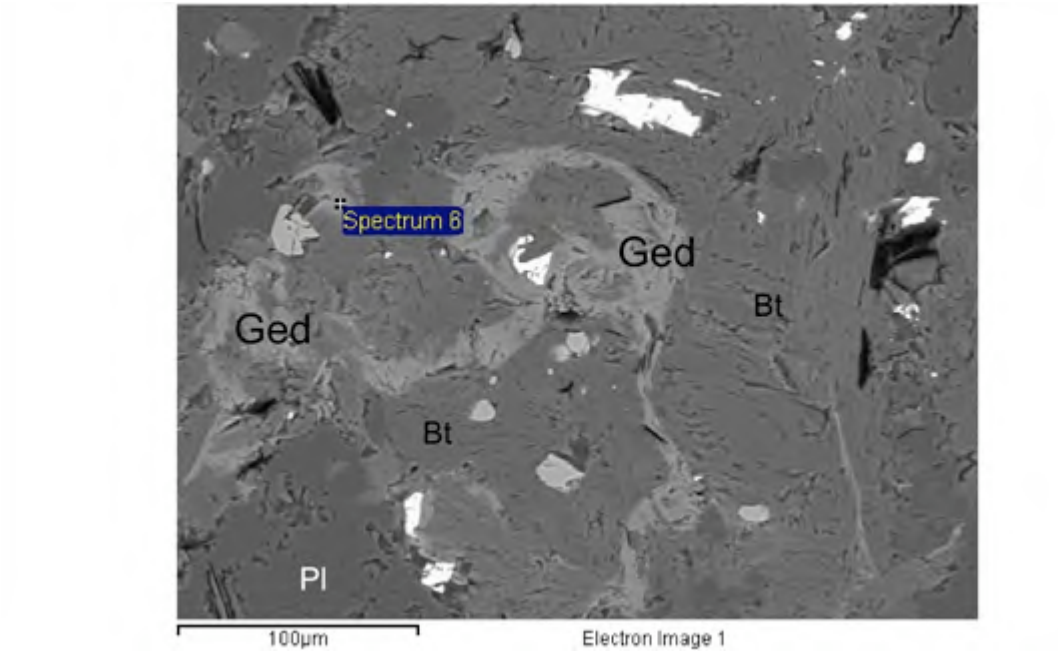

Figure 7.6. BSE image of gedrite (Ged) associated with biotite (Bt) in sample F-2-849. Gedrite and biotite are commonly found together and biotite reacts to gedrite with an increase in temperature. Gedrite commonly has an amorphous shape throughout the rock, and is never found in its common rhombohedral shape. Spectrum label represents the area of chemical composition analysis and is marked in bold on Table 7.4.

Table 7.3. Table of standardless representative analyses of garnet. All analyses performed in standardless mode and cation proportions are based on 12 oxygens.

Representative Analyses of Garnet

	Thomson Formation		
Field Site	Midway Road		
Sample No.	MR-01-A	MR-01-A	MR-01-A
Site No.	2	2	5
No. Analyses	1	1	1
Wt %			
SiO_2	41.71	41.53	41.79
TiO_2	0.00	0.00	0.00
Al_2O_3	28.75	28.30	24.77
FeO	5.72	6.36	10.94
MgO	0.00	0.00	0.00
MnO	0.00	0.00	0.00
CaO	23.82	23.81	22.50
Na_2O	0.00	0.00	0.00
K_2O	0.00	0.00	0.00
Total	100.00	100.00	100.00
Cations (Calculated on the basis of 12 oxygens)			
Norm Factor	2.73	2.72	2.67
Si	3.05	3.05	3.13
Ti	0.00	0.00	0.00
Al	2.48	2.45	2.19
Fe	0.35	0.39	0.68
Mg	0.00	0.00	0.00
Mn	0.00	0.00	0.00
Ca	1.86	1.87	1.80
Na	0.00	0.00	0.00
K	0.00	0.00	0.00
Total	**7.74**	**7.75**	**7.80**
Fe/(Fe+Mg)	1.00	1.00	1.00
Mg(Mg+Fe)	0.00	0.00	0.00
X(Fe)	0.16	0.17	0.28
X(Mg)	0.00	0.00	0.00
X(Mn)	0.00	0.00	0.00
X(Ca)	0.84	0.83	0.72

Table 7.4. Table of standardless representative analyses of gedrite. All analyses performed in standard mode and cation proportions are based on 23 oxygens.

Representative Analyses of Gedrite

	Virginia Formation				
Field Site	Section 22	Water Hen			
Sample No.	A-1-430	C-6-679	C-10-1747	C-10-1747	C-11-2914
Site No.	2	2	3	4	2
No. Analyses	1	4	10	3	1
Wt %					
SiO_2	30.340	40.020	44.930	42.350	39.240
TiO_2	0.000	0.000	0.040	0.000	0.000
Al_2O_3	25.290	14.790	10.770	12.240	14.320
FeO	29.150	23.020	26.940	28.960	27.380
MgO	14.890	21.840	16.030	15.690	18.680
MnO	0.330	0.000	0.000	0.000	0.000
CaO	0.000	0.340	1.190	0.760	0.390
Na_2O	0.000	0.000	0.090	0.000	0.000
K_2O	0.000	0.000	0.000	0.000	0.000
Total	100.000	100.010	99.990	100.000	100.010
Total Cations (Based on 23 O)					
Norm Factor	2.530	2.631	2.604	2.571	2.575
Si	4.250	5.490	6.480	6.090	5.510
Al(iv)	3.750	2.510	1.520	1.910	2.490
SUM	8.000	8.000	8.000	8.000	8.000
Al(Vi)	0.430	-0.120	0.310	0.160	-0.120
Ti	0.000	0.000	0.000	0.000	0.000
Fe	3.420	2.640	3.250	3.480	3.210
Mg	3.110	4.470	3.440	3.360	3.910
Mn	0.040	0.000	0.000	0.000	0.000
SUM	7.000	6.990	7.000	7.000	7.000
Ca	0.000	0.050	0.180	0.120	0.060
Na	0.000	0.000	0.030	0.000	0.000
K	0.000	0.000	0.000	0.000	0.000
SUM	0.000	0.050	0.210	0.120	0.060
Total	**15.000**	**15.040**	**15.210**	**15.120**	**15.060**
X(Fe)	0.524	0.371	0.486	0.509	0.451
X(Mg)	0.476	0.629	0.514	0.491	0.549

Representative Analyses of Gedrite (Cont.)

	Virginia Formation			Thomson Formation		
Field Site	Linwood Lake			Fish Lake		
Sample No.	LL-1-09	LL-1-09	LL-1-09	F-1-532	F-2-835	F-2-837
Site No.	1	3	4	1	1	6
No. Analyses	9	8	6	6	2	5
Wt %						
SiO_2	41.050	35.290	38.710	32.650	35.650	36.740
TiO_2	0.000	0.000	0.000	0.000	0.000	0.000
Al_2O_3	12.450	20.900	18.820	24.970	21.670	18.140
FeO	29.340	24.230	19.970	22.060	27.290	29.500
MgO	16.090	19.010	21.870	18.370	15.400	15.620
MnO	0.040	0.300	0.050	0.110	0.000	0.000
CaO	1.040	0.280	0.580	0.000	0.000	0.000
Na_2O	0.000	0.000	0.000	0.000	0.000	0.000
K_2O	0.000	0.000	0.000	0.490	0.000	0.000
Total	100.010	100.010	100.000	98.650	100.010	100.000
Total Cations (Based on 23 O)						
Norm Factor	2.555	2.604	2.669	2.587	2.582	2.551
Si	5.900	4.870	5.270	4.530	5.000	5.200
Al(iv)	2.100	3.130	2.730	3.470	3.000	2.800
SUM	8.000	8.000	8.000	8.000	8.000	8.000
Al(Vi)	0.010	0.270	0.290	0.620	0.580	0.220
Ti	0.000	0.000	0.000	0.000	0.000	0.000
Fe	3.530	2.790	2.270	2.560	3.200	3.490
Mg	3.450	3.910	4.440	3.800	3.220	3.290
Mn	0.000	0.040	0.010	0.010	0.000	0.000
SUM	6.990	7.010	7.010	6.990	7.000	7.000
Ca	0.160	0.040	0.080	0.000	0.000	0.000
Na	0.000	0.000	0.000	0.000	0.000	0.000
K	0.000	0.000	0.000	0.090	0.000	0.000
SUM	0.160	0.040	0.080	0.090	0.000	0.000
Total	**15.150**	**15.050**	**15.090**	**15.080**	**15.000**	**15.000**
X(Fe)	0.506	0.416	0.338	0.403	0.498	0.515
X(Mg)	0.494	0.584	0.662	0.597	0.502	0.485

Representative Analyses of Gedrite (Cont.)

	Thomson Formation				EP Basalts
Field Site	Fish Lake		Midway Road		Ely's Peak
Sample No.	F-2-843	**F-2-849**	MR-01-A	MR-01-A	EP-3-09b
Site No.	1	**6**	2	5	4
No. Analyses	1	**4**	4	1	2
Wt %					
SiO_2	34.630	**39.840**	32.380	32.380	37.100
TiO_2	0.000	**0.000**	0.090	0.000	0.000
Al_2O_3	24.440	**21.070**	23.030	21.240	19.590
FeO	18.010	**28.270**	29.410	31.880	21.990
MgO	22.450	**14.990**	14.410	14.590	19.870
MnO	0.480	**0.160**	0.490	0.000	0.440
CaO	0.000	**0.000**	0.120	0.000	1.030
Na_2O	0.000	**0.000**	0.000	0.000	0.000
K_2O	0.000	**0.090**	0.170	0.000	0.000
Total	100.010	**104.420**	100.100	100.090	100.020
Total Cations (Based on 23 O)					
Norm Factor	2.682	**2.710**	2.531	2.504	2.631
Si	4.620	**5.390**	4.580	4.590	5.130
Al(iv)	3.380	**2.610**	3.420	3.410	2.870
SUM	8.000	**8.000**	8.000	8.000	8.000
Al(Vi)	0.460	**0.750**	0.420	0.140	0.320
Ti	0.000	**0.000**	0.010	0.000	0.000
Fe	2.010	**3.200**	3.480	3.780	2.540
Mg	4.470	**3.030**	3.040	3.080	4.090
Mn	0.050	**0.020**	0.060	0.000	0.050
SUM	6.990	**7.000**	7.010	7.000	7.000
Ca	0.000	**0.000**	0.020	0.000	0.150
Na	0.000	**0.000**	0.000	0.000	0.000
K	0.000	**0.020**	0.030	0.000	0.000
SUM	0.000	**0.020**	0.050	0.000	0.150
Total	**14.990**	**15.020**	**15.060**	**15.000**	**15.150**
X(Fe)	0.310	**0.514**	0.534	0.551	0.383
X(Mg)	0.690	**0.486**	0.466	0.449	0.617

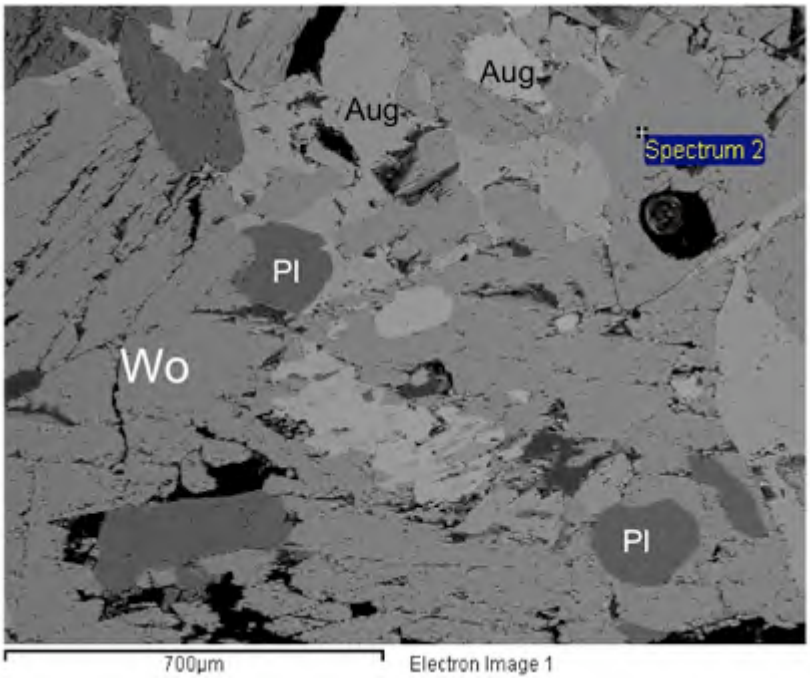

Figure 7.7. BSE image of wollastonite (Wo) closely associated with augite (Aug) taken from sample C-3-400b. Wollastonite is often misidentified as pyroxene, so EDS was needed for positive identification. Wollastonite is a good indicator mineral of contact metamorphism so its presence must be within the metamorphic aureole. Spectrum label represents the area of chemical composition analysis, which is shown in bold on Table 7.5.

Table 7.5. Table of standardless representative analyses of wollastonite. All analyses performed in standardless mode and cation proportions are based on 18 oxygens.

Representative Analyses of Wollastonite

	Virginia Formation	
Area From	Water Hen	
Sample No.	C-3-400b	**C-3-400b**
Site No.	1	**2**
No. Analyses	2	**6**
Wt %		
SiO_2	53.40	**58.10**
TiO_2	0.00	**0.00**
Al_2O_3	0.00	**0.00**
FeO	4.81	**1.46**
MgO	0.21	**0.00**
MnO	0.31	**0.42**
CaO	41.28	**32.37**
Na_2O	0.00	**7.53**
K_2O	0.00	**0.00**
Total	100.01	**99.88**
Total Cations (Based on 18 O)		
Norm Factor	2.58	**2.65**
Si	6.19	**6.56**
Al	0.00	**0.00**
Ti	0.00	**0.00**
Fe	0.47	**0.14**
Mg	0.04	**0.00**
Mn	0.03	**0.04**
Ca	5.13	**3.92**
Na	0.00	**1.65**
K	0.00	**0.00**
Total	**11.85**	**12.31**

7.4 Mineral Structure Indexing by EBSD

Electron backscatter diffraction was attempted in order to better identify cordierite. High potassium cordierite can be confused with osumilite, another high temperature silicate found in contact metamorphic regimes and some granulite terrains (Miyashiro, 1956). To distinguish between cordierite and osumilite, I determined the crystal lattice structure of the mineral by EBSD and combined that information with chemical composition to positively identify the mineral. Osumilite has a double-ring tetrahedral structure and cordierite has a single-ring structure, but compositionally they are similar (Miyashiro, 1956). The HKL NordlysII electron backscatter diffraction system was used on multiple cordierite porphyroblasts in order to determine a crystal lattice structure (Figure 7.8). Unfortunately, due to poor polish on the thin sections, there were not enough clearly-resolved Kikuchi bands developed to get an accurate structure. Ultimately the mineral was determined to be cordierite by comparing it to osumilite microprobe data collected by Grew (1982). Osumilite often has a potassium content of 8 wt% K_2O or higher (Grew, 1982), rather than the 4 wt% common in high-K cordierite (Schreyer, et. al, 1990).

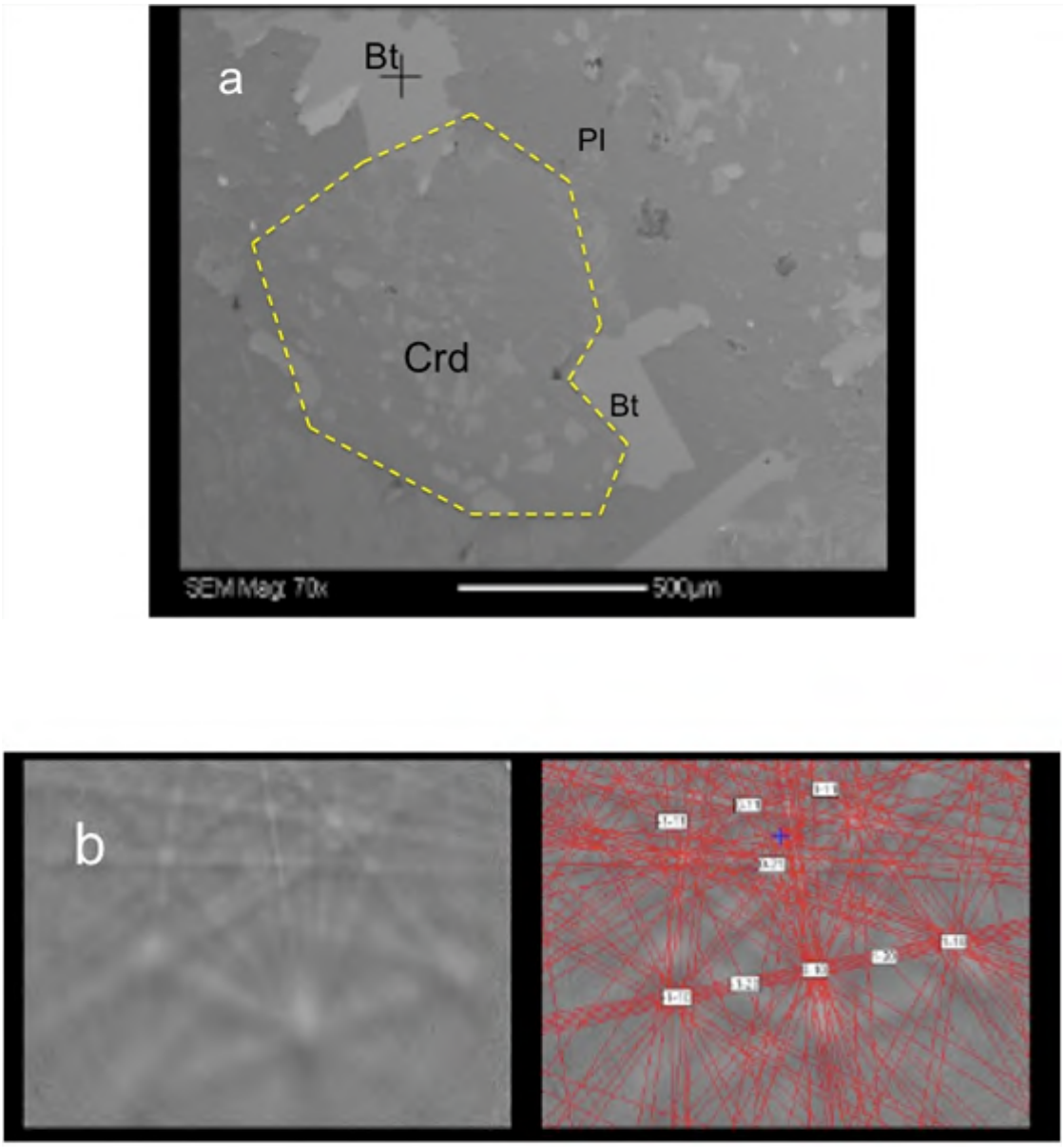

Figure 7.8. (a) SEI image of cordierite (Crd) and biotite (Bt) used for EBSD analysis. The crystal lattice structure of cordierite was to be determined by EBSD in an attempt to confirm the mineral as cordierite or osumilite. Unfortunately, the cordierite was too rough to get a good image and the smoother biotite grains produced the only usable EBSD data. In the image, the crosshairs mark where good Kikuchi bands were obtained in biotite. (b) The Kikuchi bands produced by biotite were the only ones that were accurate enough to define the mineral structure. More work could be done to determine the mineral structure of what it deduced to be cordierite, once a better polishing technique is applied.

8. THERMAL MODELING

8.1 Introduction

A one-dimensional numerical model was constructed in order to attempt to replicate thermal conditions at the time of emplacement of the Duluth Complex. Figure 8.1 demonstrates a schematic cross-section of the rocks involved in the model, and the different parameters governing them. The wall rocks were modeled to be about 10 km thick where the Duluth Complex intruded, and the intrusion itself was modeled to be approximately 5 km due to model size constraints. The Duluth Complex is estimated to have an emplacement temperature of 1200°C based on petrographic studies. The wall rocks have a geotherm that grades from 0°C at the surface to 300°C at the contact. Although the footwall is what is being modeled, the estimate of 300°C is an attempt to define country-rock temperature at the time of intrusion; therefore, the hanging wall has been used as a constraint in Figure 8.1.

The model describes heat flow via conduction from the intrusion to the wall rocks; advective heat transfer due to subsidence and/or groundwater infiltration were ignored. Relatively well-constrained parameters, such as the emplacement temperature of the Duluth Complex gabbros, and the size of the Duluth Complex intrusion, were used to inform the model. Ultimately, the slope of the thermal gradient and the temperatures of the metamorphosed wall rocks that the model predicted are compatible with those indicated by mineral stability.

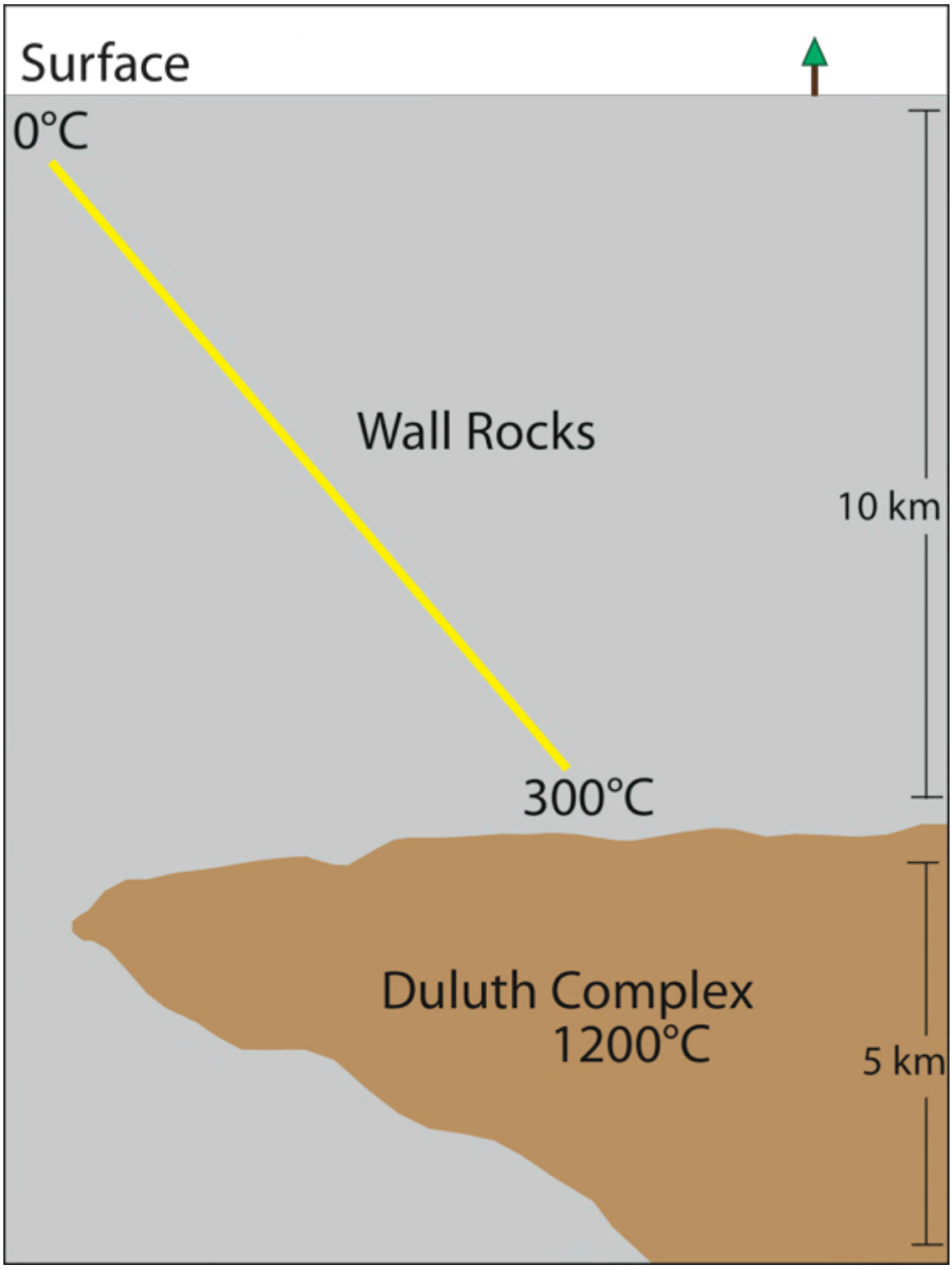

Figure 8.1. Cross-section through the Duluth Complex and the wall rocks. This simple schematic shows the depth of the intrusion and the temperatures of all rock units involved. The yellow line represents the geotherm through the wall rocks.

8.2 Emplacement Conditions of the Duluth Complex

After extensive study, the emplacement conditions of the Duluth Complex are fairly well known. Based on petrologic and geochemical studies, this igneous intrusion was approximately 1200° C at the time of emplacement, and was approximately 13 km thick (Miller, et. al, 2002). For the purpose of the model, however, a 5 km thickness was used. In general terms, the Midcontinent Rift evolved through four major magmatic pulses (Miller, et. al, 2002). It is not clear, however, how many individual injections of magma are represented by the gabbroic rocks of the Duluth Complex. If, for example, the massif was emplaced all at once, a 5 km thickness implies that the intrusion has substantial thermal power. Alternatively, if the gabbroic units were emplaced as a series of successively higher tabular sheets over a period of several million years, the thermal imprint on the wall rocks might be significantly different due to self-insulation. Furthermore, it is unclear if the magma emplacement temperature was uniform, or varied. For the purpose of the model, a uniform emplacement temperature of 1200°C and a single intrusion were assumed.

8.3 Initial Thermal State of the Wall Rocks

In contrast to the emplacement conditions of the Duluth Complex, the thermal state of the wall rocks at the time of intrusion are not well known. In addition, the stratigraphic thickness of the wall rocks is not well constrained (Severson and Peterson, 2002). However, some estimates of depth and temperature based on extrapolation of the regional geotherm can be made based on consideration of the geology. Models were run

with an initial condition of wall rock temperature at 0°C. Given some uncertainty in depth of the wall rocks during intrusion, this simplifying assumption of a starting temperature is a valid lower bound because the intrusion is much hotter than the wall rocks prior to intrusion.

Modeling with completely cooled wall rocks was a good starting point, however due to the large crystal size of the intrusion and known depths of other surrounding rocks, it is almost certain that the wall rocks were intruded at some depth, and therefore were heated to some degree. Stratigraphic thickness is almost irrelevant; the wall rocks are undoubtedly a deep pile of metasedimentary rocks, especially since they were folded and thickened, so what is important is the depth of emplacement. With a 5 km thick intrusion and a geotherm of 30°C/km, the wall rocks would have an initial starting temperature of 150°C by displacement with the gabbro. The total thickness of the North Shore Volcanic Group (sediments not included) is estimated to be 22 km, based on the seismic profile of the GLIMPCE project (Cannon et al., 1989). Measured thicknesses of normal and reversed flows on the Minnesota side of the Superior basin are approximately 10 km thick. Since the Duluth Complex intruded the North Shore Volcanics, then those volcanics were already overlying the Proterozoic metamorphic terrain. Adding 10 km of rock overlying the intrusion would bring the geotherm up to 300°C. Add to this the known burial metamorphism of the North Shore Volcanic Group in the greenschist facies (Kilburg, 1972) (which provides evidence that they experienced temperatures around 300°C), this provides the basis for running the final model with an initial wall rock temperature of 300°C.

Residual heat left over from the Penokean Orogeny was ignored because, in general, the diffusive timescale for dissipation of a thermal anomaly like the Penokean events is on the order of 100 m.y.. The Penokean predates the intrusion of the Duluth Complex by approximately 600 m.y., which allows enough time for all the excess heat associated with the earlier orogenic events to be conductively dissipated, re-estabilishing something approaching a normal crustal geotherm.

8.4 Model Description

For the construction of this model I assumed a geothermal gradient of 30°C/km prior to emplacement of the intrusion. The intrusion was modeled as an infinite horizontal slab of half-thickness 2.5 km thick at a depth of 8 km, and at time t=0. For simplicity I ignored heat production by radiogenic isotopes in the crust. The intrusion was modeled as isothermal at 1200°C and homogeneous, and the wall rocks were also modeled as thermally homogeneous.

Heat transfer was modeled by conduction alone. The temperature evolution in space and time is governed by a linear diffusion equation in the form:

$$\frac{\partial T}{\partial t} = \kappa \frac{\partial^2 T}{\partial z^2} \qquad \text{(Eq. 9.1)}$$

where time (t) is measured from the moment of emplacement, and elevation (z) is measured with respect to the midline of the intrusion. The thermal diffusivity (κ), which is the ratio of thermal conductivity (λ) to the product of density (ρ) and specific heat (c), was homogeneous in the intrusion and wall rocks (Table 8.1). Boundary conditions on Eq. 9.1 were specified temperatures at the land surface:

Table 8.1. Table of model parameters used to create the thermal model.

Model Parameters	
Initial Wall Rock Temperature (°C)	300
Initial Intrusion Temperature (°C)	1200
Thickness of the Wall Rocks (km)	10
Thickness of the Intrusion (km)	5
Thermal Diffusivity of the Wall Rocks ($\kappa=\lambda/\rho c$)	0.0000003
Thermal Diffusivity of the Intrusion ($\kappa=\lambda/\rho c$)	0.0000001
Conductivity of Wall Rocks	4
Conductivity of Intrusion	0.25
Density, ρ Wall Rocks (mg/ cm^3)	2400
Density, ρ Intrusion (mg/ cm^3)	2500
Specific Heat, c Wall Rocks (J/g*K)	500
Specific Heat, c Intrusion (J/g*K)	1000

T=0°C at z=0 km depth

and at the intrusion midline:

T=1200°C at z=0 km depth

as described above, the initial temperature profile (at T=0°C) was linear in the wall rocks and isothermal in the intrusion. Eq. 9.1 was solved using a control-volume finite-difference method implemented in a spreadsheet. The rock package was discretized into 60 m thick volumes, and the model timestep was 1 k.y..

8.5 Thermal Modeling Results

Figure 8.2 shows the evolution of the temperature distribution in the intrusion and overlying wall rocks. At the contact, the wall rocks are predicted to reach a peak temperature of 650°C. Away from the contact the rocks become steadily cooler. The length of time that has occurred since the intrusion determines the slope of the line, or how quickly the wall rocks cool down at greater distances from the contact. Ultimately the system will return to a normal equilibrium geotherm.

The thermal model calculated a peak temperature consistent with the peak temperature indicated by mineral stability. As stated previously, contact metamorphic mineral assemblages indicated that, in general, the peak metamorphic conditions in the wall rocks were between 600-700°C. The model coincides with this well, predicting a peak metamorphic condition of 650°C. The modeled contact metamorphic aureole extends out as far as 500 m, which is thicker than petrologic suggestion of a contact metamorphic aureole between 30-200 m. This suggests that although observed

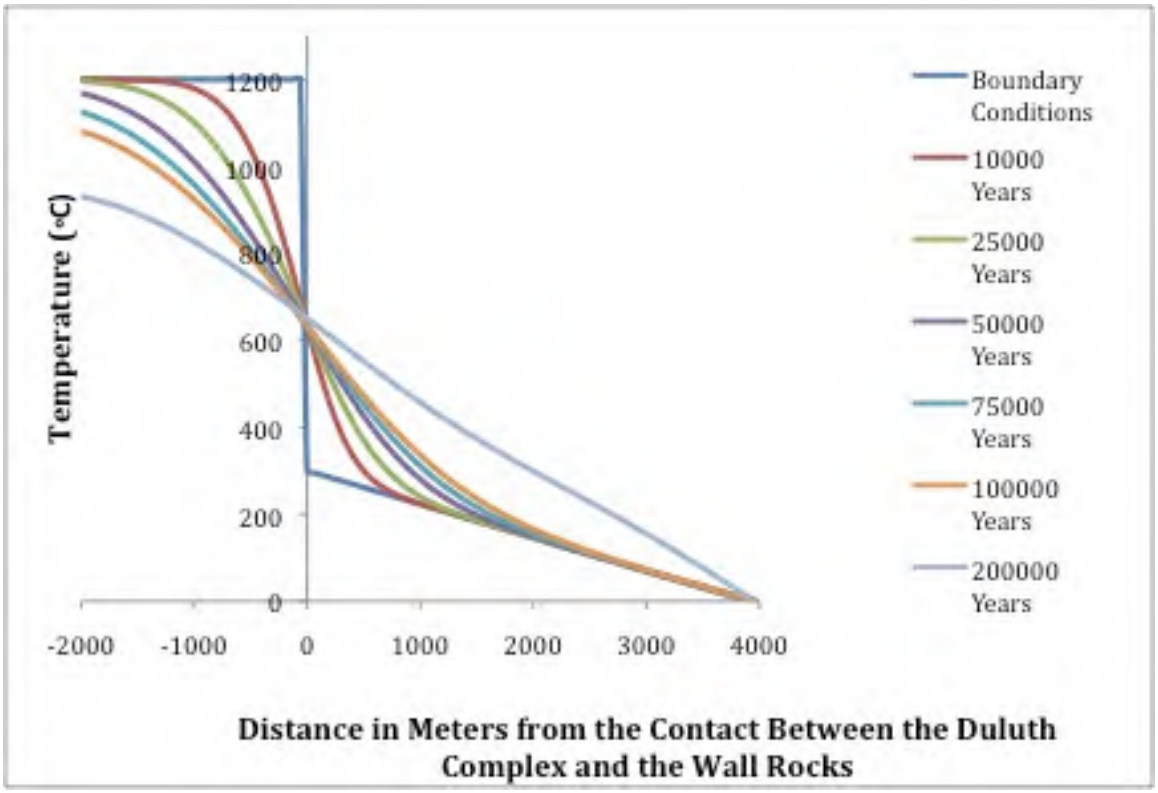

Figure 8.2. Graph of the thermal gradient of the wall rocks in relation to the Duluth Complex with decreasing time steps. The initial boundary conditions are laid out as straight lines, and the thermal gradient is laid out as curved lines with shallower slopes as time since the intrusion increases. Where the lines intersect the vertical line is the peak temperature that the wall rocks were subjected to due to the intrusion. This model almost replicates conditions seen in the real world (temperatures of 700°C or more). It reaches approximately 650°C and is within the bounds of error so it is a reasonable estimate.

evidence of metamorphism is to approximately 200 m, it is possible based on temperatures calculated in the model that contact metamorphism extended at least 500 m away from the contact. An absence of mineralogical and textural evidence for contact metamorphism beyond ~200 m is not surprising, given that rocks were previously metamorphosed to low grade during the Penokean Orogeny.

8.6 Potential Problems with Thermal Modeling

The goal of this thermal model was not to mimic the natural system, but to gain some insight into whether or not conduction alone can generate the thermal signature that is observed. However, limitations in the model may explain differences compared to observation. As stated previously, the Duluth Complex intruded in a series of magmatic events, but the one-dimensional model is limited to one large emplacement event. This difference changes the magnitude of heat flow to which the wall rocks were subjected, and ultimately changes the thermal gradient and the width of the contact aureole. In reality, modeling with multiple pulses of melt injection would probably drive the thermal gradient down a bit, because as each pulse cools, each successive pulse would affect the wall rocks less and less. The current model configuration maximizes heating of the country rocks.

Another potential problem is the initial temperature of the Duluth Complex. The model treats the gabbroic massif as a homogeneous system with an emplacement temperature of 1200°C throughout. However, in reality, the intrusion was not homogeneous because cooling would have begun to occur immediately at the margin of

the igneous body. The heterogeneous temperatures created in such a scenario would lower the thermal gradient more than the prediction of the model. Latent heat of crystallization and enthalpies of dehydration reactions in the aureole could also affect the temperature of both the intrusion and the wall rocks by adding to conduction (Docka, 1982), but these are probably balanced by heat loss at the margin. Figure 8.3 shows the Duluth Complex reaching temperatures higher than 1200°C, and ultimately creating contact metamorphic temperatures closer to 700-800°C. This is not feasible because temperatures higher than 1200°C in the Duluth Complex would not have allowed it to crystallize.

The thermal model predicts the wall rocks to reach 650°C. Mineral stability predicts conditions at a minimum of 600°C and a maximum of 700°C. This indicates that the model and the observed data coincide well. The small difference could be attributed to imprecise estimates based on mineral stability or non-ideal parameters chosen for the model.

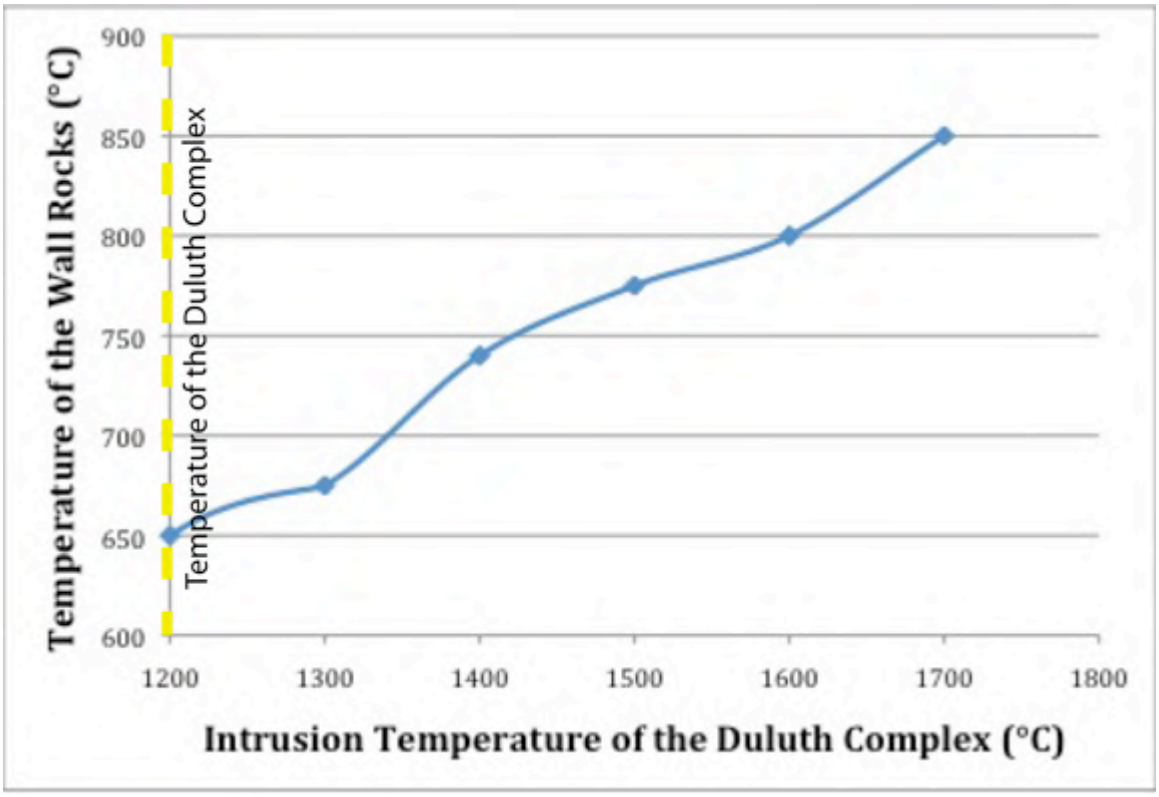

Figure 8.3. Graph of the peak temperature that the wall rocks were subjected to relative to the emplacement temperature of the Duluth Complex. The known temperature of the Duluth Complex is 1200°C, which produces a max temperature of 650°C. As the temperature of the wall rocks increases, the emplacement temperature of the Duluth Complex increases also. However, the Duluth Complex couldn't get much higher than 1200°C because it would not be able to crystallize, therefore temperatures that allow the wall rocks to reach temperatures of 700°C or above are unrealistic.

9. DISCUSSION

9.1. Contact Aureole

The contact metamorphic aureole extends from the Duluth Complex into the Animikie Group for at least 200 m based on metamorphic textures such as “spotty slate” texture. In outcrop and in core the aureole is identified where bedding becomes increasingly deformed compared to the regional fabrics. In some areas close to the contact bedding has been obliterated entirely. The aureole is petrographically defined by the presence of porphyroblasts and mortar texture (Figures 6.6-6.11). In the Ely’s Peak Basalts the aureole is slightly thinner, and extends for approximately 100 m. In outcrop and petrographically the aureole in metabasalt is identified by a granoblastic texture in which the rock takes on a hornfels texture (Figure 6.15).

Although the Duluth Complex is an extremely large, hot igneous intrusion, the wall rocks have a fairly narrow contact metamorphic aureole. This is most likely due to two factors. First, the wall rocks were fairly cool when the Duluth Complex intruded into them. They were estimated to be at a depth of about 10 km, which when taking into account the geothermal gradient, and the affect of burial metamorphism due to overhead sediments would give the rocks a temperature of approximately 300°C. This scenario of hot rock intruding into cool rock did not allow a large contact aureole to be produced. Second, and perhaps more important, the Duluth Complex intruded as a series of pulses, and perhaps after the first initial pulse the subsequent pulses were insulated, and the wall rocks were not as affected by those subsequent pulses. Both of these scenarios provide a logical explanation for the thin width of the contact aureole.

9.2. Pressure-Temperature History

Peak contact metamorphic temperatures in the wall rocks range from at least 600°C to as much as 700°C (Figure 9.1). The presence of minerals such as orthopyroxene and wollastonite confirm these temperatures. Exchange of Fe and Mg in orthopyroxene and clinopyroxene can be used as a geothermometer to determine the maximum temperature that the wall rocks experienced during intrusion (Wood and Banno, 1973). Unfortunately, due to the small grain size and lack of samples containing both types of pyroxene in textural equilibrium, I was unable to determine whether the ortho- and clinopyroxene found in this study were in chemical equilibrium; thus, the geothermometer cannot be used in this case to verify the temperature estimate.

Thermal modeling was attempted to emulate the thermal gradient attained in nature (Figure 8.1). A one-dimensional model attempted to constrain the Duluth Complex and the wall rocks using known parameters such as the emplacement temperature of the Duluth Complex, and estimating lesser-known parameters such as the depth of the wall rocks at the time of emplacement. The peak metamorphic temperature estimated by the thermal model was approximately 650°C. The estimate coincides well with temperatures given from petrography and mineral stability, especially given the lack of base conditions to use, and the complexity of modeling a natural intrusion in a one-dimensional model. Despite many uncertainties, the model also estimated a fairly thin contact metamorphic aureole when compared to the size of the Duluth Complex, which is also what is observed in the field and petrographically. The model also implies that

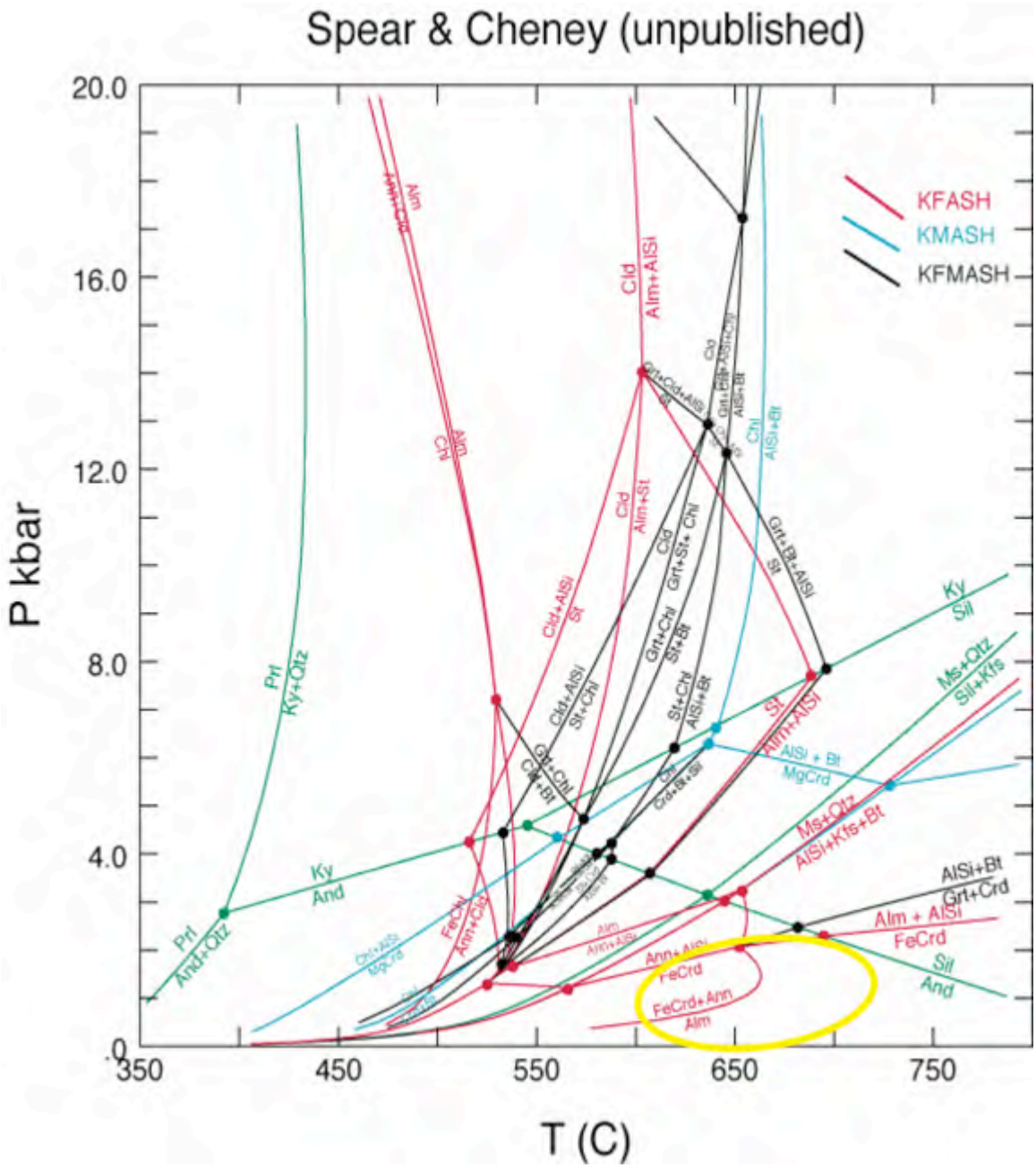

Figure 9.1. Petrogenetic grid based on the thermodynamic data set of Spear and Cheney (1989). The grid yellow circle highlights the estimated pressures and temperatures at the time of emplacement. Note that the area where iron-rich cordierite is found coincides with those temperatures and pressures estimated by petrographic and mineral stability data.

although the Duluth Complex may have intruded as a series of separate pulses, they occurred within a relatively short amount of time. In order to induce temperatures of 650°C, a large volume of magma must have been emplaced, so although there were probably multiple intrusions, their ages must be similar. One large batch of magma would still be too much magma for the temperatures seen, but many small batches in a short amount of time is a plausible idea because the intrusion rate was likely much greater than the cooling rate. This coincides with recent work done by Hoaglund (2010) which shows U-Pb ages for multiple intrusions that are less than 1 million years apart.

Mineral assemblages were not ideal for determining pressures. Pressures during the time of emplacement have been estimated by Duchesne (2004) and Kilburg (1972) as being approximately 2.5 kbar. This would mean that the Duluth Complex intruded at a depth of approximately 8 km, which would give the wall rocks an emplacement temperature of at least 250°C. For the purpose of this study, their estimates were used.

9.3. Mineral Growth

Severson and Peterson (2002) described a section of the Virginia Formation called the graphitic argillite unit that contains staurolite and sillimanite. If temperatures reached 700°C and possibly higher in the contact aureole, why were staurolite and sillimanite never found in this study? Graphitic argillite is a relatively uncommon composition in the Animikie Group and would represent a more pelitic composition as compared to the common metagraywackes. The graphitic argillite unit could be only locally present, and cores picked for this study did not contain evidence of this unit.

The lack of staurolite and sillimanite leads to another question about why certain minerals are found in certain parts of the study area and not in others. It is possible that the presence or absence of certain minerals can indicate a temperature change due to heat flow. However, the majority of the wall rocks were subjected to a similar amount of heat flow, and the minerals that grow only at certain sites form at lower temperatures than some of the more common minerals. Ultimately, parent rock composition has more importance in determining which minerals are present than the amount of heat flow. Sediments that were cemented with calcite after deposition tend to produce minerals that are more calcium-rich, such as garnet, clinopyroxene and wollastonite. Sediments that are less calcium-rich produce orthopyroxene, although both orthopyroxene and clinopyroxene have been found in certain sites. Parent rock composition combined with the heat flow from the Duluth Complex produces the complex and differing mineral arrangements found throughout the study area.

10. CONCLUSIONS

The Thomson and Virginia formations of the Animikie Group and the Ely's Peak basalts of the North Shore Volcanic Group were studied to determine how they were affected by intrusion of the Duluth Complex. Contact metamorphic mineral assemblages were identified at each field site (Figure 10.1) and their chemical composition was determined through EDS analysis. The contact metamorphic aureole was identified in both hand sample and thin section to be approximately 200 m in the Animikie Group, and 100 m in the Ely's Peak Basalts. Criteria used to define this aureole include textures such as mortar texture, spotty slate texture, and granoblastic texture, and metamorphic indicator minerals such as cordierite, garnet, wollastonite, and pyroxene. The peak pressure-temperature conditions that the wall rocks were subjected to were 600-700°C and 2.5 kbar, as determined from optical petrography, which confirm the earlier estimates provided by Severson (1995), Duchesne (2004), and Kilburg (1972). The peak metamorphic mineral assemblage found in the study area ranged from ferrosilite-gedrite-cordierite to garnet-clinopyroxene-biotite (Figure 10.1). This range is due to a change in parent composition of the original sedimentary rock. High-potassium cordierite is especially important when looking at the peak metamorphic mineral assemblages because high-potassium cordierite in an indicator mineral of high-temperature low-pressure environments such as contact metamorphic aureoles.

The width of the contact metamorphic aureole is very thin when compared to the size of the Duluth Complex, and is only 100-200 m. This suggests that the wall rocks were cool at the time of emplacement, even if they were intruded at depth. Heat transfer

could have been minimal due to the influence of fluids; for example fluids generated during dehydration reactions in the Animikie Group could have dissipated heat effectively and limited the development of a wide aureole. Multiple intrusions of the Duluth Complex also could have played a role by providing an insulating boundary layer so the rocks were only subjected to the heat from that one layer. Pressures and temperatures also provide good information about emplacement conditions. Pressures were estimated to be 2.5 kbar based on petrologic estimates from Kilburg (1972) and Duchesne (2004), and this provides information that the rocks were at approximately 8 km depth during emplacement. Temperatures were estimated to be 600-700°C and coincide with observed mineral assemblages.

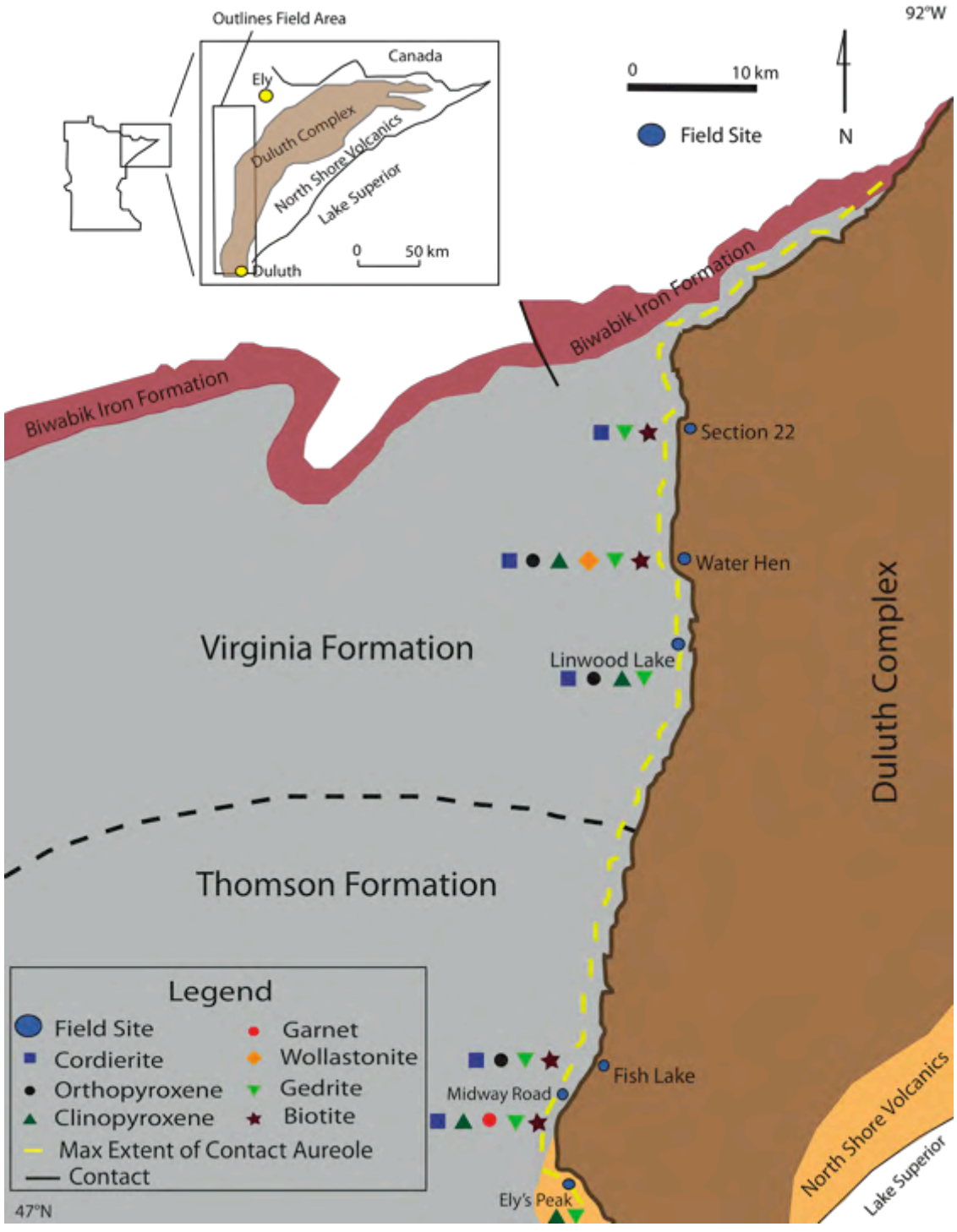

Figure 10.1. Geologic map of the Duluth Complex and the surrounding wall rocks modified after Severson (1995). The contact metamorphic aureole has been added to this map as the dashed yellow line. At each field site the main metamorphic minerals have been noted with a specific symbol (see legend.)

REFERENCES

Andrews, M. S., Ripley, E. M., 1989. Mass transfer and sulfur fixation in the contact aureole of the Duluth Complex, Dunka Road Cu-Ni Deposit, Minnesota. Canadian Mineralogist, 27 : 293-310.

Beck, J. W., 1988. Implications for Early Proterozoic tectonics and the origin of continental flood basalts, based on combined trace element and neodymium/strontium isotopic studies of mafic igneous rocks of the Penokean Lake Superior belt, Minnesota, Wisconsin and Michigan. Ph. D. dissertation, University of Minnesota, Minneapolis, Minnesota, 262 p.

Cannon, W. F., Green, A. G., Hutchinson, D. R., Lee, M., Milkereit, B., Behrendt, J. C., Halls, H. C., Green, J. C., Dickas, A. B., Morey, G. B., Sutcliffe, R., Spencer, C., 1989. The North American Midcontinent rift beneath Lake Superior from GLIMPCE seismic reflection profiling. Tectonics. 8, 2 : 305-332.

Davis, D. W., and Green, J. C., 1997. Geochronology of the North American Midcontinent rift in western Lake Superior and implications for its geodynamic evolution. Canadian Journal of Earth Sciences. 34, 4 : 476-488.

Davis, D. W., and Paces, J. B., 1990. Time resolution of geologic events on the Keweenaw Peninsula and implications for development of the Midcontinent rift system. Earth and Planetary Science Letters. 97, 54-64.

Deer, W. A., Howie, R. A., and Zussman, J., 1992. An introduction to the rock forming minerals. - 2nd ed., 696 p.

Docka, J. A., Berg, J. H., and Klewin, K. W., 1985. Thermometry in the Kiglapait aureole: Part II. Evaluation of exchange thermometry in a well-constrained thermal setting. Journal of Petrology. 27, 1 : 605-626.

Duchesne, L., 2004. Fusion partielle et microstructures associées dans l'auréole de contact du complexe igné de Duluth, Minnesota. Ph. D. dissertation. University of Quebec. 217 p.

Goldich, S. S., Nier, A. O., Baadsgaard, H., Hoffman, J. H., and Kreuger, H. W., 1961. The Precambrian geology and geochronology of Minnesota. Minnesota Geological Survey Bulletin, 41, 193 p.

Green, J. C., 1968. Varieties of flows in the North Shore Volcanic Group, Minnesota. 14th Annual Institute on Lake Superior Geology (abs.) : 20.

Green, J. C., 1972. North Shore Volcanic Group and associated minor intrusions *in* Geology of Minnesota centennial volume, University of Minnesota Press.

Green, J. C., 2002. Volcanic and sedimentary rocks of the Keweenawan Supergroup in northeastern Minnesota *in* Miller, J. D., Jr., Green, J. C., Severson, M. J., Chandler, V. W., Hauck, S. A., Peterson, D. M., and Wahl, T. E., 2002. Geology and mineral potential of the Duluth Complex and related rocks of northeastern Minnesota. Minnesota Geological Survey Report of Investigations 58, 207 p.

Grew, E. S., 1982. Osumilite in the sapphirine-quartz terrane of Enderby Land, Antarctica: implications for osumilite petrogenesis in the granulite facies. American Mineralogist, 67 : 762-787.

Hauck, S. A., Severson, M. J., Zanko, L. M., Barnes, S. J., Morton, P., Alminas, H. V., Foord, E. E., and Dahlberg, E. H., 1997. An overview of the geology and oxide, sulfide, and platinum group element mineralization along the western and northern contacts of the Duluth Complex *in* Ojakangas, R. W., Dickas, A. B., and Green, J. C., eds., Middle Proterozoic to Cambrian rifting, Central North America. Geological Society of America Special Paper 312 : 137-185.

Hemming, S., McLennan, S. M., Hanson, G. N., and Krogstad, K. M., 1990. Pb isotope systematics in quartz [abs.]: Eos, 71, 17 : 654-655.

Hentschel, G., 1977. Neufunde seltener Minerale im Laacher Vulkangebiet. Aufschluss 28 : 129-133.

Hoaglund, S., 2010. U-Pb geochronology of the Duluth Complex and related hypabyssal intrusions: investigating the emplacement history of a large multiphase intrusive complex related to the 1.1 Ga Midcontinent Rift. Master's Thesis. University of Minnesota – Duluth. 101 p.

Kilburg, J. A., 1972. Petrology, structure, and correlation of the Upper Precambrian Ely's Peak Basalts. M. S. Thesis, University of Minnesota – Duluth, Duluth, Minnesota. 97 p.

Kretz, R., 1983. Symbols for rock-forming minerals. American Mineralogist, 68 : 277-279.

Labotka, T. C., White, C. E., and Papike, J. J., 1984. The evolution of water in the contact-metamorphic aureole of the Duluth Complex, northeastern Minnesota. Geological Society of America Bulletin. 95 : 788-804.

Miller, J. D., Jr., and Vervoort, J. D., 1996. The latent magmatic stage of the Midcontinent rift: A period of magmatic underplating and melting of the lower crust. Institute on Lake Superior Geology 42nd Annual Meeting Program and Abstracts. 42, 1 : 33-35.

Miller, J. D., Jr., and Severson, M. J., 2002. Geology of the Duluth Complex *in* Miller, J. D., Jr., Green, J. C., Severson, M. J., Chandler, V. W., Hauck, S. A., Peterson, D. M., and Wahl, T. E., 2002. Geology and mineral potential of the Duluth Complex and related rocks of northeastern Minnesota. Minnesota Geological Survey Report of Investigations 58. 207 p.

Miyashiro, A., 1956. Osumilite, a new silicate mineral, and its crystal structure. American Mineralogist, 41, 104-116.

Miyashiro, A., and Iiyamo, T., 1954. A preliminary note on a new mineral, indialite, polymetamorphic with cordierite. Proceed Japan Acad 30, 8 : 746-751.

Morey, G. B., and Ojakangas, R. W., 1970. Sedimentology of the Middle Precambrian Thomson Formation, East-Central Minnesota. Minnesota Geological Survey Report of Investigation 13. 32 p.

Ojakangas, R. W., Morey, G. B., and Southwick, D. L., 2001. Paleoproterozoic basin development and sedimentation in the Lake Superior region, North America. Sedimentary Geology. 141 – 142 : 319 – 341.

Paces, J. B., and Miller, J. D., Jr., 1993. Precise U-Pb ages of Duluth Complex and related mafic intrusions, northeastern Minnesota: Geochronological insights to physical, petrogenetic, paleomagnetic and tectonomagmatic processes associated with the 1.1 Ga Midcontinent rift system. Journal of Geophysical Research. 98, B8 : 13997 – 14013.

Peterson, D. M. and Severson, M. J., 2002. Archean and paleoproterozoic rocks that form the footwall of the Duluth Complex *in* Miller, J. D., Jr., Green, J. C., Severson, M. J., Chandler, V. W., Hauck, S. A., Peterson, D. M., and Wahl, T. E., 2002. Geology and mineral potential of the Duluth Complex and related rocks of northeastern Minnesota: Minnesota Geological Survey Report of Investigations 58. 207 p.

Rao, B. V., and Ripley, E. M., 1983. Petrochemical studies of the Dunka Road Cu-Ni deposit, Duluth Complex, Minnesota. Economic Geology. 78 : 1222-1238.

Ripley, E. M., 1981. Sulfur isotopic studies of the Dunka Road Cu-Ni deposit, Duluth Complex, Minnesota. Economic Geology, 76 : 610-620.

Ripley, E. M., 2001. Ore genesis related to the development of the 1.1 Ga Midcontinent Rift system. Abstracts with Programs – Geological Society of America. 33, 4, 20 p.

Ripley, E. M., 2001. Re-Os isotopic composition and PGE contents of Proterozoic carbonaceous argillites, Virginia Formation, northeastern, Minnesota. Organic Geochemistry. 32, 6 : 857-866.

Sandberg, A. E., 1938. Section across Keweenawan lavas at Duluth, Minnesota. Geological Society of America Bulletin. 49 : 795-830.

Sawyer, E. W., 1999. Criteria for the recognition of partial melting: Physics and Chemistry of the Earth. 24, 3 : 269-279.

Schreyer, W., Maresch, W. V., Daniels, P., and Wolfsdorff, P., 1990. Potassic cordierites: characteristic minerals for high temperature, very low pressure environments. Contributions to Mineralogy and Petrology. 105 : 162-172.

Schwartz, G. M., 1949. The geology of the Duluth metropolitan area. Minnesota Geological Survey Bulletin. 33, 136 p.

Severson, 1994. Igneous Stratigraphy of the South Kawishiwi intrusion, Duluth Complex, northeastern Minnesota. Natural Resources Research Institute, Technical Report NRRI/TR-93/34. 210 p.

Severson, M. J., 1995. Geology of the southern portion of the Duluth Complex. Natural Resources Research Institute, Technical Report NRRI/TR-95/26. 185 p.

Severson, M. J., Patelke, R. L., Hauck, S. A., and Zanko, L. M., 1996. The Babbitt copper-nickel deposit, part C: Igneous geology, footwall lithologies, and cross sections. Natural Resources Research Institute, Technical Report NRRI/TR-94/21c. 79 p.

Spear, F. S., 1993. Metamorphic phase equilibria and pressure-temperature-time paths. Mineralogical Society of America. 799 p.

Spear, F. S., and Cheney, J. T., 1989. A petrogenetic grid for pelitic shists in the system SiO_2-Al_2O_3-FeO-MgO-K_2O-H_2O. Contributions to Mineralogy and Petrology. 101, 2 : 149-164.

Winchell, N. H., 1899. Geology of Minnesota. Minnesota Geological Survey final report, 4, 630 p.

Wood, B. J., and Banno, S., 1973. Garnet-orthopyroxene and orthopyroxene-clinopyroxene relationships in simple and complex systems. Contributions to Mineralogy and Petrology. 42 : 109-124.

Zanko, L. M., Severson, M. J., and Ripley, E. M., 1994. Geology and mineralization of the Serpentine copper-nickel deposit. Natural Resources Research Institute, Technical Report NRRI/TR-93/52. 90 p.

Zartman, R. E., Nicholson, S. W., Cannon, W. F., and Morey, G. B., 1997. U-Th-Pb zircon ages of some Keweenawan Supergroup rocks from the south shore of Lake Superior, *in* Bornhorst, T, J., ed., Petrology and metallogeny of intraplate mafic and ultramafic magmatism. Canadian Journal of Earth Sciences. 34, 4 : 549-561.

Appendix A

Abbreviations

Abbreviations

The following is a list of mineral abbreviations devised by Kretz (1983) that are used throughout the text.

Ap : Apatite

Aug : Augite

Bt : Biotite

Cal : Calcite

Chl : Chlorite

Cpx : Clinopyroxene

Crd : Cordierite

Fs : Ferrosilite

Ged : Gedrite

Grt : Garnet

Ilm : Ilminite

Kfs : Potassium Feldspar

Ms : Muscovite

Ol : Olivine

Opx : Orthopyroxene

Pent* : Pentlandite

Pl : Plagioclase

Py : Pyrite

Qtz : Quartz

Rt : Rutile

Sph* : Sphalerite

Spl : Spinel

Spn : Sphene

Tur : Tourmaline

Wo : Wollastonite

Zr : Zircon

*Mineral abbreviations not from Kretz (1983).

Appendix B

Chemical Analyses of Minerals Found in the Study Area

Representative Analyses of Biotite

	Virginia Formation					Thomson Fm.	
Field Site	Section 22	Water Hen				Fish Lake	
Sample No.	A-1-430	C-6-698	C-11-2873	C-11-2914	C-11-2914	F-1-493	F-1-683
Site No.	2	1	1	2	3	2	1
No. Analyses	1	1	2	3	4	1	2
Wt %							
SiO_2	38.990	39.760	39.340	40.410	41.710	39.280	39.670
TiO_2	4.530	2.950	4.500	0.000	2.500	4.510	3.360
Al_2O_3	16.870	17.700	18.290	16.950	16.050	16.640	18.320
FeO	22.080	20.130	20.840	19.420	21.300	19.790	19.780
MgO	7.900	10.770	7.280	18.420	9.760	9.690	9.470
MnO	0.000	0.000	0.000	0.000	0.000	0.000	0.000
CaO	0.000	0.000	0.000	0.000	0.000	0.000	0.000
Na_2O	0.000	0.000	0.000	0.000	0.000	0.000	0.000
K_2O	9.630	8.690	9.750	4.820	8.690	9.830	9.410
Total	100.000	100.00	100.00	100.020	100.010	99.740	100.010
Total Cations (Based on 22 O)							
Norm Factor	2.509	2.553	2.530	2.618	2.549	2.526	2.549
Si	5.039	4.981	5.077	4.681	5.364	5.037	5.028
Al(iv)	2.961	3.019	2.923	3.319	2.636	2.963	2.972
SUM	8.000	8.000	8.000	8.000	8.000	8.000	8.000
Al(vi)	1.652	1.601	1.914	0.939	1.596	1.590	1.795
Ti	0.440	0.278	0.437	0.000	0.242	0.435	0.320
Fe	2.386	2.109	2.249	1.881	2.291	2.122	2.096
Mg	1.522	2.012	1.401	3.181	1.871	1.852	1.789
Mn	0.000	0.000	0.000	0.000	0.000	0.000	0.000
SUM	6.000	6.000	6.000	6.000	6.000	6.000	6.000
Ca	0.000	0.000	0.000	0.000	0.000	0.000	0.000
Na	0.000	0.000	0.000	0.000	0.000	0.000	0.000
K	1.587	1.389	1.605	0.712	1.426	1.608	1.521
SUM	1.587	1.389	1.605	0.712	1.426	1.608	1.521
Total	**15.587**	**15.38**	**15.60**	**14.712**	**15.426**	**15.608**	**15.521**
X(Fe)	0.611	0.512	0.616	0.372	0.550	0.534	0.540
X(Mg)	0.389	0.488	0.384	0.628	0.450	0.466	0.460

Representative Analyses of Biotite (Cont.)

	Thomson Formation					
Area From	Fish Lake			Midway Road		
Sample No.	F-1-683	F-2-835	F-2-837	MR-01-E	MR-03-B	MR-03-B
Site No.	2	1	6	4	2	3
No. Analyses	6	1	1	8	3	2
Wt %						
SiO_2	41.470	47.090	42.000	41.970	42.760	39.400
TiO_2	2.830	0.000	0.860	1.230	2.120	2.890
Al_2O_3	18.500	18.450	15.640	21.400	21.470	19.830
FeO	18.940	20.450	13.270	18.050	18.580	20.780
MgO	9.320	9.480	22.390	9.980	7.460	7.700
MnO	0.000	0.000	0.000	0.000	0.000	0.000
CaO	0.000	0.000	0.000	0.220	0.000	0.000
Na_2O	0.000	0.000	0.000	0.090	0.000	0.000
K_2O	8.950	4.530	5.840	7.050	7.610	9.420
Total	100.010	100.000	100.000	99.990	100.000	100.020
Total Cations (Based on 22 O)						
Norm Factor	2.581	2.673	2.677	2.632	2.628	2.543
Si	5.276	5.919	4.818	5.172	5.395	5.017
Al(iv)	2.724	2.081	3.182	2.828	2.605	2.983
SUM	8.000	8.000	8.000	8.000	8.000	8.000
Al(vi)	1.947	2.074	0.824	2.193	2.436	2.050
Ti	0.271	0.000	0.074	0.114	0.201	0.277
Fe	2.015	2.149	1.273	1.860	1.960	2.212
Mg	1.768	1.776	3.829	1.833	1.403	1.461
Mn	0.000	0.000	0.000	0.000	0.000	0.000
SUM	6.000	6.000	6.000	6.000	6.000	6.000
Ca	0.000	0.000	0.000	0.029	0.000	0.000
Na	0.000	0.000	0.000	0.022	0.000	0.000
K	1.452	0.726	0.855	1.108	1.225	1.530
	1.452	0.726	0.855	1.159	1.225	1.530
Total	**15.452**	**14.726**	**14.855**	**15.108**	**15.225**	**15.530**
X(Fe)	0.533	0.548	0.250	0.504	0.583	0.602
X(Mg)	0.467	0.452	0.750	0.496	0.417	0.398

Representative Analyses of Muscovite

	Thomson Formation			
Field Site	Fish Lake			Midway Road
Sample No.	F-1-532	F-2-843	F-2-849	MR-01-E
Site No.	1	1	3	4
No. Analyses	3	6	4	2
Wt %				
SiO_2	50.05	52.50	53.10	53.28
TiO_2	0.11	0.00	0.00	0.48
Al_2O_3	34.58	31.83	32.70	28.30
FeO	1.82	2.26	2.05	5.02
MgO	2.13	3.40	3.99	2.82
MnO	0.00	0.00	0.00	0.00
CaO	0.00	0.00	0.00	0.72
Na_2O	0.31	0.32	0.00	0.80
K_2O	11.01	9.68	8.17	8.61
Total	100.01	99.99	100.01	100.03
Total Cations (Based on 22 O)				
Norm Factor	2.88	2.90	2.94	2.87
Si	6.36	6.62	6.62	6.80
Al(iv)	1.64	1.38	1.38	1.20
SUM	8.00	8.00	8.00	8.00
Al(vi)	5.18	4.73	4.80	4.26
Ti	0.01	0.00	0.00	0.05
Fe	0.19	0.24	0.21	0.54
Mg	0.40	0.64	0.74	0.54
Mn	0.00	0.00	0.00	0.00
SUM	5.79	5.61	5.76	5.37
Ca	0.00	0.00	0.00	0.10
Na	0.08	0.08	0.00	0.20
K	1.79	1.56	1.30	1.40
Total	**15.65**	**15.25**	**15.06**	**15.07**

Representative Analyses of Chlorite

	Virginia Formation			
	Area 22			Water Hen
Field Site	A-1-430	A-1-476	A-1-476	C-6-679
Sample No.	2	2	2	2
Site No.	7	5	9	14
No. Analyses				
Wt %				
SiO_2	33.06	37.01	35.52	37.42
TiO_2	0.00	0.00	2.09	0.00
Al_2O_3	24.98	22.82	20.07	19.77
FeO	25.33	23.48	27.18	23.41
MgO	16.05	14.65	13.07	18.81
MnO	0.00	0.38	0.00	0.00
CaO	0.00	0.00	0.00	0.00
Na_2O	0.00	0.00	0.00	0.00
K_2O	0.57	1.67	2.07	0.59
Total	99.99	100.01	100.00	100.00
Total Cations (Based on 22 O)				
Norm Factor	2.59	2.61	2.55	2.62
Si	4.68	5.19	5.11	5.23
Al(iv)	3.32	2.81	2.89	2.77
SUM	8.00	8.00	8.00	8.00
Al(vi)	4.17	3.77	3.40	3.25
Ti	0.00	0.00	0.23	0.00
Fe	3.00	2.75	3.27	2.73
Mg	3.39	3.06	2.80	3.92
Mn	0.00	0.05	0.00	0.00
SUM	10.55	9.63	9.70	9.90
Ca	0.00	0.00	0.00	0.00
Na	0.00	0.00	0.00	0.00
K	0.10	0.30	0.38	0.11
SUM	0.10	0.30	0.38	0.11
Total	18.65	17.93	18.08	18.01
X(Fe)	0.53	0.53	0.46	0.59
X(Mg)	0.47	0.47	0.54	0.41

Representative Analyses of Alkali Feldspar

	Virginia Formation			Thomson Formation		
Field Site	Section 22	Water Hen		Fish Lake		
Sample No.	A-1-476	C-6-698	C-11-2873	F-2-835	F-2-837	F-2-849
Site No.	2	1	1	1	6	3
No. Analyses	1	2	3	5	2	1
Wt %						
SiO_2	66.290	66.840	66.360	65.740	66.010	66.450
TiO_2	0.000	0.000	0.000	0.000	0.000	0.000
Al_2O_3	17.450	18.040	18.000	19.450	17.950	17.820
FeO	0.000	0.000	0.330	0.000	0.650	0.410
MgO	0.000	0.000	0.000	0.000	0.000	0.000
MnO	0.000	0.000	0.000	0.000	0.000	0.000
CaO	0.000	0.000	0.000	0.170	0.000	0.000
Na_2O	0.000	1.640	1.880	1.140	0.000	1.070
K_2O	16.260	13.690	13.430	13.500	15.410	14.250
Total	100.000	100.210	100.000	100.000	100.020	100.000
Total Cations (Based on 8 O)						
Norm Factor	2.886	2.921	2.910	2.919	2.892	2.904
Si	3.058	3.047	3.037	2.999	3.040	3.047
Al(iv)	-0.058	-0.047	-0.037	0.001	-0.040	-0.047
SUM	3.000	3.000	3.000	3.000	3.000	3.000
Al(vi)	0.949	0.969	0.971	1.046	0.974	0.963
Ti	0.000	0.000	0.000	0.000	0.000	0.000
Fe	0.000	0.000	0.013	0.000	0.025	0.016
Mg	0.000	0.000	0.000	0.000	0.000	0.000
Mn	0.000	0.000	0.000	0.000	0.000	0.000
SUM	0.949	0.969	0.983	1.046	0.999	0.979
Ca	0.000	0.000	0.000	0.008	0.000	0.000
Na	0.000	0.145	0.167	0.101	0.000	0.095
K	0.957	0.796	0.784	0.786	0.905	0.833
SUM	0.957	0.941	0.951	0.895	0.905	0.929
Total	**4.906**	**4.910**	**4.934**	**4.940**	**4.904**	**4.907**

Representative Analyses of Alkali Feldspar (Cont.)

	Thomson Formation			Ely's Peak Basalts	
Field Site	Midway Road			Ely's Peak	
Sample No.	MR-01-A	MR-01-A	MR-03-B	EP-6-09	EP-7-09
Site No.	2	5	3	2	1
No. Analyses	2	2	4	5	4
Wt %					
SiO_2	66.070	66.230	66.430	65.340	66.730
TiO_2	0.000	0.000	0.120	0.000	0.000
Al_2O_3	17.730	17.970	17.480	18.130	17.470
FeO	0.170	0.000	1.190	0.000	0.330
MgO	0.000	0.000	0.180	0.000	0.000
MnO	0.000	0.000	0.160	0.000	0.000
CaO	0.000	0.000	0.290	0.000	0.000
Na_2O	0.570	0.750	1.740	0.000	0.000
K_2O	14.800	14.780	11.900	14.940	15.470
Total	99.340	99.730	99.490	98.410	100.000
Total Cations (Based on 8 O)					
Norm Factor	2.883	2.896	2.905	2.861	2.898
Si	3.051	3.045	3.045	3.041	3.066
Al(iv)	-0.051	-0.045	-0.045	-0.041	-0.066
SUM	3.000	3.000	3.000	3.000	3.000
Al(vi)	0.965	0.974	0.944	0.995	0.946
Ti	0.000	0.000	0.004	0.000	0.000
Fe	0.007	0.000	0.046	0.000	0.013
Mg	0.000	0.000	0.012	0.000	0.000
Mn	0.000	0.000	0.006	0.000	0.000
SUM	0.972	0.974	1.013	0.995	0.959
Ca	0.000	0.000	0.014	0.000	0.000
Na	0.051	0.067	0.155	0.000	0.000
K	0.872	0.867	0.696	0.887	0.907
SUM	0.923	0.934	0.865	0.887	0.907
Total	**4.894**	**4.908**	**4.877**	**4.882**	**4.866**

Representative Analyses of Plagioclase Feldspar

	Virginia Formation					
Field Site	Section 22	Water Hen				
Sample No.	A-1-430	C-3-324	C-3-400b	C-10-1747	C-11-2873	C-11-2914
Site No.	2	1	1	4	1	2
No. Analyses	1	3	1	2	3	5
Wt %						
SiO_2	66.460	47.830	48.020	58.770	63.820	61.170
TiO_2	0.000	0.000	0.000	0.000	0.000	0.000
Al_2O_3	21.310	34.190	24.820	26.630	22.990	24.910
FeO	0.000	0.000	0.280	0.000	0.000	0.000
MgO	0.000	0.000	0.000	0.000	0.000	0.000
MnO	0.000	0.000	0.000	0.000	0.000	0.000
CaO	3.190	16.810	26.880	8.260	4.170	6.510
Na_2O	8.550	1.170	0.000	6.340	9.020	7.410
K_2O	0.490	0.000	0.000	0.000	0.000	0.000
Total	100.000	100.000	100.000	100.000	100.000	100.000
Cations (Calculated on the basis of 8 oxygens)						
Norm Factor	3.033	2.911	2.806	2.983	3.014	2.998
Si	2.918	2.188	2.278	2.623	2.819	2.717
Al(iv)	0.082	0.812	0.722	0.377	0.181	0.283
SUM	3.000	3.000	3.000	3.000	3.000	3.000
Al(vi)	1.103	1.843	1.388	1.401	1.197	1.304
Ti	0.000	0.000	0.000	0.000	0.000	0.000
Fe	0.000	0.000	0.011	0.000	0.000	0.000
Mg	0.000	0.000	0.000	0.000	0.000	0.000
Mn	0.000	0.000	0.000	0.000	0.000	0.000
SUM	1.103	1.843	1.399	1.401	1.197	1.304
Ca	0.150	0.824	1.366	0.395	0.197	0.310
Na	0.728	0.104	0.000	0.549	0.773	0.638
K	0.027	0.000	0.000	0.000	0.000	0.000
Total	**5.008**	**5.770**	**5.765**	**5.344**	**5.167**	**5.251**
X(Ca)	0.166	0.888	1.000	0.419	0.203	0.327
X(Na)	0.804	0.112	0.000	0.581	0.797	0.673
X(K)	0.030	0.000	0.000	0.000	0.000	0.000
X(An)	0.112	1.737	1.973	0.537	0.186	0.360
X(Ab)	0.793	0.107	0.000	0.652	0.883	0.752
X(Or)	0.030	0.000	0.000	0.000	0.000	0.000

Representative Analyses of Plagioclase Feldspar (Cont.)

	Virginia Fm.	Thomson Formation				
Field Site	Linwood Lake	Fish Lake				
Sample No.	LL-1-09	F-1-532	F-1-683	F-2-835	F-2-837	F-2-843
Site No.	1	1	1	1	6	1
No. Analyses	2	1	3	1	2	1
Wt %						
SiO_2	44.940	69.910	66.130	65.080	70.590	69.640
TiO_2	0.000	0.000	0.000	0.000	0.000	0.000
Al_2O_3	35.880	18.690	21.310	21.390	18.070	18.640
FeO	0.470	0.000	0.000	0.000	0.000	0.000
MgO	0.000	0.000	0.000	0.000	0.000	0.000
MnO	0.000	0.000	0.000	0.000	0.000	0.000
CaO	18.710	0.240	2.990	4.440	0.000	0.160
Na_2O	0.000	11.160	9.570	9.090	11.350	11.560
K_2O	0.000	0.000	0.000	0.000	0.000	0.000
Total	100.000	100.000	100.000	100.000	100.010	100.000
Cations (Calculated on the basis of 8 oxygens)						
Norm Factor	2.886	3.054	3.029	3.015	3.058	3.049
Si	2.073	3.048	2.907	2.874	3.074	3.041
Al(iv)	0.927	-0.048	0.093	0.126	-0.074	-0.041
SUM	3.000	3.000	3.000	3.000	3.000	3.000
Al(vi)	1.951	0.960	1.104	1.113	0.927	0.959
Ti	0.000	0.000	0.000	0.000	0.000	0.000
Fe	0.018	0.000	0.000	0.000	0.000	0.000
Mg	0.000	0.000	0.000	0.000	0.000	0.000
Mn	0.000	0.000	0.000	0.000	0.000	0.000
SUM	1.969	0.960	1.104	1.113	0.927	0.959
Ca	0.925	0.011	0.141	0.210	0.000	0.007
Na	0.000	0.943	0.816	0.778	0.958	0.979
K	0.000	0.000	0.000	0.000	0.000	0.000
Total	**5.893**	**4.915**	**5.060**	**5.102**	**4.886**	**4.946**
Ca+Na+K	0.925	0.954	0.956	0.988	0.958	0.986
X(Ca)	1.000	0.012	0.147	0.213	0.000	0.008
X(Na)	0.000	0.988	0.853	0.787	1.000	0.992
X(K)	0.000	0.000	0.000	0.000	0.000	0.000
X(An)	2.057	0.005	0.107	0.167	0.000	0.004
X(Ab)	0.000	0.902	0.888	0.848	0.880	0.936
X(Or)	0.000	0.000	0.000	0.000	0.000	0.000

Representative Analyses of Plagioclase Feldspar (Cont.)

Field Site	Thomson Fm.	Ely's Peak Basalts		
	Midway Road	Ely's Peak		
Sample No.	MR-01-A	EP-3-09b	EP-6-09	EP-7-09
Site No.	2	5	2	1
No. Analyses	2	3	2	4
Wt %				
SiO_2	41.710	67.750	56.650	57.330
TiO_2	0.000	0.000	0.000	0.000
Al_2O_3	28.750	20.010	27.760	27.160
FeO	5.720	0.250	0.000	0.000
MgO	0.000	0.000	0.000	0.000
MnO	0.000	0.000	0.000	0.000
CaO	23.820	1.420	10.140	9.320
Na_2O	0.000	10.380	5.190	5.930
K_2O	0.000	0.190	0.260	0.260
Total	100.000	100.000	100.000	100.000
Cations (Calculated on the basis of 8 oxygens)				
Norm Factor	2.734	3.035	2.964	2.966
Si	2.032	2.972	2.545	2.574
Al(iv)	0.968	0.028	0.455	0.426
SUM	3.000	3.000	3.000	3.000
Al(vi)	1.650	1.034	1.470	1.437
Ti	0.000	0.000	0.000	0.000
Fe	0.233	0.009	0.000	0.000
Mg	0.000	0.000	0.000	0.000
Mn	0.000	0.000	0.000	0.000
SUM	1.883	1.044	1.470	1.437
Ca	1.243	0.067	0.488	0.448
Na	0.000	0.883	0.452	0.516
K	0.000	0.011	0.015	0.015
Total	**6.127**	**5.004**	**5.425**	**5.416**
Ca+Na+K	1.243	0.960	0.955	0.979
X(Ca)	1.000	0.070	0.511	0.458
X(Na)	0.000	0.919	0.473	0.527
X(K)	0.000	0.011	0.016	0.015
X(An)	2.199	0.042	0.732	0.644
X(Ab)	0.000	0.912	0.531	0.607
X(Or)	0.000	0.011	0.018	0.018

Representative Analyses of Quartz

	Virginia Formation				
Field Site	Section 22	Water Hen			
Sample No.	A-1-430	C-3-324	C-3-400b	C-6-698	C-11-2873
Site No.	2	1	2	1	1
No. Analyses	2	1	1	1	1
Wt %					
SiO_2	100.00	100.00	96.13	99.28	89.70
TiO_2	0.00	0.00	0.00	0.00	0.00
Al_2O_3	0.00	0.00	0.81	0.00	2.90
FeO	0.00	0.00	0.46	0.00	3.41
MgO	0.00	0.00	0.00	0.00	0.99
MnO	0.00	0.00	0.00	0.00	1.04
CaO	0.00	0.00	2.60	0.00	0.00
Na_2O	0.00	0.00	0.00	0.00	0.00
K_2O	0.00	0.00	0.00	0.00	1.96
Total	100.00	100.00	100.00	99.28	100.00
Cations (Calculated on the basis of 2 oxygens)					
Norm Factor	3.32	3.32	3.27	3.30	3.17
Si	1.00	1.00	0.98	1.00	0.94
Al	0.00	0.00	0.01	0.00	0.04
Ti	0.00	0.00	0.00	0.00	0.00
Fe	0.00	0.00	0.00	0.00	0.03
Mg	0.00	0.00	0.00	0.00	0.02
Mn	0.00	0.00	0.00	0.00	0.01
Ca	0.00	0.00	0.03	0.00	0.00
Na	0.00	0.00	0.00	0.00	0.00
K	0.00	0.00	0.00	0.00	0.03
Total	**1.00**	**1.00**	**1.02**	**1.00**	**1.06**

Representative Analyses of Quartz (Cont.)

	Virginia Formation		Thomson Formation		
Field Site	Water Hen	Linwood Lake	Fish Lake		
Sample No.	C-11-2914	LL-1-09	F-1-532	F-1-683	F-2-835
Site No.	2	4	1	2	1
No. Analyses	2	2	1	1	1
Wt %					
SiO_2	100.00	99.40	93.95	100.00	100.00
TiO_2	0.00	0.00	0.00	0.00	0.00
Al_2O_3	0.00	0.00	2.03	0.00	0.00
FeO	0.00	0.27	2.84	0.00	0.00
MgO	0.00	0.00	1.19	0.00	0.00
MnO	0.00	0.00	0.00	0.00	0.00
CaO	0.00	0.33	0.00	0.00	0.00
Na_2O	0.00	0.00	0.00	0.00	0.00
K_2O	0.00	0.00	0.00	0.00	0.00
Total	100.00	100.00	100.01	100.00	100.00
Cations (Calculated on the basis of 2 oxygens)					
Norm Factor	3.32	3.31	3.25	3.32	3.32
Si	1.00	1.00	0.96	1.00	1.00
Al	0.00	0.00	0.02	0.00	0.00
Ti	0.00	0.00	0.00	0.00	0.00
Fe	0.00	0.00	0.02	0.00	0.00
Mg	0.00	0.00	0.02	0.00	0.00
Mn	0.00	0.00	0.00	0.00	0.00
Ca	0.00	0.00	0.00	0.00	0.00
Na	0.00	0.00	0.00	0.00	0.00
K	0.00	0.00	0.00	0.00	0.00
Total	**1.00**	**1.01**	**1.03**	**1.00**	**1.00**

Representative Analyses of Quartz (Cont.)

	Thomson Formation					
Field Site	Fish Lake			Midway Road		
Sample No.	F-2-837	F-2-843	F-2-849	MR-01-A	MR-01-E	MR-03-B
Site No.	6	1	3	5	4	2
No. Analyses	1	1	2	3	2	3
Wt %						
SiO_2	98.91	100.00	100.00	100.00	98.32	98.84
TiO_2	0.00	0.00	0.00	0.00	0.00	0.00
Al_2O_3	0.00	0.00	0.00	0.00	1.12	0.68
FeO	0.60	0.00	0.00	0.00	0.30	0.48
MgO	0.49	0.00	0.00	0.00	0.00	0.00
MnO	0.00	0.00	0.00	0.00	0.00	0.00
CaO	0.00	0.00	0.00	0.00	0.00	0.00
Na_2O	0.00	0.00	0.00	0.00	0.00	0.00
K_2O	0.00	0.00	0.00	0.00	0.26	0.00
Total	100.00	100.00	100.00	100.00	100.00	100.00
Cations (Calculated on the basis of 2 oxygens)						
Norm Factor	3.30	3.32	3.32	3.32	3.30	3.31
Si	1.00	1.00	1.00	1.00	0.99	0.99
Al	0.00	0.00	0.00	0.00	0.01	0.01
Ti	0.00	0.00	0.00	0.00	0.00	0.00
Fe	0.01	0.00	0.00	0.00	0.00	0.00
Mg	0.01	0.00	0.00	0.00	0.00	0.00
Mn	0.00	0.00	0.00	0.00	0.00	0.00
Ca	0.00	0.00	0.00	0.00	0.00	0.00
Na	0.00	0.00	0.00	0.00	0.00	0.00
K	0.00	0.00	0.00	0.00	0.00	0.00
Total	**1.01**	**1.00**	**1.00**	**1.00**	**1.01**	**1.01**